The Physics of Phase Transition Phenomena Enhanced by Nanoparticles

Liu Yang[1,*], Jialu Tian[1], Yulong Ding[2], Avinash Alagumalai[3], Fatih Selimefendigil[4,5], Mortaza Aghbashlo[6], Meisam Tabatabaei[7,8], L. Godson Asirvatham[9], Somchai Wongwises[10], S.A. Sherif[11], Efstathios E. Michaelides[12], Christos N. Markides[13], Omid Mahian[14,**]

N.B.: This is the ACCEPTED MANUSCRIPT version of this article. The final, published version of the article can be found at: https://doi.org/10.1063/5.0200714

[1] *Key Laboratory of Energy Thermal Conversion and Control of Ministry of Education, School of Energy and Environment, Southeast University, Nanjing, 210096, China*

[2] *Birmingham Centre for Energy Storage & School of Chemical Engineering, University of Birmingham, Edgbaston, Birmingham B15 2TT, UK*

[3] *Department of Mechanical Engineering, GMR Institute of Technology, Rajam 532127, India*

[4] *Department of Mechanical Engineering, College of Engineering, King Faisal University, Al Ahsa 31982, Saudi Arabia*

[5] *Department of Mechanical Engineering, Celal Bayar University, 45140 Manisa, Turkey*

[6] *Department of Mechanical Engineering of Agricultural Machinery, Faculty of Agricultural Engineering and Technology, College of Agriculture and Natural Resources, University of Tehran, Karaj, Iran*

[7] *Higher Institution Centre of Excellence (HICoE), Institute of Tropical Aquaculture and Fisheries (AKUATROP), Universiti Malaysia Terengganu, 21030, Kuala Nerus, Terengganu, Malaysia*

[8] *Department of Biomaterials, Saveetha Dental College, Saveetha Institute of Medical and Technical Sciences, Chennai, 600 077, India*

[9] *Department of Mechanical Engineering, Karunya Institute of Technology and Sciences, Coimbatore 641114, India*

[10] *Fluid Mechanics, Thermal Engineering and Multiphase Flow Research Lab (FUTURE), Department of Mechanical Engineering, Faculty of Engineering, King Mongkut's University of Technology Thonburi, Bangmod, Bangkok 10140, Thailand*

[11] *Department of Mechanical and Aerospace Engineering, University of Florida, 1064 Center Drive, 181 NEB Building, Gainesville, Florida 32611, USA*

[12] *Department of Engineering, TCU, Fort Worth, TX, 76129, USA*

[13] *Clean Energy Processes (CEP) Laboratory, Department of Chemical Engineering, Imperial College London, London SW7 2AZ, UK*

[14] *Zhejiang Provincial Engineering Research Center for the Safety of Pressure Vessel and Pipeline, Faculty of Mechanical Engineering and Mechanics, Ningbo University, Ningbo 315211, China*

Corresponding authors E-mails: yang_liu@seu.edu.cn(Liu Yang); omid.mahian@gmail.com (Omid Mahian)

Abstract

Phase transitions are fundamental phenomena in physics that have been extensively studied owing to their applications across diverse industrial sectors, including energy, power, healthcare, and the environment. An example of such applications in the energy sector is thermal energy storage using phase change materials. In such systems, and indeed in many other thermal systems, an emerging and promising approach involves the use of nanoparticles, which have been extensively studied for their potential to enhance the performance of thermal systems. However, conducting thermodynamic analyses of thermal systems in the presence of nanoparticles proves to be complex and resource-consuming because of the involvement of many parameters, including (i) temperature, molecular structure, and composition of the host fluid in which nanoparticles are either dispersed or in physical contact; (ii) nanoparticle morphology, size, type, and concentration; and (iii) complex interactions between the nanoparticles and the base fluid. This article reviews recent studies on the role of nanoparticles in phase transition processes such as freezing, melting, boiling, evaporation, and condensation. It begins with an overview of phase transition phenomena without nanoparticles, emphasizing the most important controlling parameters, and then examines the underlying physics of nanoparticle-involved phase transitions, critically examining their impact on process speed (transport rates). The article also explores physical phenomena, such as Brownian motion, thermophoresis, microconvection, and nanoparticle agglomeration, and considers their contribution to rate control (enhancement or reduction). Finally, the article presents challenges, research gaps, and suggestions for future exploration, aimed at offering a comprehensive understanding of the complex interplay between the presence of nanoparticles and the phase transition processes.

***Keywords*:**

Boiling; Condensation; Evaporation; Freezing; Melting; Nanoparticles; Phase change

Table of contents

1. Introduction
2. Phase change heat transfer at the nanoscale
    2.1. Effects of nanoparticle concentration and morphology
        2.1.1. Nanoparticle type and concentration
        2.1.2. Aspect ratio of nanoparticles
    2.2. Surface factors
        2.2.1. Surface tension
        2.2.2. Surface wettability
    2.3. Effects of the external field
    2.4. Motion of nanoparticles due to field gradient
    2.5. Extended surface heat transfer
3. Freezing (solidification)
    3.1. Effects of nanoparticle concentration and morphology
    3.2. Environmental factors
        3.2.1. Surfactants
        3.2.2. Temperature and pressure
    3.3. Effects of the external field and microphysical influence mechanisms
        3.3.1. Magnetic/electric field
        3.3.2. Motion of nanoparticles due to field gradient
        3.3.3. Rejection of nanoparticles from a liquid-solid solidification front
        3.3.4. Agglomeration
        3.3.5. Micro-nano bubbles
4. Melting
    4.1. Effects of nanoparticle concentration and morphology
    4.2. External magnetic field
    4.3. Other factors
5. Boiling
    5.1. Effects of nanoparticle concentration and morphology
        5.1.1. Nanoparticle type and concentration
        5.1.2. Nanoparticle size
    5.2. Surface factors
        5.2.1. Surface tension
        5.2.2. Wettability
        5.2.3. Surface roughness

5.2.4. Deposition

5.3. Experimental conditions

5.3.1. Surfactants

5.3.2. Pressure

5.4. External field and microphysical influence mechanisms

5.4.1. Magnetic field

5.4.2. Motion of nanoparticles due to field gradients

5.4.3. Aggregation and contact angle

5.4.4. Nanoparticle migration

6. Evaporation

6.1. Effects of nanoparticle concentration and morphology

6.1.1. Nanoparticle type

6.1.2. Nanoparticle concentration

6.1.3. Nanoparticle size

6.2. Surface factors

6.2.1. Surface tension

6.2.2. Wettability

6.3. Microphysical influence mechanisms

6.3.1. Motion of nanoparticles due to field gradient

6.3.2. Microconvection

6.3.3. Nanoparticle migration

6.3.4. Radiation

6.3.5. Sonication

7. Condensation

7.1. Effects of nanoparticle concentration and morphology

7.1.1. Nanoparticle type

7.1.2. Nanoparticle concentration

7.1.3. Nanoparticle size

7.2. Surface and environmental factors

7.2.1. Wettability

7.2.2. Temperature and pressure

7.3. Microphysical influence mechanisms

7.3.1. Motion of nanoparticles due to field gradient

7.3.2. Agglomeration

7.3.3. Nanoparticles migration

8. Outlook, challenges, and future scope

9. Conclusions

1. Introduction

Phase change is ubiquitous in processes, such as water evaporation and lake water freezing under cold conditions. In this context, the word “phase” signifies a state of matter characterized by uniform chemical composition and physical attributes [1]. The term “phase transition” denotes the rapid alteration of a substance from one state to another, which is influenced by changing external parameters. The chemical composition remained constant before and after a phase change, highlighting that phase transitions are physical processes devoid of chemical reactions. From a thermodynamic perspective, this transformation can be categorized into primary and secondary phase changes. During a phase transition, volume changes occur, defining a “primary phase change,” exemplified by the transition between the ice and water states. Conversely, a “secondary phase change” entails changes in the heat capacity, thermal expansion coefficient, and compression coefficient without modifications in volume or heat, as observed in the transition from a conventional conductor to a superconductor.

Phase changes involve the formation or disruption of intermolecular bonds, driven by intermolecular forces. At the macroscopic scale, under standard conditions, matter exhibits three distinct phases: solid, liquid, and gas, with each phase reflecting the molecular arrangement of the substance. Solids feature densely packed molecules in a fixed pattern, which is characterized by robust intermolecular forces. Conversely, liquids lack a defined arrangement among molecules while maintaining their proximity, similar to solids. In contrast, gases lack both fixed patterns and have molecules traversing considerable distances, resulting in weaker forces. This understanding underpins phase transformation as a process in which distances and configurations among constituent particles are altered, ultimately converging into a new stable state [2].

Phase changes encompass a wide range of processes including freezing, melting, boiling, evaporation, condensation, transitions between solid crystalline phases, and transitions between crystalline and amorphous phases. These phenomena have applications in diverse fields such as

materials chemistry, thermal engineering, and meteorology. These transformations are useful in diverse contexts; for instance, liquid-vapor phase change processes play a pivotal role in thermal energy storage and release applications. This uniqueness stems from the very high equivalent heat storage of phase change materials (PCMs) at a constant temperature, which leads to solidification or melting across temperature ranges rather than at specific points [2]. When a phase change occurs between the vapor and liquid phases, as seen in evaporation and condensation processes, scrutinizing the interfacial resistance in liquid-vapor mixtures provides insights into interfacial heat and mass transfer intricacies [3]. Therefore, understanding the essence of phase change phenomena and its multifaceted influencing factors is imperative to enhance the efficacy of systems reliant on these processes.

Nanoparticles are minute entities whose definitions, as adopted by various organizations in Figure 1, converge to characterize them as particles with at least one dimension measuring less than 100 nm [4]. These nanoparticles exhibit diverse morphologies, including spherical, flaky, dendritic, tubular, rod-shaped, and numerous others. The categorization shown in Figure 2 highlights eight classes: (a) carbon-based nanoparticles, (b) metal nanoparticles, (c) ceramic nanoparticles, (d) semiconductor nanoparticles, and (e) polymer nanoparticles [5]. Given this diversity, the creation of nanoparticles with precise sizes and morphologies necessitates the implementation of precise and sophisticated synthesis techniques.

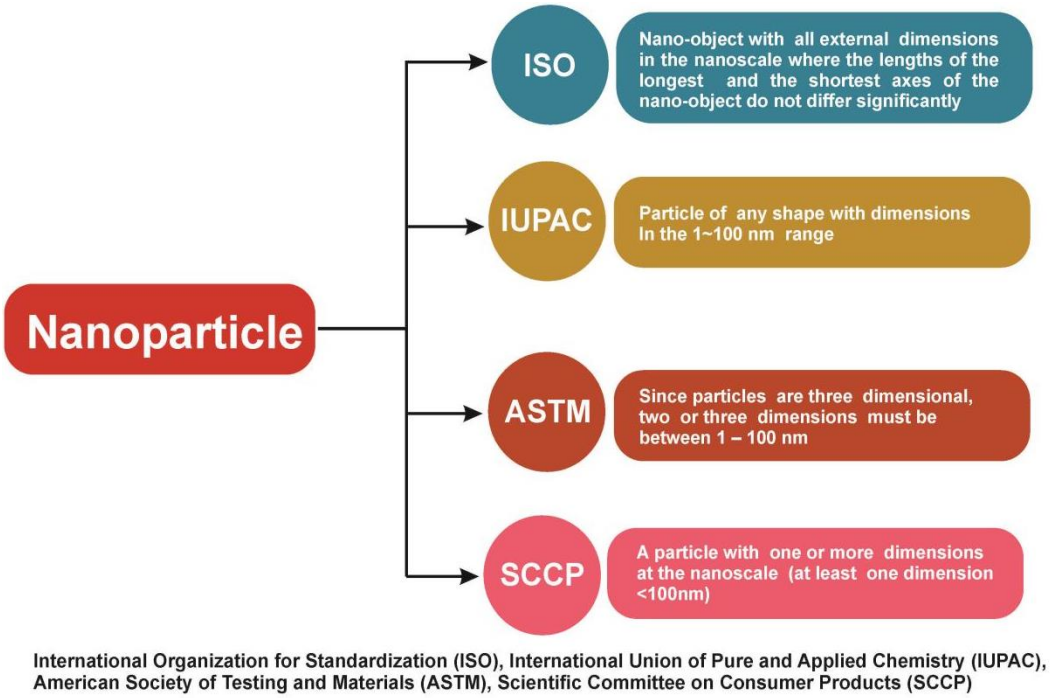


Figure 1. Definition of nanoparticles provided by different organizations.

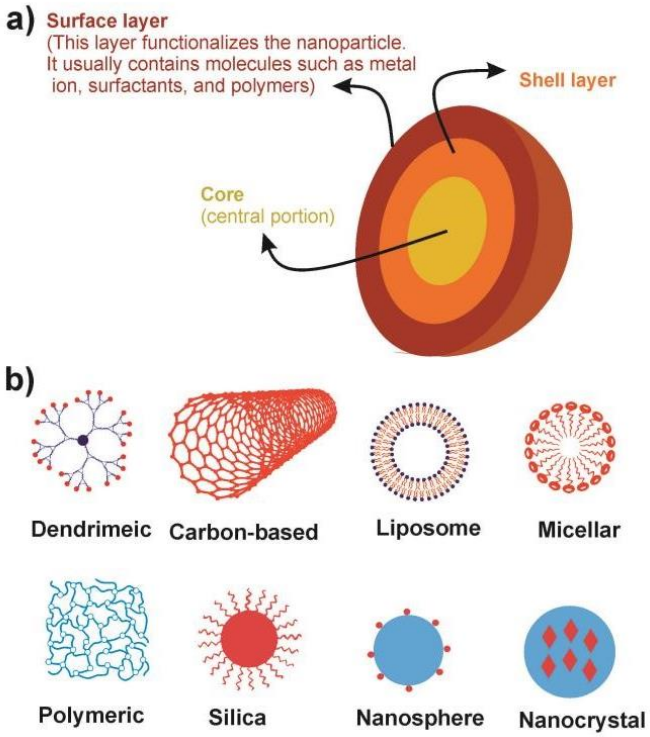


Figure 2. a) Layers of nanoparticles. b) Main classes of nanoparticles [5].

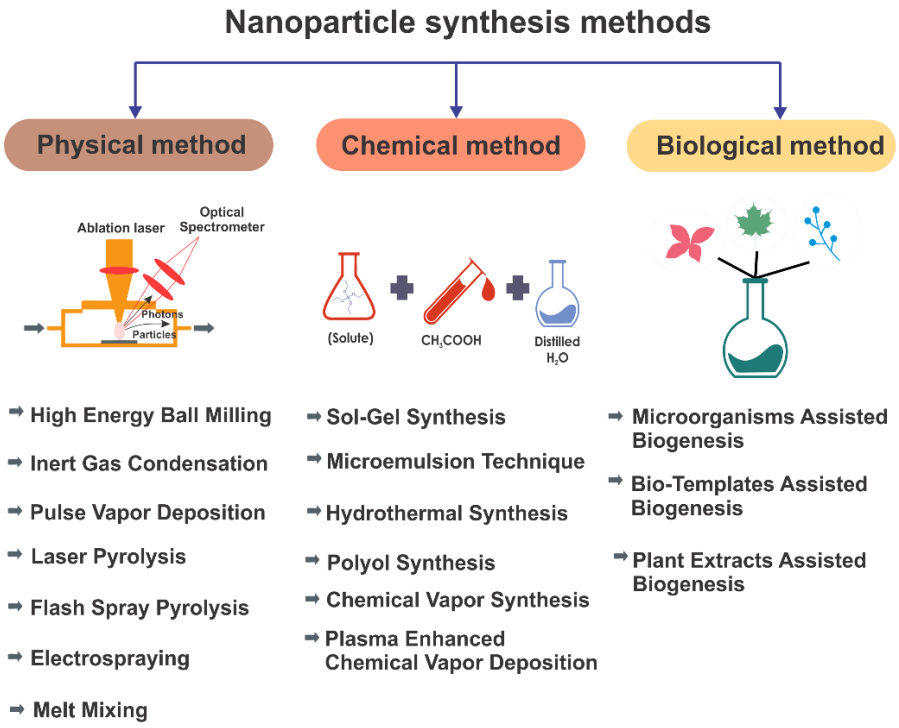


Figure 3. Methods for nanoparticle synthesis. Adapted from Ref. [6].

As shown in Figure 3, the nanoparticles were synthesized using various methods. Their remarkable electronic, optical, magnetic, mechanical, and thermal attributes render them immensely valuable [6]. Notably, the first three qualities have practical applications in sensor production [5]. Owing to their diminutive size, distinct optical traits, and limited surface area, these nanoparticles have garnered widespread use across diverse domains, including medicine, energy, and sensing. A case involving gold nanoparticles leveraged as contrast agents for X-ray and MRI imaging because of their light absorbing and scattering capabilities. Tailored to bind selectively to specific cell types, these nanoparticles enable targeted drug delivery and permit drug release monitoring via their optical attributes. They also enhance light absorption in solar cells, thus boosting the energy conversion efficiency.

In addition, nanoparticles, especially those containing Pt and Pd, serve as crucial catalysts [7] and augment the sensitivity of surface plasmon resonance. Owing to their small dimensions, nanoparticles offer a platform for nanoengineering surfaces and fabrication of application-

specific nanostructures [8]. The incorporation of nanoparticles into fluids has several advantages. Their addition elevates the thermal conductivity and specific heat capacity of the mixture, while the size of the nanoparticles increases the viscosity, which is beneficial in lubrication applications. Furthermore, nanoparticles enhance thermal stability by increasing the thermal resistance and thwarting thermal degradation [9-13]. Figure 4 elucidates the impact of nanoparticle dispersion on the thermal and physical properties of the base liquid, revealing influential properties [14, 15].

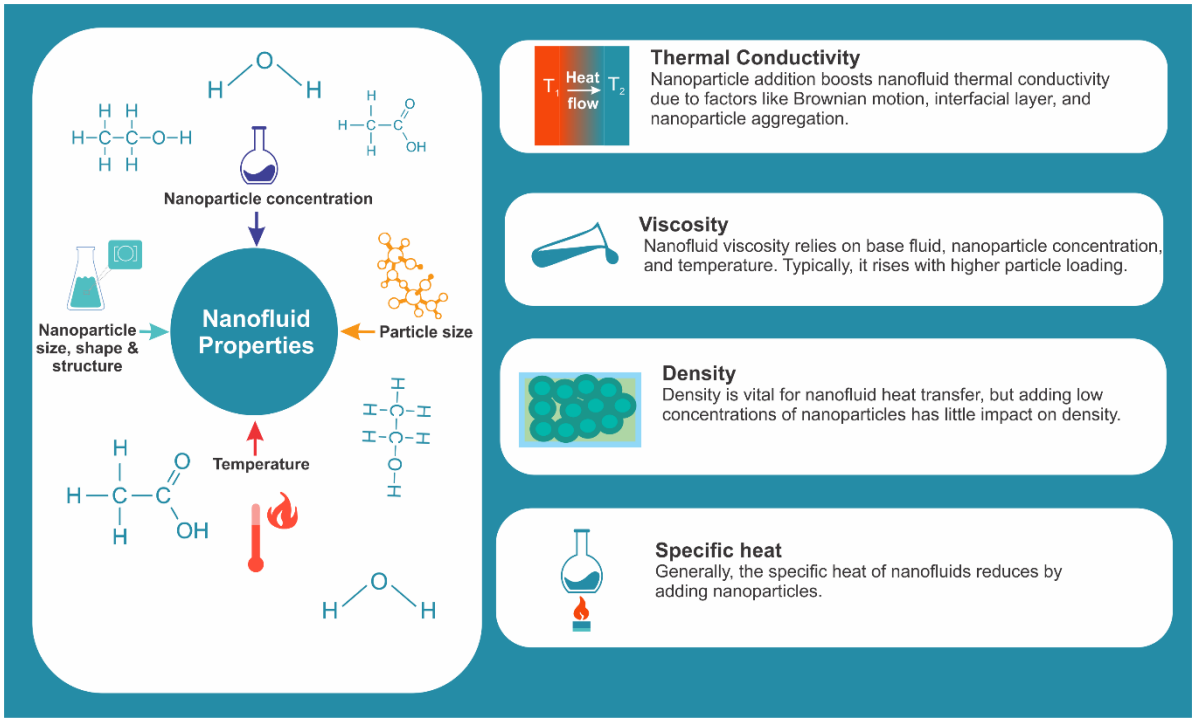


Figure 4. Effects of nanoparticle suspension on thermophysical properties of fluids [14, 15].

In recent years, the drive to harness renewable and low-grade waste energy has propelled energy storage technology into a major field of research. Among the research efforts underway, phase-change energy storage has gained significant attention and applications. PCMs have emerged as notable latent thermal energy storage media that maintain nearly constant temperatures during phase transitions and transfer thermal energy through latent heat. Leveraging the PCM's

latent heat characteristics, phase-change energy storage offers the potential to mitigate heat source temperature fluctuations and enhance the overall system temperature stability. As a result, it holds promise across diverse domains, such as battery thermal management, industrial waste heat recovery, solar thermal energy utilization, and building thermal control.

Nevertheless, PCMs often suffer from low thermal conductivity, impair or reduce heat transfer, and affect the system efficiency and thermal performance. To address this issue, the integration of nanoparticles into PCMs has emerged as an effective solution. Nanoparticles augment the latent heat capacity of PCMs, thus facilitating greater heat absorption or release during the phase transitions. In addition, nanoparticle inclusion curtails particle agglomeration, improving the thermal and chemical stability of the mixtures, and enhancing PCM resilience. Moreover, nanoparticle integration curbs the degradation of PCMs during repetitive thermal cycles, thus improving their durability [16, 17].

This article marks the first comprehensive review of the interplay between nanoparticles and phase transformations, such as freezing, melting, evaporation, boiling, and condensation. A synoptic overview of this study is shown in Figure 5. This work is a critical and methodical exploration that offers a systematic assessment of nanoparticle performance within the phase transformation process. This review examines in detail the multifaceted factors that impact nanoparticles during their involvement in enhancing the phase-change heat transfer and thermal energy storage. The aim is to refine the optimization of thermal conductivity enhancement facilitated by nanoparticles, leading to diminished energy storage requirements, heightened work efficiency, and realization of energy conservation goals. Moreover, this review addresses pivotal challenges and proposes future research directions within this realm, aiming to steer advancements that build on the potential of nanoparticles for efficient energy management.



Figure 5. Graphical illustration of the present work [18].

2. Phase change heat transfer at the nanoscale

Before examining nanoscale phase change heat transfer, a comprehensive understanding of the foundational theory and underlying physics of phase change is imperative. The Landau phase transition theory is the cornerstone for this understanding, providing fundamental insights into first- and second-order phase transitions [18]. This theory posits that equilibrium is attained under constant volume and temperature conditions when minimizing the Helmholtz free energy function or under constant pressure and temperature by minimizing the Gibbs free energy. Within this framework, non-zero-order parameters signify an ordered state, whereas order parameters with a zero value indicate a disordered state. Illustrative instances of order parameters include the magnetization of a ferromagnetic system, dielectric polarization within a ferroelectric system, and the superfluid density inherent in superconducting and superfluid states.

According to Landau, the Helmholtz free energy of a system can be expressed as a power series[19]

$$F(\xi, T) = -g_1\xi + \frac{1}{2}g_2\xi^2 + \frac{1}{4}g_4\xi^4 + \frac{1}{6}g_6\xi^6 + \cdots \quad (1)$$

where ξ denotes the order parameter and the multiplier parameters g_i are functions of temperature: $g_i = g_i(T)$. It is important to recognize that a first-order transition necessitates a discontinuous change in entropy, which gives rise to latent heat. Consequently, for such transitions, the free energy must exhibit discontinuity. In contrast, a second-order transition mandates that the order parameter (ξ) is zero at temperatures equal to or surpassing a specific critical temperature (T_c) while assuming a finite value below T_c.

Any phase transition initiates with the emergence of a novel phase, which becomes evident through changes in thermodynamic properties. First-order phase transitions occur when the first-order derivative of the thermodynamic potential characterizes the new phase. Conversely, second-order phase transitions occur when a new phase emerges with a second-order derivative of thermodynamic potential. This transition phenomenon, known as nucleation, is a hallmark of first-order phase changes [20]. Nucleation, a fundamental process in generating new phases, has been demonstrated in scenarios, such as the condensation of dispersed vapor molecules into a liquid state. This concept was introduced by Gibbs in 1878 through classical nucleation theory [21], according to which fluctuating nuclei develop under substantial driving forces. Exploring the foundational principles of the classical nucleation theory and its subsequent evolution provides a profound comprehension of nucleation within the realm of nanoscience.

In addition to the various theories outlining the phase transition phenomena, several equations have been introduced to articulate and characterize the process. The Clausius-Clapeyron relation [22] and the Laplace-Young equation [23, 24] are pivotal examples. The Clausius-Clapeyron relation establishes a foundation for assessing the properties within two-phase regions. Specifically, for liquid evaporation, the Clausius-Clapeyron relation is expressed as

$$\frac{dp}{dT} = \frac{s_g - s_f}{v_g - v_f} = \frac{s_{fg}}{v_{fg}} = \frac{h_{fg}}{T.v_{fg}} \quad (2)$$

where s_g and s_f are the specific entropy of the saturated vapor and saturated liquid, v_g and v_f are the specific volumes of the saturated vapor and saturated liquid, respectively; and s_{fg}, v_{fg}, and h_{fg} represent the change in specific entropy, specific volume, and specific enthalpy (latent heat) over the phase transition, respectively.

The Laplace-Young equation establishes a connection between the higher pressure and the force arising from the surface tension [24]:

$$p_c = \sigma \left[\frac{1}{R_1} + \frac{1}{R_2}\right] \quad (3)$$

where p_c is the pressure difference over the interface between two immiscible fluids, σ is the surface tension, and R_1 and R_2 are the principal radii of curvature.

In addition to theories concerning phase transitions, recent strides in experimental and numerical methodologies have yielded insights and outcomes for enhancing phase transitions through nanoparticle integration. The morphology of nanoparticles, influence of external forces induced by magnetic or electrical fields, and motion of nanoparticles prompted by temperature or velocity gradients stand out as pivotal factors driving heat transfer enhancement.

2.1. Effects of nanoparticle concentration and morphology

2.1.1. Nanoparticle type and concentration

Researchers have employed various techniques to identify the most suitable nanoparticle concentration and loading for phase change applications. These investigations have predominantly highlighted the augmentation of the phase-change processes and heat storage rates. Nanoparticles can potentially enhance the phase change phenomena at specific loading levels. Notably, the introduction of nanoparticles can lead to an increase in fluid viscosity,

thereby curbing convective motion within the fluid. This effect might counterbalance or diminish the heightened heat-transfer rates [25].

2.1.2. Nanoparticle aspect ratio

Nano-enhanced phase change materials (NePCMs) offer a deeper understanding of the heat transfer mechanisms during the melting and solidification processes. When considering the melting of PCMs encapsulated within elliptical cylinders, the melting process can be categorized into two distinct types: constrained and unconstrained. In the former, the melting section does not make direct contact with the adjacent layer, whereas in the latter, the solid phase moves noticeably between the solid and liquid phases owing to the density differences. The aspect ratio governs the melting and solidification phase change processes. Recent studies have explored how nanoparticle aspect ratios influence the enhancement of the phase transition. An elliptical capsule with various aspect ratios (5, 1, and 2) was studied in one such investigation utilizing Cu nanoparticles through numerical analysis. The study revealed that the melting rate was the fastest, with an aspect ratio of 2, whereas it was the slowest, with an aspect ratio of 1 [10].

In another study investigating the effects of aspect ratio on heat storage rate, Li et al. [26] employed a graphene nanoplatelet-based nanofluid (with concentrations of 0, 1, and 3% by weight) as the working fluid. They examined the flow patterns within differentially heated rectangular cavities. The experimental findings revealed that employing highly loaded NePCM (3% by weight) could introduce a swifter heat storage rate initially. However, at intermediate stages, the heat storage rate exhibited an inverse correlation with loading (3% by weight was the slowest). Moreover, the study highlighted the substantial impact of increasing the aspect ratios on heat storage rates.

2.2. Surface factors

2.2.1. Surface tension

Surface tension determines the surface wettability and bubble growth, establishing its significance in boiling and condensation phenomena [27]. This interplay is shown in Figure 6, elucidating how nanoparticle attributes, such as nature, size, and shape, in conjunction with other parameters, affect the surface tension of nano-dispersed fluids [27]. In boiling heat transfer, the liquid-vapor interface is the origin of bubbles, which grow or shrink depending on the mutual attraction between interface molecules and the surface tension of the liquid [28]. Indeed, a significant aspect of enhancing the boiling heat transfer revolves around reducing surface tension. This reduction facilitated bubble formation and release, ultimately leading to an enhancement of the overall heat transfer process.

The heat transfer correlation within the nucleate boiling regime introduced by Rohsenow in 1952 [28] indicates that the nucleate heat flux ($q'_{nucleate}$) can be increased by reducing the surface tension force as follows:

$$q'_{nucleate} = \mu_l h_{fg} \left[\frac{g(\rho_l - \rho_v)}{g_0 \sigma}\right]^{0.5} \left(\frac{c_{p,l}\Delta T_e}{C_{s,f} h_{fg} {Pr_l}^n}\right)^3 \quad (4)$$

where μ is the viscosity, g is the gravitational acceleration, g_0 is the force conversion factor, ρ is the density, σ is the surface tension force, c_p is the isobaric heat capacity, ΔT_e is the excess temperature, h_{fg} is the latent heat of vaporization, and P_r is the Prandtl number. The values of the coefficients $C_{s,f}$ and exponent n are contingent upon the characteristics of the solid-liquid interface, with the subscripts l and v designating the liquid and vapor phases, respectively.

The boiling heat transfer involves a pivotal dimensionless parameter known as the Bond number [29], which represents the relationship between gravity and surface tension forces:

$$Bo = \frac{(\rho - \rho')L^2 g}{\sigma} \quad (5)$$

where ρ' represents the density of the surrounding medium and L denotes the characteristic length. As the surface tension decreases, the Bond number increases, which increases the heat-transfer coefficient (HTC) [30].

Regarding external flow convection boiling, a phenomenon prevalent in heat exchangers, the convective heat flux hinges on a dimensionless parameter known as the Weber number:.

$$We = \frac{\rho v^2 L}{\sigma} \tag{6}$$

This parameter represents the ratio of inertial force to surface tension force [31].

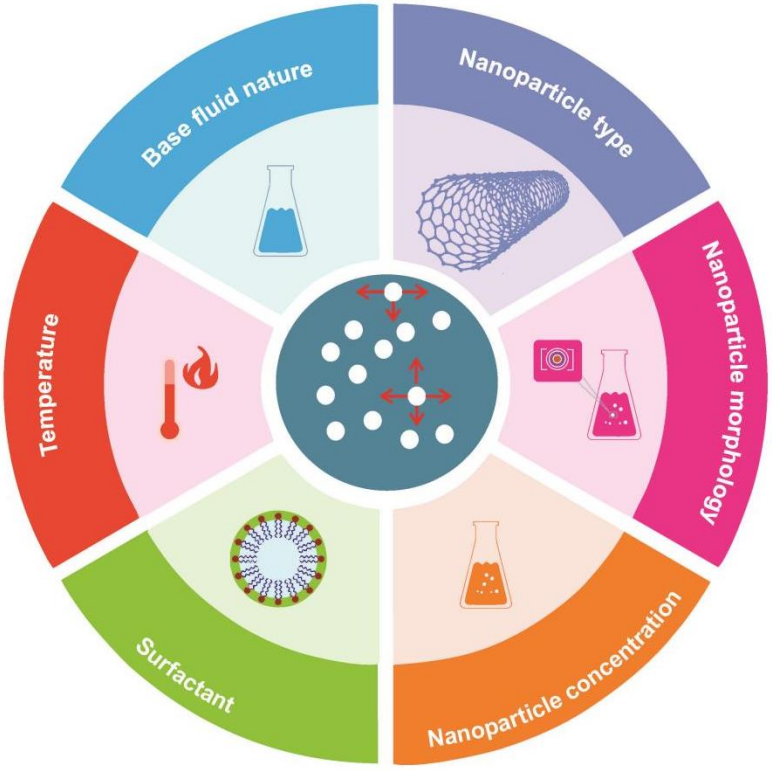


Figure 6. Factors affecting the surface tension of nanofluids. Adapted from Ref. [27].

2.2.2. Surface wettability

Bubbles in the boiling process and droplets in the condensation process are inherently influenced by surface wettability. This link is illustrated in Figure 7, where bubbles and droplets exhibit both static and dynamic wetting behaviors on both the plain and micro/nanostructured surfaces.

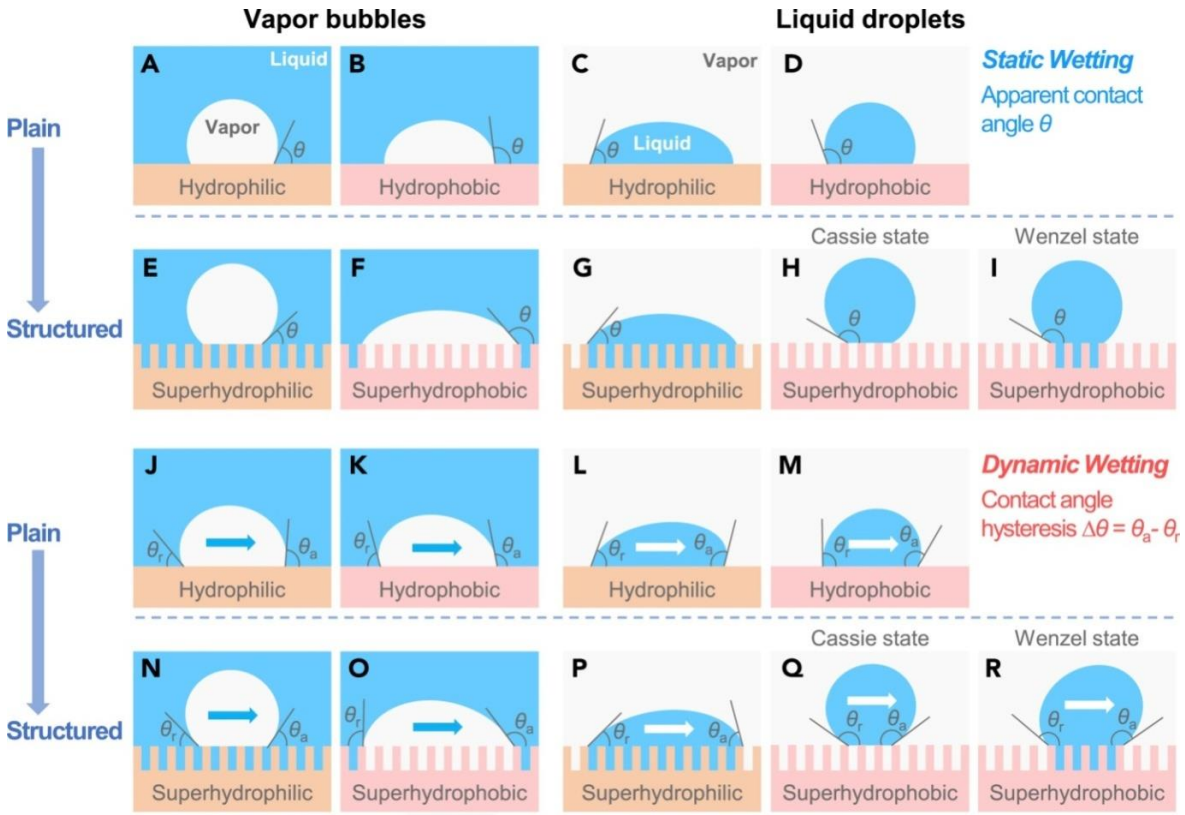


Figure 7. Representation of static and dynamic wetting states of bubbles and droplets on plain and structured surfaces. A, B, E, and F show the static wetting of vapor bubbles on the plain (A, B) and the structured surface (E, F). C, D, G, H, I show the static wetting of liquid droplets on the plain (C, D) and the structured surface (G, H, I). Likewise, J, K, N, O, and L, M, P, Q, and R show the dynamic wetting states of bubbles and droplets on plain and structured surfaces. Reproduced with permission from Joule. 2(11), 2307-2347 (2018). Copyright 2018 Elsevier Inc.[32]

Determining the wetting surfaces during boiling and condensation depends on the intrinsic contact angle. The contact angle denotes the angle formed between the liquid and solid interfaces within the liquid medium. Surfaces with high and low intrinsic contact angles are referred to as hydrophobic and hydrophilic, respectively [33]. A range of diverse surfaces in the vapor bubbles and liquid droplets relative to the contact angle is shown in Fig. 7. Evidence

suggests that the introduction of nanoparticles can ameliorate wetting on surfaces with poor characteristics [34, 35]. Incorporating nanoparticles into the base fluid in boiling heat-transfer scenarios can alter the contact angle and bubble volume.

Conversely, nanoparticles deposited on heating surfaces can diminish the thermal resistance of condensers or evaporators [34]. The wetting behavior of certain nano-dispersed fluids is contingent on the surfactants utilized [36, 37]. Researchers have further demonstrated that nanoparticle surfaces exhibiting intertwined wetting behaviors are advantageous for enhancing condensation heat transfer rates, especially when gravitational forces fail to facilitate droplet sweeping [38]. In addition, the influence of nanoparticle concentration on the wetting and evaporation behavior of sessile nanodroplets has been linked to the surface wettability [39].

2.3. Effect of external fields

The impact of external fields, such as magnetic or electric fields, on fluids has long been a subject of research because of their capacity to amplify heat-transfer mechanisms [40]. To elucidate the dynamics of electrically or magnetically conducting fluids, the Navier-Stokes equation requires augmentation in the form of an electromagnetic body force [41]. The electromagnetic force (F_{em}) is composed of three distinct components:

$$F_{em} = F_{es} + F_m + F_{mp} \tag{7}$$

where F_{es}, F_m, and F_{mp} are the electrostatic, magnetic, and magnetophoretic forces, respectively.

Frequently, electrostatic and magnetic forces are amalgamated into what is known as the Lorentz force (F_{Lor}), providing an alternative representation:

$$F_{em} = F_{Lor} + F_{mp} \tag{8}$$

where the Lorentz force per unit volume is a function of the charge density q (C/m^2) and the current density J (A/m^2).

$$F_{Lor} = qE + J \times B \tag{9}$$

The magnetophoretic force per unit volume is associated with a magnetic field gradient:

$$F_{mp} = \frac{\Delta\chi}{\mu_0}(B \cdot \nabla)B \tag{10}$$

where $\Delta\chi$ represents the magnetic susceptibility difference between the nanoparticles and the surrounding fluid. The vacuum permeability μ_0 has a value $\mu_o = 4\pi \times 10^{-7}$ (N/A^2).

When there is an electrolyte solution with ionic species, the Nernst-Planck equation expresses the Coulomb electrostatic force (the first term of the Lorentz force) acting on it:

$$F_{Coul} = C_F \nabla\Phi \sum_{i=1}^{n} Z_i C_i \tag{11}$$

where C_F is the Faraday constant, Φ is the electric potential, and Z_i and C_i are the valence and concentration of i^{th} ionic species in the electrolyte solution, respectively. The Coulomb electrostatic and magnetophoretic forces are zero under a uniform electric potential and magnetic fields.

Based on these criteria, the Navier-Stoke equations can be expressed as:

$$\nabla . v = 0 \tag{12}$$

$$\frac{\partial v}{\partial t} + (v.\nabla v) = -\frac{1}{\rho}\nabla p + v\nabla^2 v + F_{em}$$

$$\rho c\left[\frac{\partial T}{\partial t} + (v.\nabla)T\right]_p = k\nabla^2 T + \frac{1}{\sigma_{el}} J.J + \Phi$$

where v is the flow velocity, σ_{el} indicates the electrical conductivity of the solution, $\frac{1}{\sigma_{el}} J.J$ represents the Joule heating term, and Φ is the viscous dissipation.

In phase-change applications, important dimensionless numbers, such as the magnetic Reynolds ($Re = \frac{vl}{\lambda}$) and Hartmann ($Ha = Bl\sqrt{\frac{\sigma_{el}}{\mu}}$) numbers, are used to describe the magnetohydrodynamic effect on thermal fluids. Studies have reported that the heat transfer rates can be increased or decreased when the Hartmann number is decreased or increased, respectively.

Applying an electric field to a nano-dispersed fluid increases the heat-transfer rate by enhancing the thermal conductivity of the fluid. The electric field exerts forces on the nano-dispersed fluid, encompassing electrophoretic, dielectrophoretic, and electrostriction forces, collectively contributing to the heat transfer improvement [40]. In the presence of a magnetic field, the heat transfer rate of a nano-dispersed fluid is enhanced up to a certain magnetic field strength, beyond which it diminishes with further increase in the magnetic field intensity. During the solidification of ferrofluids, it has been observed that the impact of a magnetic field on the solidification process is negligible for both non-electrically conductive and electrically conductive ferrofluids [42]. Applying a magnetic field to nanoparticle-enhanced boiling heat transfer leads to an augmented HTC up to a specific magnetic field intensity, followed by a decrease with further intensity increments [43].

2.4. Motion of nanoparticles due to field gradient

Brownian motion describes the random movement of particles in a fluid. This motion occurs as particles collide with the surrounding molecules and undergo erratic trajectories owing to these molecular impacts. The phenomenon, named after Robert Brown, who initially described it, is a consequence of the molecular agitation that suspended particles experience in a fluid medium. This molecular agitation leads to the movement of particles, essentially constituting a form of diffusion. In the context of spherical particles undergoing Brownian motion, Stokes' law can be used to compute their hydrodynamic diameter (d_h)[44]:

$$d_h = \frac{K_B T}{3\pi\mu D_T} \tag{13}$$

where K_B is Boltzmann's constant, T is the absolute temperature (K), μ is the viscosity of the fluid, and D_T is the translational dispersion coefficient. Brownian motion depends on particle size, with a larger dispersion coefficient corresponding to smaller particles [45]. Brownian motion greatly influences nanoparticles owing to their small size and inertia.

Thermophoresis was originally discovered in the 19th century by Professor Tait [46]. Thermophoresis is the manifestation of Brownian motion under the influence of a temperature gradient, and drives the particles to the side of the lower temperature. The average thermophoretic velocity of the nanoparticles can be predicted by the random thermophoretic force due to molecular collisions [47]. Because of their small size, submicron particles are particularly prone to being influenced by thermophoresis [48]. A schematic representation of Brownian motion and thermophoresis effects is shown in Figure 8.

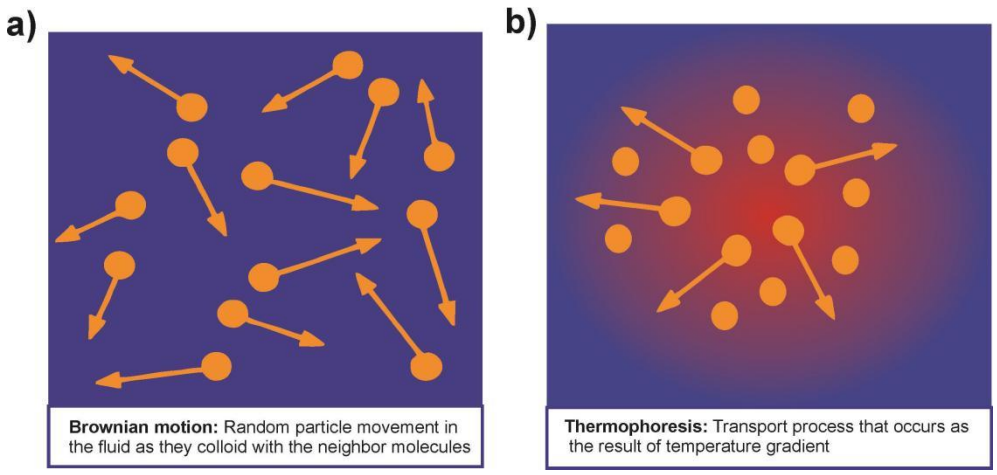


Figure 8. a) Brownian motion. b) Thermophoresis [48].

Examinations centered on the boundary layer evolution within Maxwell fluids have highlighted the interplay between Brownian motion and thermophoresis [49]. These influences resonate with the velocity, concentration, and temperature fields of particles. In particular, increased Brownian motion and thermophoretic velocity tend to modify the concentration field of particles, leading to hindered diffusion in narrow flow domains [50]. In a distinct inquiry, exploring nanofluid flow over stretching plates influenced by a magnetic field illuminates the intricate relationship among concentration profiles, Brownian motion, and thermophoretic parameters [49]. This investigation revealed a positive correlation between Brownian motion

parameters and concentration, juxtaposed with an inverse relationship between thermophoretic parameters and concentration.

Further research explored the utilization of a two-dimensional non-Newtonian Sisko nanofluid flow pattern over a stretching sheet, revealing heightened thermophoresis, Brownian motion, and temperature ascent [51]. This phenomenon occurs because the nanofluid generates more heat, which is attributed to the kinetic energy acquired from the initial temperature. As the initial temperature increased the kinetic energy of the nanofluid, the particles within the nanofluid exhibited heightened activity over time, resulting in an increase in temperature. In addition, a numerical analysis of the Williamson nanofluid subjected to the influence of Brownian motion and thermophoresis underscores a substantial surge in temperature when both thermophoretic and Brownian motion parameters assume larger values, as the higher thermal conductivity of the fluid contributes to this phenomenon [52].

2.5. Extended surface heat transfer

Following Newton's law of cooling, the heat transfer occurring between a surface and its surrounding environment, characterized by the surface temperature T_s and the surrounding temperature T_∞, can be mathematically represented as follows (Eq. 14) [28] :

$$Q_{conv} = hA_s\,(T_s - T_\infty) \tag{14}$$

Thus, the rate of convective heating can be increased by increasing either the surface area (A_s) or convective HTC (h). In practical scenarios, increasing the value of h necessitates supplementary installations such as pumps or fans. Alternatively, the surface area can be increased by employing extended surfaces commonly known as fins.

The use of fins can potentially increase the melting and solidification rates in latent heat storage systems [28]. In this case, several parameters are considered, including the fin conductivity, fin length, number of fins, fin arrangement, and temperature of the hot wall. Research has

demonstrated that including short fins can expedite phase-change processes, such as melting, especially when longer fins are absent [53]. Moreover, research results have indicated that combining fins with nanoparticles can substantially enhance the phase change process [54, 55]. In addition to these factors, the effects of nanoparticle migration, surface roughness, deposition, agglomeration, and other environmental elements also exert their influence. A comprehensive examination of these elements and their impacts on phase transition phenomena is discussed in subsequent sections.

3. Freezing (solidification)

The onset of the solidification process commences when the liquid attains its freezing point temperature and continues to release heat to its surroundings. This process requires the release of a substantial amount of latent heat, which, if not dissipated promptly, has the potential to impede the entire solidification trajectory. Throughout solidification, the heat transfer mechanism manifests in distinct modalities contingent on the prevailing state of the substance. Heat is conveyed via both conduction and convection within the liquid at the interface separating the liquid and solid phases, whereas conduction remains the sole mode of heat transfer within the solid phase. This progression prevails as long as the ambient temperature remains below the freezing point of the substance, causing the layer of frozen material to incrementally increase in thickness [56].

Phase-change energy storage has emerged as a promising technology for mitigating the disparity between energy supply and demand. The performance of energy storage systems is intricately linked to the attributes of PCMs [57]. However, the occurrence of subcooling during solidification is a prevalent issue in numerous PCMs, leading to diminished heat-transfer rates. Subcooling entails the liquid temperature dropping below the freezing point without initiating condensation, thereby endangering the desired energy storage. The resultant low thermal

conductivity results in a decrease in the cooling storage capacity over time, coupled with a reduced energy storage efficiency. Various methodologies have been explored to expedite the heat transfer from PCMs to solids [9], as shown in Figure 9. A particularly effective strategy involves the integration of nanoparticles into the PCMs. This addition substantially bolsters the thermal conductivity of the PCM and concurrently serves as a substrate for nucleation, thereby fostering heterogeneous nucleation. This endeavor can potentially curtail the requisite solidification subcooling, thereby enhancing the efficacy of latent heat storage systems. Figure 10 shows the diverse geometrical arrangements of NePCMs during the solidification process. The following sections examine the multiple effects of distinct variables on the solidification rate, including nanoparticle type and concentration, surfactant incorporation, temperature, pressure, agglomeration, wettability, surface tension, electric or magnetic fields, Brownian motion, micro-convection, and micro-nano bubbles.

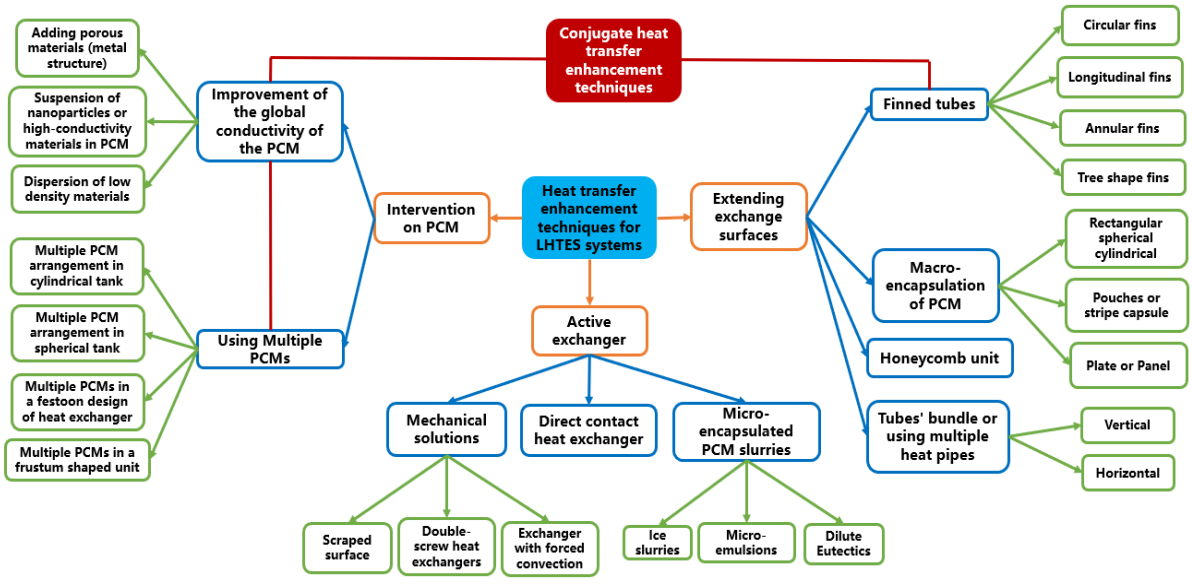


Figure 9. Techniques for improving heat transfer to enhance the efficiency of latent heat storage systems. Adapted from Ref. [58].

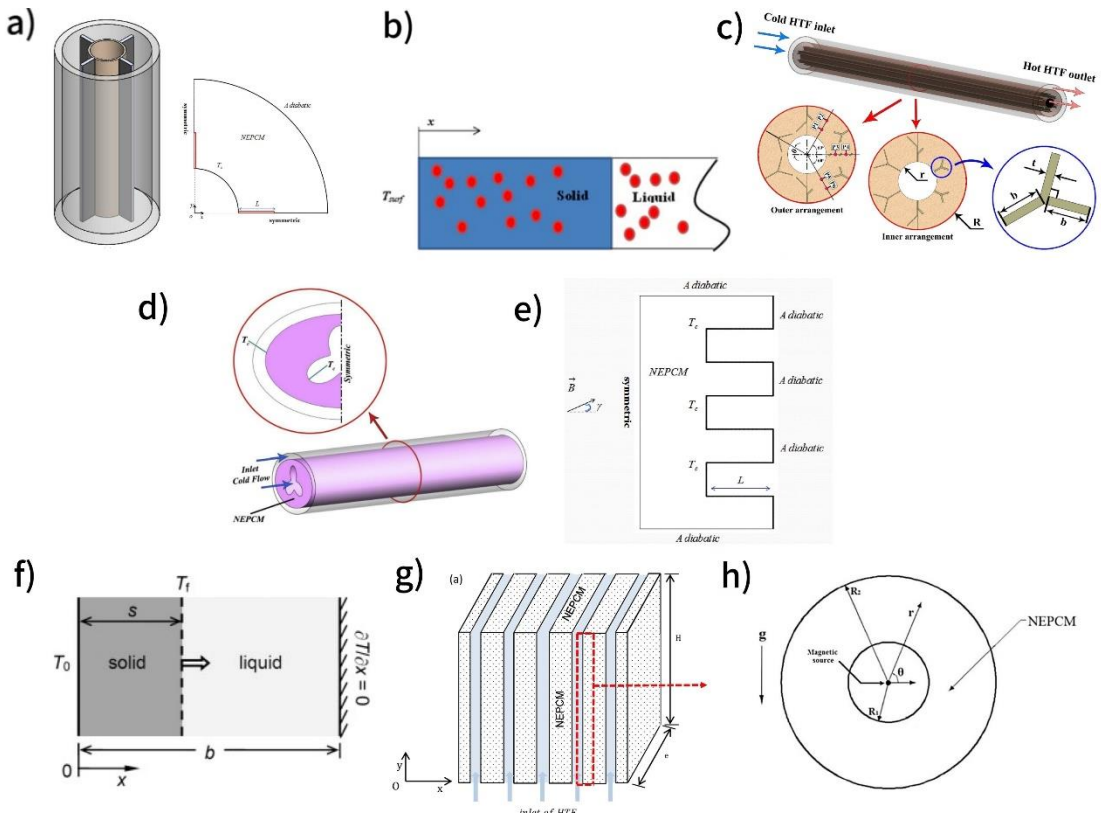


Figure 10. Different geometries considered for NePCM solidification: a) enclosure with metallic fin. Reproduced with permission from J. Mol. Liq. 259, 424-438 (2018). Copyright 2018 Elsevier B.V.[59] b) unidirectional freezing. Reproduced with permission from Int. J. Heat Mass Transfer. 67, 202-213 (2013). Copyright 2013 Elsevier Ltd.[60] c) Y-shaped fins triplex tube. Reproduced with permission from J. Energy Storage. 46, 103878 (2022). Copyright 2021 Elsevier Ltd.[61] d) triplex-tube. Reproduced with permission from J. Mol. Liq. 296, 111731 (2019). Copyright 2019 Elsevier B.V.[62] e) heat storage system. Reproduced with permission from Int. Commun. Heat Mass Transfer. 117, 104715 (2020). Copyright 2020 Elsevier Ltd.[63] f) unidirectional freezing in a finite slab. Reproduced with permission from Int. J. Therm. Sci. 62, 120-126 (2012). Copyright 2011 Elsevier Masson SAS.[64] g) rectangular latent heat storage unit. Reproduced with permission from Energy Build. 153, 1-17 (2017). Copyright 2017 Elsevier B.V.[65] h) annulus enclosure. Reproduced with permission from Energy Convers. Manage. 171, 879-889 (2018). Copyright 2018 Elsevier Ltd.[42].

3.1. Effects of nanoparticle concentration and morphology

Nanoparticles exhibit crystalline structures and small contact angles, which facilitate heterogeneous liquid nucleation, thereby mitigating subcooling. Increasing the nanoparticle concentration and size further augments the nucleation effect and enhances the solidification rates [59]. In addition, increasing the fin length and radiation parameters reduced the solidification rate. A study conducted by El Hasadi and Khodadadi [66], employing copper nanoparticles at a concentration of 10% by weight, revealed significant alterations in the freezing rates, depending on the nanoparticle size and shape. For nanoparticle diameters of 5 and 2 nm, accelerated freezing was observed due to heightened thermal conductivity inducing supercooling, leading to a commensurate increase (or decrease) in colloidal layer thickness with larger (or smaller) nanoparticle sizes.

In another investigation, El Hasadi and Khodadadi numerically explored copper nanoparticles with diameters of 7, 5, and 2 nm in a cyclohexane solvent. This study showed that nanoparticles were repelled from the solidification front, resulting in a heightened nanoparticle concentration near the solid-liquid interface. This augmented liquid nanoparticle concentration near the solid interface decelerates the rate of solid-liquid interface formation compared to pure cyclohexane [60]. Notably, the influence of the particle size was more pronounced. The study by Wang et al. [62], employing numerical simulations, examine solidification in copper oxide/water nanofluids with a nanomaterial concentration close to 0.04%. This investigation reported a reduced solidification time when nanomaterials were combined with pure water and attributed the reduction to an amplified shape factor.

The increase in the surface-to-volume ratio of nanomaterial surface atoms significantly influences the freezing temperature, as observed by Zhu and Li [67] using a numerical model involving metallic and semi-metallic nanoparticles. Moreover, Fan et al. [68] documented the fastest solidification rate in NePCM, ascribed to the integration of high-thermal-conductivity

nanoparticles, thereby enhancing the overall thermal conductivity of the PCMs. The maximum particle loading for 1% expedited solidification was 34%. Their study was underpinned by a developed unidirectional solidification model employing a highly conductive nanofluid composed of graphene nanoplatelets and dodecanol ($C_{12}H_{260}$) in their numerical analysis.

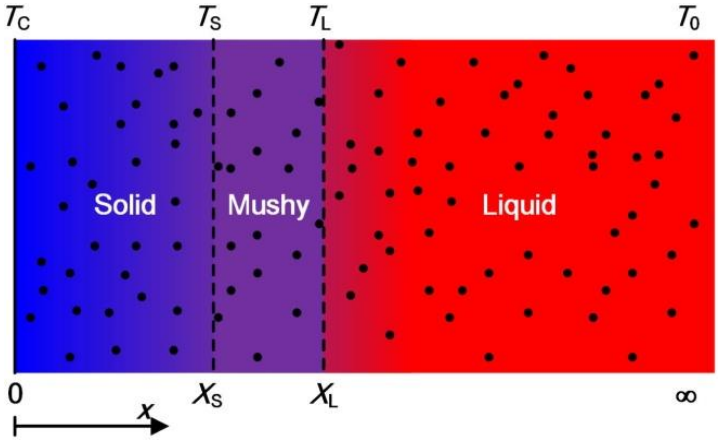


Figure 11. Unidirectional solidification model. Reproduced with permission from Int. J. Heat Mass Transfer. 86, 478-481 (2015). Copyright 2015 Elsevier Ltd.[68].

Khodadadi and Hosseinizadeh [69] conducted a numerical investigation involving a copper nanoparticle-water mixture with concentrations ranging from 0% to 0.2%. Their findings revealed that NePCM displayed superior thermal conductivity to the base material during solidification. This enhancement was particularly high when the nanofluid underwent phase change. In a separate experimental study focused on organic PCMs laden with nanoparticles, Mishra et al. [70] observed an interesting phenomenon in which nanomaterials tended to aggregate within grain boundaries. This arrangement led to the formation of an almost two-dimensional network characterized by high thermal conductivity pathways during the freezing process of the NePCMs.

3.2. Environmental factors

3.2.1. Surfactants

Mo et al. [71] investigated the role of surfactants in altering the freezing rates of nanofluids. Their study involved the preparation of nanofluids using carbon nanotube (CNT) particles with diameters ranging from 10 to 30 nm and a concentration of 0.1% by weight. By incorporating surfactants at concentrations of 0.05, 0.10, and 0.16% by weight, they effectively reduced the surface tension of the liquid. Interestingly, researchers found that CNT nanofluids demonstrated similar supercooling and freezing characteristics to deionized water when the diameter of the CNT particles was considerable. They also observed a direct correlation between the amount of surfactant and the degree of subcooling and phase transition time of the nanofluid.

In a separate investigation, Wang et al. [72] examined the impact of surfactants on expanded graphite nanofluids. Through their experiments, they utilized expanded graphite samples with a mass fractions of 93% octanoic acid and myristic acid. introduction these surfactants led to a substantial improvement in thermal conductivity, registering an impressive increase of >230%. Building on these findings, You et al. [73] conducted another study, revealing insights into the role of dispersants in modulating the supercooling of alumina-based nanofluids. Specifically, their research highlighted the fact that the effect of dispersants on nanofluid supercooling was more pronounced compared to the impact of nanoparticles alone, particularly for a nanofluid containing 3.6% alumina nanoparticles.

3.2.2. Temperature and pressure

Fan and Khodadadi [64] conducted an experimental study using cyclohexane-based suspensions infused with copper oxide nanoparticles to understand the influence of nanoparticles on the phase-change dynamics. Their observations revealed substantial fluctuations in the temperature and pressure during the phase change process. The experimental data showed a nonlinear relationship between the particle concentration and solidification rate during unidirectional freezing. This complexity was attributed to the non-monotonic increase

in thermal conductivity with concentration throughout the solidification process. In addition to experimental investigations, the authors developed numerical tools to comprehensively analyze the interplay of temperature and pressure on solidification kinetics.

Elbahjaoui and El Qarnia [65] numerically assessed the impact of initial temperature on the solidification of a NePCM within a heat exchanger. They found that decreasing the initial temperature of the heat exchanger resulted in a significant enhancement of sensible and latent heat release, thereby significantly accelerating the solidification rate. Meanwhile, in a distinct numerical exploration, Sharma et al. [74] utilized computational fluid dynamics to simulate the solidification of Cu-water nanofluids in a horizontal trapezoidal cavity under diverse boundary conditions. Their study discovered a correlation between the heat flux and aspect ratio of the trapezoidal cavity. Throughout the solidification process, the nanofluid exhibited an increase in thermal resistance, causing a reduction in the heat flux. Importantly, the simulation results emphasize that the initial temperature of the nanofluid did not exert a discernible influence on the overall duration of the solidification process.

3.3. Effect of external fields and microphysical influence mechanisms

3.3.1. Magnetic/electric field

Manipulation of ferromagnetic nanoparticles through electric and magnetic fields has emerged as a promising avenue to influence the motion dynamics of these particles, particularly at the solid-liquid interface. This effect has garnered significant attention, prompting analyses and experimental investigations to elucidate its impact on the solidification process of PCMs. Jia et al. [75] investigated this subject by scrutinizing the influence of electromagnetic fields on graphene/water nanofluids. They discovered a fascinating phenomenon by employing magnetic fields with an intensity of 1.2 T and a range of current intensities (0.02 to 0.15 A). The electromagnetic field induces graphene to adsorb a substantial amount of surfactant (carboxymethyl cellulose), thereby

triggering heterogeneous nucleation. This interaction between electromagnetic fields and nanoparticles offers a novel avenue for manipulating nucleation processes.

In a distinct experimental study conducted by Zhang et al. [76], the impact of magnetic fields on ferrofluid droplets was examined. By actively controlling the direction and magnitude of the magnetic field, researchers can modify the shape of magnetic nanodroplets, resulting in an alteration in the time required for fluid solidification. This capability to modulate the solidification process by adjusting the magnetic field direction and strength could underscore the potential of external fields in shaping the phase-change behavior. Figure 12 shows the forces acting on a ferrofluid droplet during magnetic lift and squeezing, offering insight into the intricate interplay between magnetic forces and solidification dynamics.

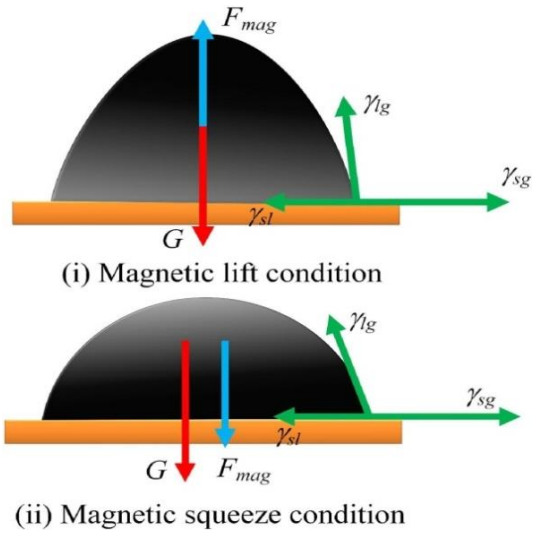


Figure 12. Forces acting on a ferrofluid droplet under: (i) magnetic lift, and (ii) magnetic squeeze. Reproduced with permission from Appl. Therm. Eng. 176, 115444 (2020). Copyright 2020 Elsevier Ltd.[76].

A comprehensive exploration of the impact of magnetic and electric fields on diluted copper oxide nanofluids was conducted by Shah et al. [63], which involved statistical analysis to reveal intriguing relationships. Their findings indicated an inverse relationship between

the strength of the magnetic field and entropy production, while the buoyancy force exhibited a direct proportionality relationship. This statistical investigation could illuminate the intricate interplay between the external fields and thermodynamic factors, providing insights into how these factors orchestrate solidification.

In a similar vein, Sheikholeslami and colleagues embarked on a similar numerical analysis [77], setting the internal surface temperature to 240 K. This study introduced the concept of Lorentz force to PCMs, showing how its incorporation augments the discharge rate and enhances heat transfer. This augmentation was attributed to the interplay between the nanoparticles, buoyancy effects, and Lorentz force. The interaction between the Lorentz force and buoyancy was identified as a significant contributor to expediting solidification in various PCMs, facilitated by a non-uniform transverse magnetic field. Conductive magnetic fluids were observed to engage with both ferrohydrodynamics and magnetohydrodynamics during solidification, in contrast to non-conductive magnetic fluids, which only interact with ferrohydrodynamics. This distinction could effectively reduce the solidification time, a finding substantiated by numerical analysis of magnetic oxide (Fe_3O_4)/seawater under the influence of electromagnetic fields [42]. Recent research by Shi et al. [78] revealed that applying a magnetic field with an intensity of 50 mT yielded remarkable results, significantly boosting the solidification rate while curtailing the time required for energy release. This finding could underscore the potential of magnetic fields to efficiently shape and optimize phase-change processes.

3.3.2. Motion of nanoparticles due to field gradient

Incorporating nanoparticles with high thermal conductivity into PCMs offers a substantial avenue for enhancing heat transfer efficiency. This enhancement is further amplified by Brownian motion, which not only boosts the phase transition rate but also enhances the convective heat transfer properties. Jamalabadi and Park [79] explored this phenomenon

through numerical analysis involving a diluted Cu nanofluid, aiming to elucidate the impact of Brownian motion on fluid behavior. The findings show a clear pattern: Brownian motion significantly accelerates the phase change rates.

3.3.3. Rejection of nanoparticles from a liquid-solid solidification front

Nanoparticle-infused PCMs encounter a propensity for aggregation during solidification, driven by the repulsion of nanoparticles at the solid-liquid interface. This phenomenon leads to an uneven distribution of the particles within the solid phase. An in-depth exploration of this nanoparticle repulsion effect at the solid-liquid interface was undertaken by El-Hasadi and Khodadadi [60]. Their investigations discovered some interesting insights: an escalation in the particle volume fraction is correlated with a deceleration in the formation of solid-liquid interfaces. Moreover, particle size has a more pronounced influence on the interface growth rate. In another computational study, the same researchers examined the effect of distinct copper nanoparticle sizes on the solid-liquid solidification interface [66]. They found that, as the particle size decreased, the interface shifted from a planar to an unstable dendritic structure. This transition is attributed to Brownian diffusion and solution convection, allowing smaller nanoparticles to be discharged more easily.

Saint-Michel et al. [80] conducted solidification experiments employing suspensions within a Hele-Shaw cell, employing a setup designed to study the impact of multi-particle interactions on particle repulsion at the solid-liquid interface. The experiments highlight the formation of a concentrated particle layer at the solidification front, shedding light on its pivotal role in the trapping mechanism. These findings collectively provide a foundational understanding of the intricate process of particle repulsion at the solid-liquid interface during solidification.

3.3.4. Agglomeration

Li et al. [81] conducted tests to investigate the agglomeration effects of various nanofluids, including graphene-water, silicon dioxide-water, and titanium dioxide-water. This study highlighted the fact that graphene tends to agglomerate because of its hydrophobic nature, especially in the absence of surfactants. The graphene-water system exhibited superior freezing characteristics compared to the other nanofluids studied. In a separate study, Nespoulous et al. [82] examined the effect of agglomeration on amorphous silica. Their experiment involved the cyclic freezing and thawing of the fluid. Over the cycles, the silica nanoparticles aggregated into microbeads, revealing a close link between morphological changes and particle concentration. In a study involving temperature gradients, Michaelides [83] demonstrated that a higher concentration of particles in colder parts of the flow domain, such as freezing surfaces, increases their local concentration. This enhancement in the local concentration can lead to nanoparticle agglomeration and may even cause a transition to non-Newtonian behavior.

Jia et al. [81] experimentally explored the role of surfactants in preventing collisional aggregation of particles. Their experiments involved titanium dioxide nanofluids with sodium dodecyl sulfate. They observed that surfactant adsorption on nanoparticle surfaces or agglomerates effectively hindered particle aggregation, thereby enhancing the nucleation mechanism. In a study focused on solidification behavior, Singh et al. [84] investigated energy storage systems equipped with graphene nanoflake fins at medium temperatures. Numerical simulations were performed to investigate the influence of natural convection on the solidification rate. Notably, natural convection played a significant role in the initial stages, whereas the later stages were primarily dictated by heat conduction owing to the absence of the molten PCMs. Adopting finned systems led to a remarkable 49% reduction in solidification time, highlighting how natural convection currents and flow cells contributed to accelerating the solidification rate.

3.3.5. Micro-nano bubbles

In a study conducted by Zhu et al. [85], the impact of micro-nano bubbles on the nucleation and crystal growth of sucrose and maltodextrin solutions was explored during an ultrasound-assisted freezing process. The phenomenon of cavitation bubbles creates high-pressure conditions and microturbulence upon their rupture, facilitating both primary heterogeneous nucleation and secondary nucleation. Notably, the presence of micro-nano bubbles were found to play a pivotal role in enhancing the nucleation rate and crystal growth. This effect, in turn, reduces the phase transition time, thereby contributing to an overall improvement in solidification efficiency. The intricate interplay of various factors influencing the nano-enhanced solidification process is summarized in Figure 13.

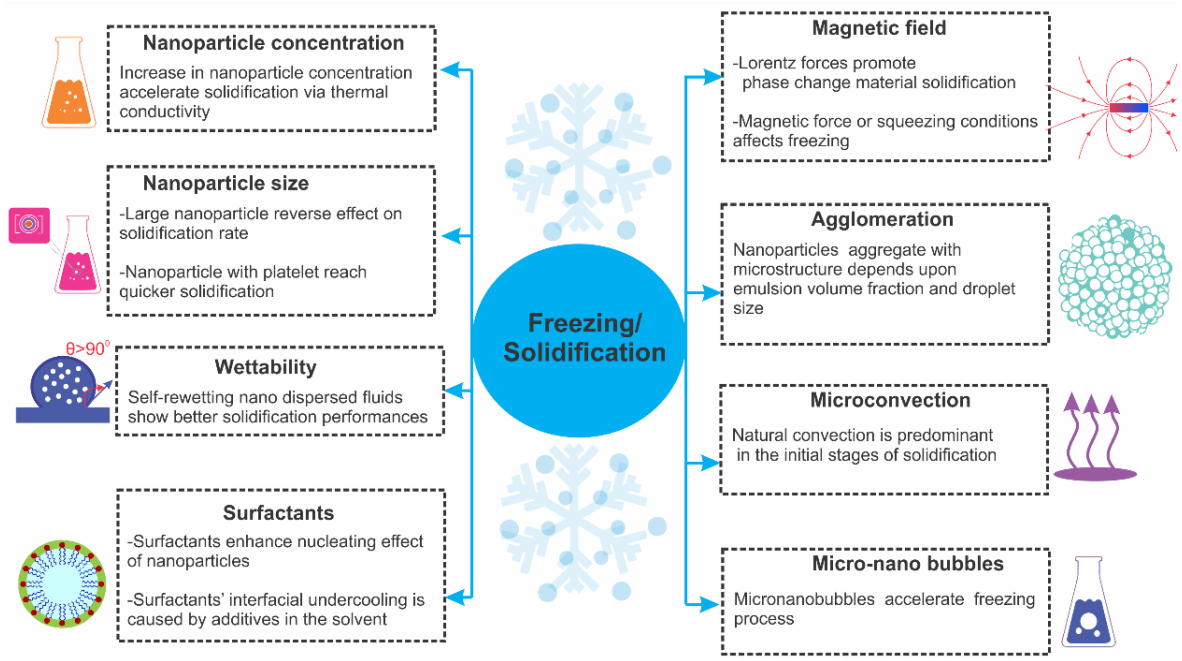


Figure 13. Effects of different factors on nano-enhanced solidification process [85].

4. Melting

Melting, or fusion, is a transformative process through which a solid material such as metal or paraffin transitions into a liquid or colloidal state. Metamorphosis involves the absorption of

thermal energy. Crystalline solids are characterized by a specific temperature at which they melt, known as the melting point, whereas non-crystalline materials lack a fixed melting point. The melting point corresponds to the temperature at which the endothermic process of the crystal transformation is initiated. The crystal progressively transformed into a liquid as the temperature surpassed the melting point. This phase transition, referred to as the melting point of the crystal, marked the onset of melting. Following the complete liquefaction, the temperature continued to increase. Conversely, solidification is the reverse process of crystal melting and is characterized by the coexistence of solid and liquid phases within the crystal. The temperature remained constant during solidification until the crystal fully transitioned to the liquid state. Diverse geometrical configurations utilized by researchers to investigate the melting behavior of NePCMs are illustrated in Figure 14.

PCMs have a remarkable ability to cyclically absorb and release substantial amounts of heat, making them efficacious for storing thermal energy. During utilization, PCMs exhibit stability, robust resistance to interference, and strong reversibility. These attributes have led to the widespread adoption of nanoparticles across various industrial applications, including thermal energy storage at both high and low temperatures. This potential promotes solar heating and supports the decarbonization of the energy sector [86]. Thermal energy storage is frequently employed in industrial waste heat recovery owing to its reliable low-temperature heat retrieval capabilities, which minimize heat losses and enhance thermal energy round-trip efficiency [10]. Although latent heat storage is a superior option to other thermal energy storage methods, it has limitations, such as restricted thermal conductivity and problems in the melting processes. These drawbacks contribute to increased industrial costs. Consequently, the focus shifts to exploring the influences of various factors, such as nanoparticle concentration and type, presence of surfactants or magnetic fields, and other operational parameters, on the melting rate of NePCMs under diverse operating conditions.

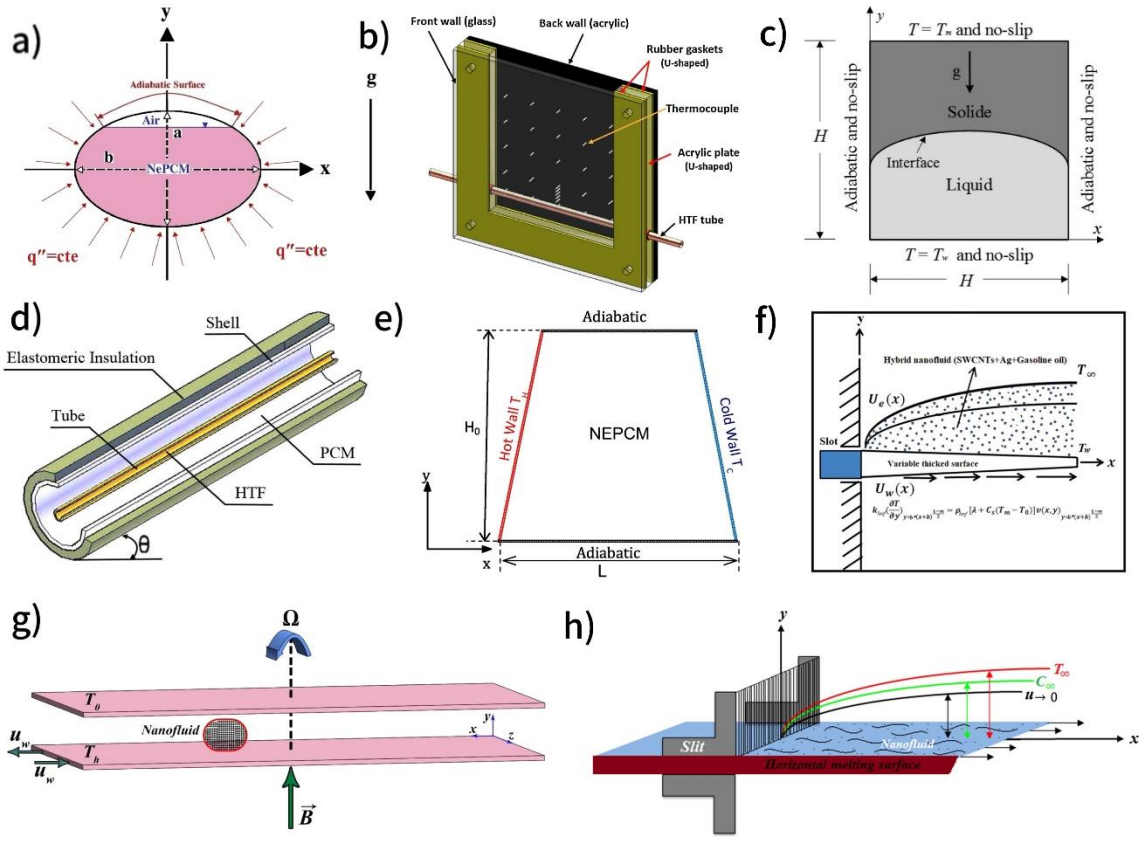


Figure 14. Different geometries considered for NePCM melting: a) elliptical capsule. Reproduced with permission from Int. J. Mech. Sci. 149, 164-177 (2018). Copyright 2018 Elsevier Ltd.[10] b) rectangular enclosure. Reproduced with permission from J. Energy Storage. 18, 485-497 (2018). Copyright 2018 Elsevier Ltd.[87] c) bottom-heated rectangular cavity. Reproduced with permission from Int. J. Heat Mass Transfer. 81, 415-425 (2015). Copyright 2014 Elsevier Ltd.[88] d) inclined shell-and-tube heat exchanger. Reproduced with permission from Appl. Therm. Eng. 112, 1497-1509 (2017). Copyright 2016 Elsevier Ltd.[89] e) trapezoidal cavity. Reproduced with permission from J. Mol. Liq. 292, 110592 (2019). Copyright 2019 Elsevier B.V.[90] f) variable thicked surface. Reproduced with permission from Int. Commun. Heat Mass Transfer. 121, 104805 (2021). Copyright 2020 Elsevier Ltd.[91] g) Stretching sheet. Reproduced with permission from Physica A. 541, 123036 (2020). Copyright 2019 Elsevier B.V.[92] h) Sisko fluid over a moving surface. Reproduced with

permission from Int. J. Heat Mass Transfer. 126, 1034-1042 (2018). Copyright 2018 Elsevier Ltd.[51].

4.1. Effects of nanoparticle concentration and morphology

Several studies have documented the impact of nanoparticles on the melting rates of NePCMs. Existing studies suggest that nanoparticles have a negligible influence on the early stages of the melting process, where heat conduction predominantly governs the heat transport mechanisms. However, as time progressed, the effect of nanoparticles became increasingly pronounced, particularly as the volume percentage of nanoparticles within the NePCM increased. This phenomenon results in a reduction in the volume change of NePCM and an increase in the melting rate [93]. Cui et al. [94] investigated the thermodynamic characteristics of integral melting of copper nanoparticles with sizes ranging from 25.6 to 65.7 nm. The observed trend revealed a linear correlation between the melting temperature, melting enthalpy, and melting entropy and the reciprocal of the particle size. Notably, the thermodynamic properties of these molten systems deteriorated more significantly by decreasing the size of the Cu nanoparticles.

Boukani et al. [10] highlighted the positive impact of copper nanoparticles at concentrations of 0.1% and 3% and aspect ratios of 2.0, 1.0, and 0.5, on the melting characteristics of NePCMs. Elbahjaoui and El Qarnia [95] revealed through the iterative explicit lattice Boltzmann method that a single MgO nanoparticle of 0.01 volume fraction inside a bi-lobe capsule can reduce the pure PCM melting time by 55% and minimize the elapsed time. An experimental investigation conducted by Bashar and Siddiqui [87] presented a comparison of four distinct nanofluids—silver (1% by weight), copper oxide (concentrations of 1, 3, 6, 8, and 10% by weight), aluminum oxide (1% by weight), and multi-walled carbon nanotubes (MWCNT) (1% by weight concentration). The findings of their study indicated that silver and copper oxide

nanoparticles exhibited superior thermal performance, with copper oxide nanoparticles at a 6% concentration demonstrating accelerated melting compared to the other nanofluids.

Ho and Gao [96] investigated the influence of aluminum oxide nanoparticles on the heat transfer efficiency within the melted region of an enclosure. The study examined varying mass fractions of dispersed nanoparticles in the PCM, encompassing concentrations of 0, 5, and 10% by weight, under specific flow conditions (Reynolds number Re= 1.71×10^{6}–5.67×10^{7}; Stanton number St = 0.037–0.108; subcooling parameter = 0.042–0.537). The research revealed that as the mass fraction of nanoparticles was increased in NePCMs, the natural convection heat transfer rate and the total energy transfer rate to the outer shell of the melted region exhibited significant decreases compared with pure PCMs. This phenomenon could be attributed to the higher dynamic viscosity induced by the dispersed nanoparticles, which counteracted the expected enhancement in heat transmission through natural convection during the melting process. These findings could provide valuable insights for future investigations into the heat transfer characteristics of nano-phase transition materials [96].

Several researchers have employed numerical simulations and experimental investigations to explore the influence of the nanoparticle type and concentration on the melting rate of PCMs. Feng et al. [88] conducted a numerical study on copper nanoparticles with 0, 0.05, and 0.1% volumetric concentrations. The incorporation of nanoparticles enhances the melting rate and heat transfer efficiency of PCMs. This improvement was attributed to the increased thermal conductivity and reduced fusion enthalpy of the materials. Shojaeefard et al. [97, 98] discovered that hybrid nanoparticles can reduce the complete melting time and increase the thermal storage capacity of a thermal energy storage (TES) system through different Boltzmann models, and the extent of the time reduction is associated with the type of particles, weight ratio, and volumetric concentration. An increase in the nanoparticle volume fraction also resulted in a larger proportion of melted material, higher

stored energy, and faster advancement of the melting interface. These insights offer valuable guidance for optimizing the performance of NePCMs. Adding only 1% volume of copper oxide nanoparticles can notably accelerate the melting process, particularly when the material is equipped with shorter fins and heated from the bottom [99].

Experimental investigations have also highlighted the effects of nanoparticle addition on NePCMs [100]. This addition could decrease the latent heat of fusion while simultaneously enhancing the thermal conductivity and dynamic viscosity. In the initial stages of melting, the solid-liquid interface maintained a consistent size and shape owing to the dominance of the heat conduction. As time passed, natural convection became increasingly significant, altering the shape of the phase-change interface and accelerating the melting process near the inclined shell outlet. Overall, the nanoparticle addition enhances the thermal performance of PCMs and introduces innovative design possibilities for phase-change energy storage systems.

Furthermore, numerical analyses provided insights into the effects of nanoparticle concentration on melting rates. Ebrahimi and Dadvand [101] studied aluminum oxide-paraffin wax composites with 0, 2, and 5 wt% by weight aluminum oxide concentrations. They found that a volumetric concentration of 2% nanoparticles resulted in the highest melting rate. Another numerical investigation by Darzi et al. [102] demonstrated that higher copper oxide nanoparticle concentrations (0, 2, and 4 vol.%) enhanced the melting rates.

The impact of graphene nanoparticle concentrations (0.5 and 2% by weight) on the melting rate of NePCM was the subject of a numerical investigation conducted by Lachachene et al. [90]. Their results revealed a nonmonotonic trend in the melting rate with varying nanoparticle concentrations. Similarly, in studies encompassing both experimental and numerical approaches, Al-Jethelah et al. [103] found that the inclusion of copper oxide nanoparticles at concentrations of 0, 2, and 4 vol% by volume accelerated heat transfer and accelerated the progression of the interface during the regime of diminishing solids. This

finding implies that copper oxide nanoparticles can enhance the heat transmission efficiency and expedite solidification in these proportions. A study by Muhammad et al. [91] conducted a numerical examination on a hybrid nanofluid (consisting of single-walled carbon nanotubes (SWCNTs) with silver and gasoline and oil), revealing an effective melting behavior.

The choice of nanomaterial incorporated into PCM plays a decisive role in determining its melting characteristics. A numerical study conducted by Faraji et al. [104] discovered that employing a blend of nanoparticles (aluminum oxide, zinc oxide, copper oxide, and copper nanoparticles) at varying concentrations (0, 1, 2, 3, and 4 vol%) could significantly enhance the thermal diffusivity of NePCMs. A numerical investigation by Mahdia and Nsofor [105] reported that by dispersing aluminum oxide nanoparticles at concentrations of 0, 1, 3, and 5 vol% (with porous foam porosity of 0.95 and 0.98), the time required for PCM melting could be remarkably reduced by up to 90% when metal foams were present. They also reported that two key factors governed this reduction in melting time: the type of metal foam employed and the concentration of nanoparticles utilized. Parsazadeh and Duan [106] examined the heat transfer rate of a nanofluid comprising copper oxide and water, specifically by examining concentrations ranging from 0 to 4 vol%. Their findings demonstrated that the material melted faster when an optimal quantity of nanoparticles was introduced.

However, an adverse melting characteristic of NePCM was apparent with an excessive increase in nanoparticle concentration beyond the optimal amount. In contrast, according to a numerical analysis conducted by Sebti et al. [107], increasing the nanoparticle concentration enhanced the heat transmission properties of the copper-paraffin nanofluid at the expense of the melting rate. Their study suggested that augmenting the heat transfer performance and reducing the melting rate could be achieved by harnessing suspended nanoparticles to amplify the thermal conductivity of the PCMs. In a numerical study by Tasnim et al. [108], the addition of copper oxide nanoparticles at a concentration of 10 vol% was explored, revealing a reduction in both the

conduction and convection heat transport modes within a rectangular cavity. Furthermore, their investigation revealed that incorporating these nanoparticles resulted in a slower progression of PCM melting, as evidenced by the position of the melting front. Ghalambaz et al. [109] discovered that the addition of hybrid nanomaterials (consisting of magnesium oxide and silver) enhanced the thermal conductivity, subsequently enhancing the melting rate.

4.2. External magnetic field

The presence of a magnetic field can exert a considerable influence on the melting behavior of PCM [110]. Dibavar et al. [42] numerically investigated an Fe_3O_4-water nanofluid with concentrations of 5 and 10 vol% and observed a decrease in the melting rate as the magnetic field strength increased. Researchers have demonstrated that, while an increase in the Hartmann number slows down the melting process, an increase in the magnetic field strength leads to a more uniform and rapid melting process within a circular shell. Moreover, a higher electrical conductivity results in longer melting times and reduced natural convection rates. Sheikholeslami [59] conducted a numerical study on copper-water nanofluids, with copper concentrations of 0–4 vol%, Hartmann number of 0–40, melting parameter of 0–0.2, and Rayleigh number of 500–5000 using a magnetic field, which resulted in a decrease in the strength of convective flow due to increased conductive heat transfer. In addition, their study revealed that the temperature gradient was increased by increasing the melting parameter and the Reynolds number.

Another study by Hayat et al. [111] demonstrated that the concentration of copper-water (1, 5, 10, and 20 vol%) influences melting behavior, where higher melting points allow for increased molecular movement, promoting fluid flow. However, an increase in the melting parameter thickens the material layer in contact with a surface at a different temperature, potentially reducing the heat transfer effectiveness. An experimental investigation by Sadegh et al. [112] using Fe_3O_4 magnetic nanoparticles (0, 0.5, 1, and 2 wt% by weight) determined that the

nanoparticles decreased the temperature difference and reduced the melting time. This outcome is attributed to the improved thermal conductivity and accelerated melting process owing to the presence of a magnetic field. Selimefendigil and Oztop [113] explored the impact of a magnetic field on the heat transfer rate and melt time in a corrugated cavity using a CNT-water nanofluid with a CNT content ranging from 0 to 4 vol%. The study revealed that increasing the height of the corrugated cavity decreased the heat transfer rate and significantly affected the melting time.

Furthermore, numerical research by Gireesha et al. [114] has highlighted the potential of hydromagnetic fields to enhance electromagnetic induction and temperature profiles. This study also revealed that dispersed nanoparticles in a fluid can improve the heat transmission capacity of the base fluid. The study found that the magnetic field influences phenomena such as thermophoresis and Brownian motion, and these effects were observed across a range of values for the magnetic parameter, Prandtl number, and magnetic Prandtl number. This result underscores the potential advantages of utilizing hydromagnetic fields and suspended nanoparticles in fluid systems to enhance the heat transfer efficiency. Mabood et al. [115] conducted a numerical investigation of hybrid nanofluids, specifically copper-aluminum oxide-water mixtures, and demonstrated that adding nanoparticles at different concentrations led to varying entropy generation rates. The study also indicated that stronger magnetic fields and higher nanoparticle volumes resulted in thicker thermal boundary layers. The relationship between the Bejan and Eckert numbers exhibited a decline, whereas the Brinkman number increased proportionally to the entropy generation rate. These parameters significantly influenced the behavior of the hybrid nanofluids. In addition, in a study by Mabood and Mastroberardino [116], second-order slip influenced the nanofluid flow over a stretched sheet, revealing that a higher magnetic field decreased heat and mass transfer while increasing skin friction. The higher melting and slide parameters significantly influenced the behavior of the nanofluid flow across a stretched sheet.

4.3. Other factors

Drawing insights from combined experimental and numerical studies, Dhaidan et al. [117] discovered the potential of employing an eccentric shell-and-tube configuration to expedite NePCM melting. This result was achieved by strategically lowering the center of the internal cylinder or tube, thereby increasing the exposed area, volume, and number of NePCM segments influenced by buoyancy-driven convective forces. However, it is important to consider that elevated viscosity, agglomeration, and nanoparticle precipitation can counteract the acceleration of the melting process. Notably, the thermal energy required for melting results in a decrease in flow temperature. Furthermore, the rheopectic phenomenon, which significantly affects brick particles, was observed in a numerical study involving zirconium dioxide-water systems with concentrations of 0%, 2%, 4%, and 6% [118].

With complex fluid dynamics, the interplay of parameters reveals significant trends: the skin friction coefficient decreases with the melting parameter, whereas the heat and mass transmission rates increase with parameters such as thermal radiation. An increase in the power law index also triggers a decline in the velocity, temperature, and concentration distribution. An amplified power-law index was consistently linked to augmented skin friction, heat transmission, and mass transfer rates, as revealed by a numerical analysis of a non-Newtonian Sisko fluid study conducted by Soomro et al. [51]. These complex dynamics are schematically summarized in Figure 15, which shows the multifaceted effects of different parameters on the nano-enhanced melting process.

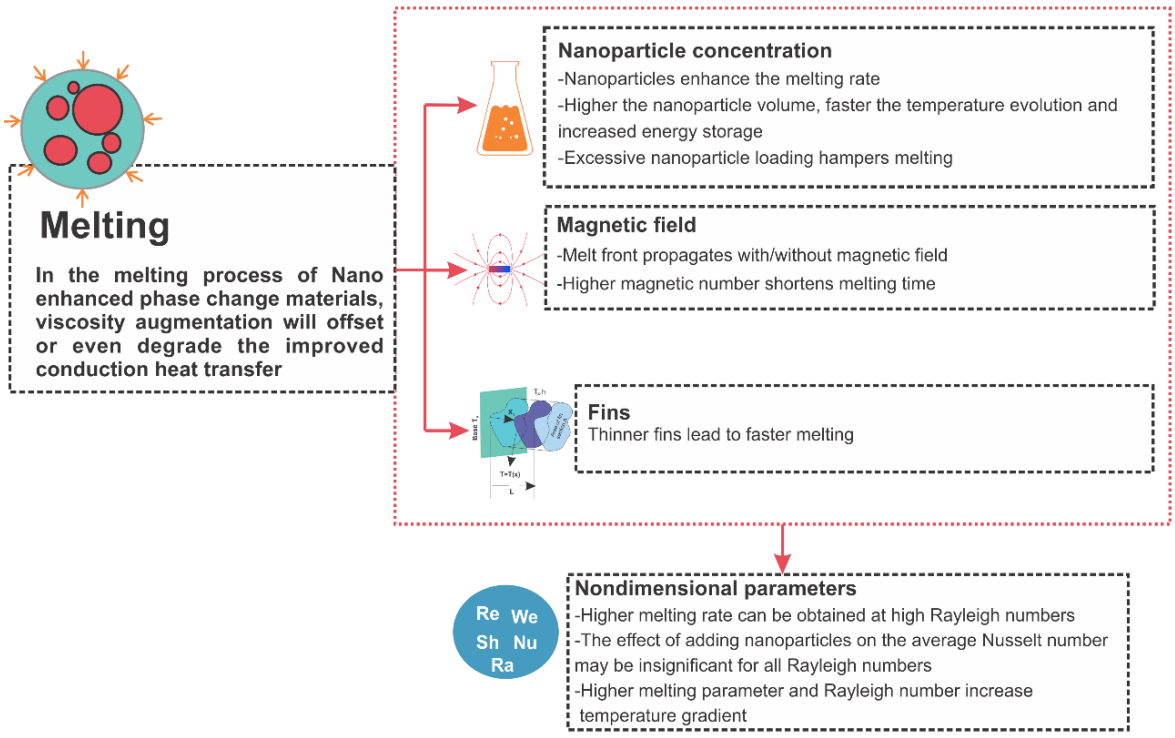


Figure 15. Effects of various factors on the melting process for nano-enhanced materials [51].

5. Boiling

Evaporation and boiling are two distinct mechanisms by which a substance transitions from liquid to gas or vapor. Evaporation involves the gradual conversion of a liquid into gas or vapor by absorbing thermal energy. This transformation occurs when the molecules within a liquid acquire sufficient energy to overcome the cohesive forces that bind them together, thus escaping as individual gas molecules into the surrounding environment. Evaporation can occur at various temperatures. Boiling refers to the rapid process of heating a liquid to a point where it swiftly transitions into a gas or vapor state. As the liquid attains its boiling point, the energy input propels its molecules to break free from intermolecular bonds, shifting the substance from liquid to gas. During this transformation, bubbles formed within the liquid, signifying the onset of boiling. The rapid generation of these bubbles, followed by their ascent to the liquid surface, distinguishes the boiling phenomenon. Figure 16 illustrates the evaporation and boiling processes.

In the context of boiling, heat transfer is intricately linked to the formation and expansion of bubbles. The inception of bubbles depends on specific conditions: (1) the liquid must be superheated beyond its boiling point, and (2) a vaporization nucleus, or core, must be present. These conditions are intricately determined by the balance of forces and heat exchange between the bubble and the surrounding liquid [119]. Using the mechanical equilibrium with surface tension forces, the vapor pressure within the bubble is given by

$$p_v = p_e + \frac{2\sigma}{R} \tag{15}$$

where p_v represents the pressure of the surrounding liquid, which is equal to the saturated vapor pressure (p_s) when the static pressure of the liquid column is disregarded. where R denotes the radius of the bubble and σ is the surface tension force of the liquid. Given that p_v surpasses p_s , the vapor confined within the bubble must have a saturation temperature that surpasses the saturation temperature linked to the corresponding saturation vapor pressure. Consequently, for the liquid to transform into steam within the bubble, its temperature must either attain or exceed the saturation point associated with the steam inside the bubble.

Boiling processes can be categorized into two fundamental types: pool and flow boiling. Pool boiling when considering the boiling process without factoring in bulk fluid flow. Conversely, if the influence of the bulk fluid flow is significant, the boiling process is termed as flow boiling [28, 120]. A visualization of these types of boiling is illustrated in Figures 16 and 17. Numerous researchers have introduced nanoparticles into various boiling scenarios to better understand the impact of nanoparticles on heat transmission.

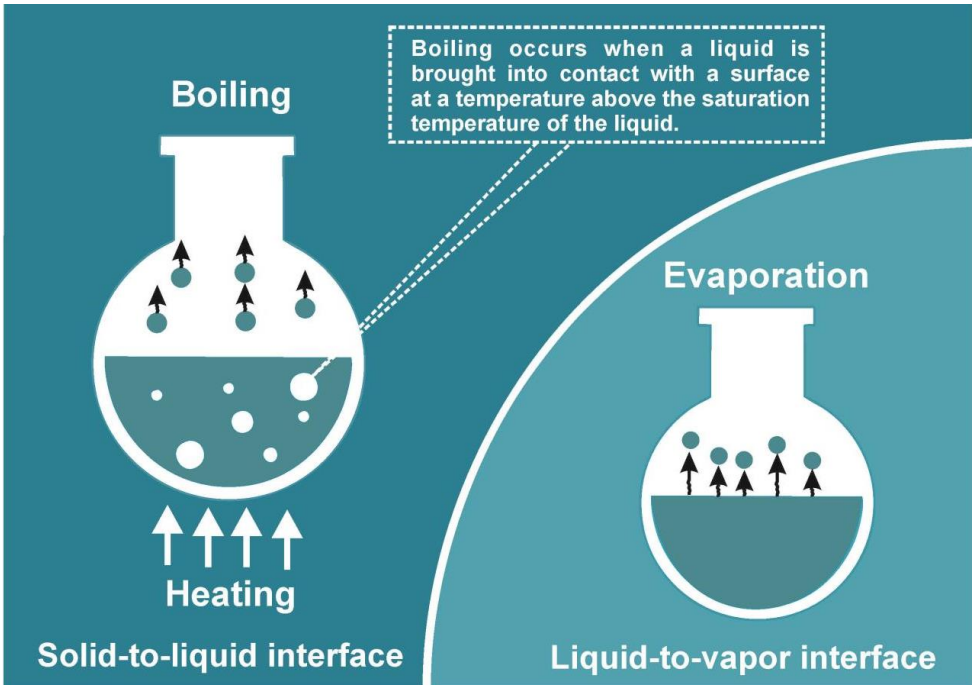


Figure 16. Infographic representation of boiling and evaporation [28].

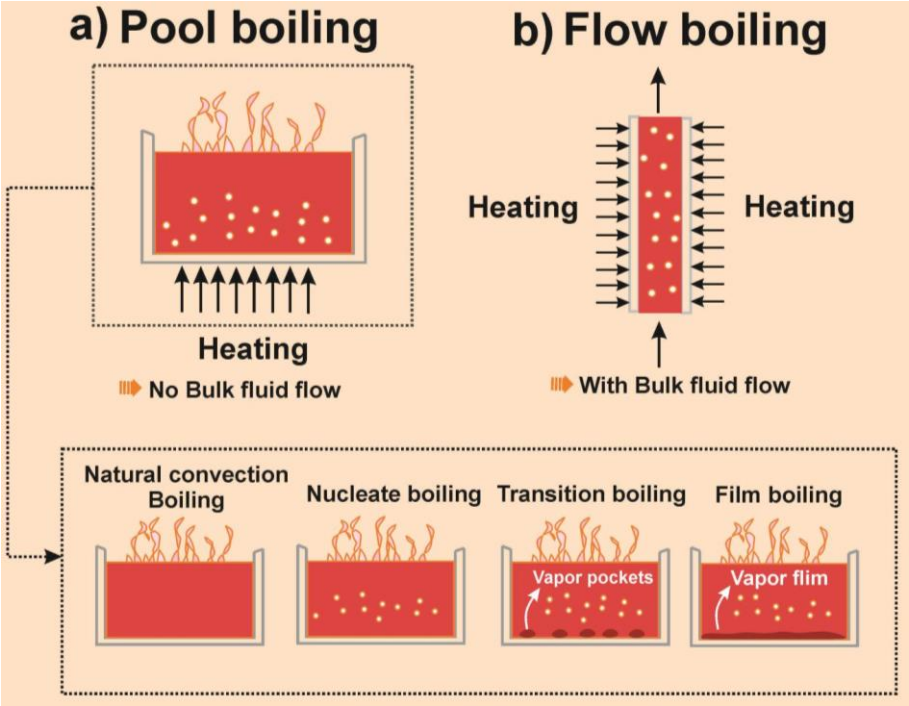


Figure 17. Representation of different types of boiling [28].

Figure 18 shows a schematic representation of the experimental setup devised to investigate how nanoparticles enhance the heat transfer during boiling. The following sections include a critical discuss the influence of nanoparticles and other boiling mechanisms on the heat-transfer rate.

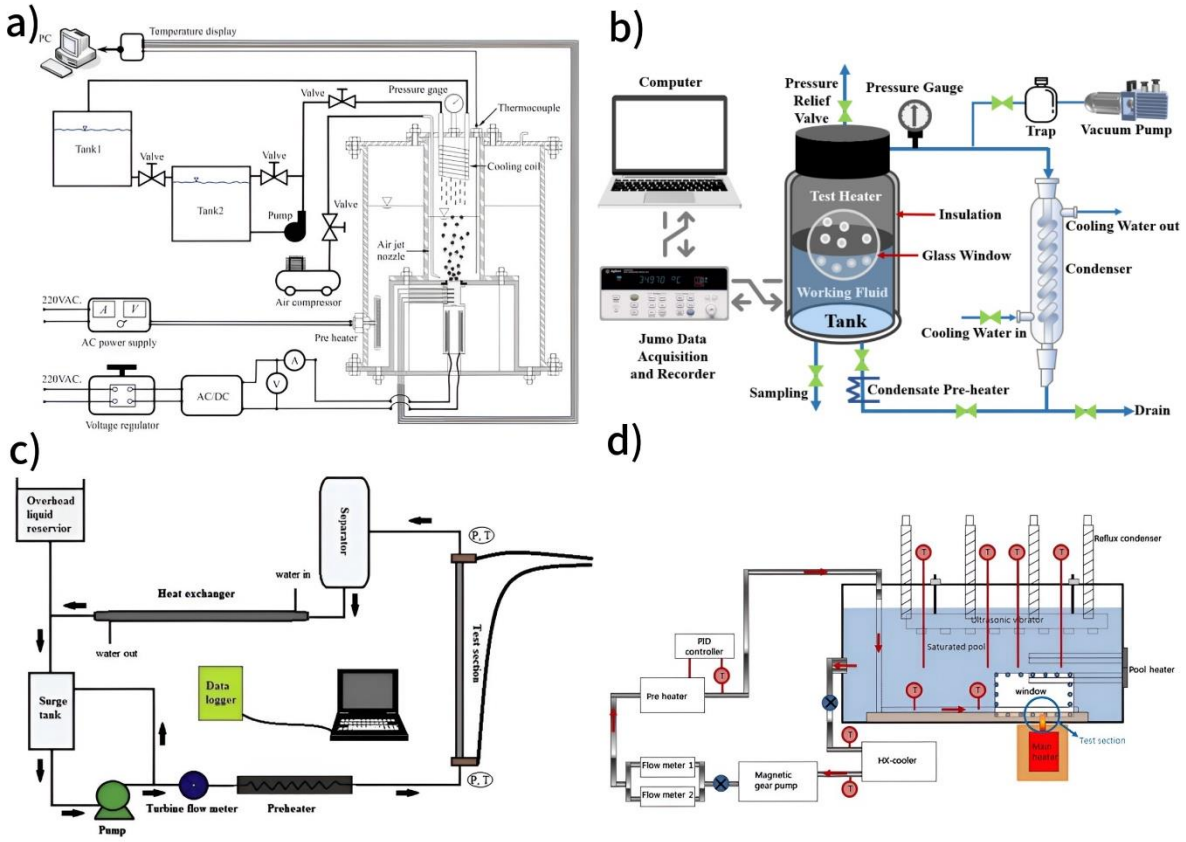


Figure 18. Schematic diagrams of experiments designed to study how nanoparticles enhance boiling heat transfer, a) nucleate pool boiling setup. Reproduced with permission from Exp. Therm Fluid Sci. 34(8), 992-999 (2010). Copyright 2010 Elsevier Inc.[121] b) pool boiling apparatus. Adapted from Ref. [122], c) flow boiling setup. Reproduced with permission from Exp. Therm Fluid Sci. 58, 156-169 (2014). Copyright 2014 Elsevier Inc.[123] d) flow boiling critical heat flux (CHF) experimental loop. Reproduced with permission from Int. J. Multiphase Flow. 36(5), 375-384 (2010). Copyright 2010 Elsevier Ltd. [124].

5.1. Effects of nanoparticle concentration and morphology

5.1.1. Nanoparticle type and concentration

The HTC and critical heat flux (CHF) are notably affected by nanoparticle type and concentration [125]. Research has demonstrated that the introduction of nanoparticles can reduce the effectiveness of boiling heat transfer by varying the extent of this reduction. This effect became more pronounced as the heat flow intensified. It is worth noting that the impact of pressure on convection boiling HTC diminishes with increasing heat flux and nanoparticle concentration [126]. This diminishing impact can be attributed to the aggregation of nanoparticles on the surface, which shifts the boiling characteristics in an unfavorable direction. As a result, the boiling rate exhibits an inverse relationship with the volume concentration of the nanoparticles [127].

Sarafraz and Hormozi [128] conducted experiments on nucleate pool boiling using an aluminum oxide/ethylene glycol nanofluid. The nanofluid contained nanoparticles with a size of 45–50 nm and a concentration ranging from 0.1 to 0.3% by weight, with a pH of 10.2. Their findings indicated that an increase in the nanofluid concentration led to the adsorption of nanoparticles of similar sizes, resulting in a significant reduction in the surface roughness. This reduction in roughness led to a decrease in the HTC owing to a decrease in the number of nucleation sites [128]. Another study conducted by Bang and Chang [129] focused on nucleate pool boiling heat transfer involving an aluminum oxide/water-based nanofluid with concentrations of 0.5, 1, 2, and 4 vol%. The study found an inverse relationship between HTC and concentration, indicating that higher concentrations weakened the heat exchange during pool nucleation boiling.

In a pioneering study by Park et al. [130], the film-boiling method was employed with nanofluids composed of aluminum oxide and deionized water. Nanoparticles with an average diameter of 33.1 nm were used at concentrations of 5, 10, and 20 vol.%. The results of the

study revealed that the heat transfer rate and HTC in the nanofluids were lower than those in pure water. Moreover, it was observed that concentrations above 5 vol.% had a minimal impact on film boiling. The deposition of nanoparticles on the surface of a heated sphere led to rapid cooling of the object, showcasing the unique effects of nanoparticles in film-boiling scenarios.

In addition to film boiling, researchers have investigated the effects of nanoparticle type and concentration on flow boiling heat transfer. Sun and Yang [131] conducted experiments using three different nanofluids: aluminum oxide/R141b, copper oxide/R141b, aluminum/R141b, and copper/R141b. These nanofluids contained nanoparticles with a diameter of 40 nm and varying concentrations (0.1, 0.2, and 0.3% by weight). The aim was to study the influence of the nanoparticle concentration and type on heat transfer. Their findings indicated a direct proportionality between the HTC and the mass fraction. Different nanoparticles had varying effects on the HTC of nano-refrigerants, with copper nanoparticles demonstrating the most effective improvement in the heat transfer efficiency.

In an interesting study on flow boiling, a nanofluid consisting of copper oxide/R113 nanoparticles [12]. The nanoparticles had an average diameter of 40 nm, and the nanofluid was tested at different concentrations (0.1, 0.2, and 0.5% by weight) without adding surfactants. This research focused on how the flow boiling heat transfer of the nanofluid changed with increasing nanoparticle concentration. Two primary factors contributed to this increase. First, the nanoparticles were found to reduce the thickness of the boundary layer, which impedes heat transfer. Second, nanoparticles exhibited the ability to adsorb liquid molecules and create a layer on their surface, further enhancing the heat transfer process.

In a study by Cieśliński and Kaczmarczyk [132], a pool boiling experiment was conducted on a porous coating using deionized water together with aluminum oxide and copper nanoparticles. The purpose of this study was to investigate the effects of concentration and pressure. The aluminum oxide particles had an average diameter of 47 nm, whereas the copper

particles measured 48 nm in diameter. The behavior of the nanoparticles during pool boiling on a porous coating is shown in Figure 19. With an increase in the nanoparticle concentration, the pH of the copper nanofluids decreased. For concentrations of 0.01, 0.1, and 1% by weight, the pH values were 7.44, 6.30, and 6.87, respectively. On the other hand, the pH of aluminum oxide nanofluids at concentrations of 0.01, 0.1, and 1% by weight was observed to be 6.51, 7.48, and 8.11, respectively. It was concluded that HTC was inversely proportional to the nanoparticle concentration. Furthermore, the pressure exhibited direct proportionality with the HTC, regardless of the particle concentration [132].

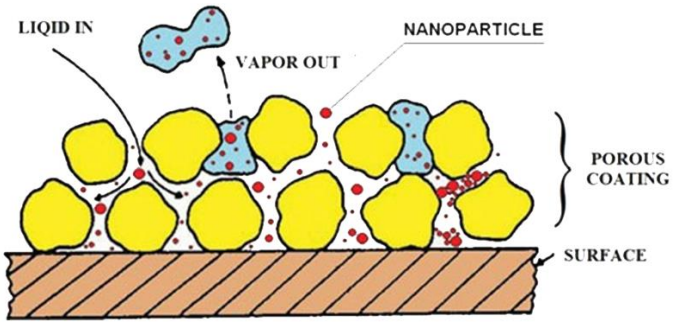


Figure 19. Nanoparticle behavior during pool boiling on porous coating [133].

In another study conducted by Soltani et al. [134], a pool boiling approach was employed using a non-Newtonian nanofluid consisting of γ-aluminum oxide/carboxymethyl cellulose in water. The nanofluid contained nanoparticles with sizes ranging from 20 to 30 nm, and the concentration of carboxymethyl cellulose in water ranged from 0.5 to 10% by weight, while the aluminum oxide concentration ranged from 0.8 to 1.4% by weight. Researchers observed that the collision between the nanoparticles and the heating surface increased the turbulence of the solution, leading to a significant enhancement in the HTC. Furthermore, they noted that the HTC of the boiling heat exchange increased with higher nanoparticle concentrations.

The effects of the concentration and aggregation on the nanofluids were also investigated. Wen and Ding [135] conducted a study using a nanofluid composed of aluminum oxide and water with nanoparticle sizes ranging from 90 to 450 nm and a pH value of 9.1. Test concentrations of the nanofluid were set at 0.32, 0.71, 0.95, and 1.25% by weight. Their findings indicated that the heat transfer enhancement was directly proportional to the particle concentration, with the highest enhancement of 40% observed at 1.25% by weight. The presence of the aggregates significantly affected the performance of the nanofluids. In another investigation by Lee et al. [136], a flow boiling method was employed using a nanofluid consisting of GO and water, with a nanoparticle concentration of 0.01 vol% and nanoparticle thickness of less than 1 nm. This study aimed to understand the influence of particle type and deposition. The study found that the CHF increased significantly when GO particles were deposited on the surface compared with silicon carbide or aluminum oxide. This enhancement was attributed to the improved wettability of the GO/water nanofluid [136].

5.1.2. Nanoparticle size

Numerous studies have investigated the impact of nanoparticle size on boiling heat transfer. Milanova and Kumar [137] conducted a nucleate pool boiling experiment using silicon dioxide/water nanofluids containing 10-and 20-nm nanoparticles. The nanofluids were at concentrations of 0.5 vol% and had different pH levels of 3, 4, 7, and 10. They observed that nanofluids containing smaller silica nanoparticles (10 nm) exhibited the best CHF performance, regardless of the pH value. Interestingly, among all the surfaces tested, the CHF performance of the Nichrome wire was the highest. This result was attributed to the oxidation of the Nichrome material due to the porosity of the silica deposits [137]. In another investigation, Vassallo et al. [138] studied the influence of nanoparticle size on the heat flux using the same nanofluid (silicon dioxide and water) through a nucleate boiling method. They used nanoparticle sizes of 15, 50,

and 3000 nm at a concentration of 0.5 vol% and found that the nanofluid with 50 nm nanoparticles allowed for the highest heat transfer rate. This heat transfer rate was nearly three times that of pure water and double that of a nanofluid containing 3000 nm nanoparticles.

Amiri et al. [139] conducted a pool boiling test using CNT/water nanofluids at concentrations of 0.01, 0.05, and 0.1% by weight. They investigated the influence of nanoparticle size, deposition, and concentration. They used CNTs with diameters ranging from 10 to 60 nm and lengths of 5—15 μm to achieve this. The study revealed that the HTC and CHF values depended on the diameter of the CNTs, with larger-diameter CNTs leading to decreased HTC and CHF values. They also observed a significant increase in the CHF due to the deposition layer formed by the CNTs on the surface. Because CNTs are non-covalent nanofluids, an increase in the CNT concentration led to a decrease in the HTC.

Sarafraz and Hormozi [140] investigated the impact of different nanoparticle types using a similar pool-boiling technique. They studied nanofluids consisting of copper oxide, aluminum oxide, and multi-walled carbon nanotubes (MWCNTs) diluted with deionized water. Their findings indicated that adding nanoparticles to the boiling surface reduced the number of nucleation sites and the surface roughness, resulting in a lower rate of surface heat transfer. Among the three nanofluids, MWCNTs demonstrated lower fouling resistance and better performance than those of the other two. In another noteworthy study, Yao et al. [141] employed the pool boiling method with nanofluids composed of aluminum oxide/water (30 nm) and silicon dioxide/water (50 nm) at a mass ratio of 1:1 and a concentration of 0.01% by weight. The research showed a clear correlation between the boiling heat transfer efficiency and nanoparticle size. Comparing the two nanofluids, they found that the silicon dioxide surface was smoother, which led to reduced vaporization of the core and bubble production. In contrast, aluminum oxide produced smaller bubbles with a higher separation frequency.

5.2. Surface factors

5.2.1. Surface tension

In experiments conducted by Kumar and Milanova [142] using SWCNT at a concentration of 0.1 vol% and an ionic surfactant, it was found that as surface tension relaxed, the percentage change in boiling heat transfer was increased steadily, reaching a maximum improvement of 270% for the case of 0.1% concentration. Aluminum oxide, silicon dioxide, and zinc oxide were used in a pool boiling experiment by Sayahi and Bahrami [122], who discovered that the surface tension had the greatest impact. The pool-boiling HTC of clean water was enhanced using aluminum oxide nanoparticles. However, because of the effects of surfactants on the increased viscosity of the nanofluid, the addition of surfactants reduced the propensity of the nanofluid for nucleation and boiling. Furthermore, the viscosity increased with increasing temperature, whereas the surface tension of the fluid exhibited a slight decrease. On the other hand, in the case of the silica nanofluid, both surface tension and dynamic viscosity contributed to lowering the HTC, which resulted in a decrease in the boiling ability of the base fluid. In the case of zinc oxide, the study exhibited the highest heat dissipation and cooling capability among the investigated nanofluids.

5.2.2. Wettability

In an experimental investigation on pool boiling conducted by Xunyan et al. [143], where a copper/water nanofluid with nanoparticles of 2 nm diameter was used, the results revealed that the deposited nanoparticles enhanced the surface wettability, thereby improving the heat transfer rate. Interestingly, increasing the particle size decreased the heat transfer rate. Another study by Coursey and Kim [35] involved the use of pool boiling with aluminum oxide/water nanofluid (concentration: 2–7% by weight) and aluminum oxide/ethanol nanofluid (concentration: 0.5–20% by weight), both with an average particle diameter of 45 nm. They

found that nanoparticles had a greater impact on systems with initially poor wetting characteristics, whereas systems with better wetting properties showed less change with nanoparticle addition. In a separate pool boiling experiment, Song et al. [144] utilized a silicon-carbide/water nanofluid at concentrations of 0.0001, 0.001, and 0.01 vol%. Their findings highlighted the influence of wettability variations on the CHF enhancement. They observed a high consistency between the CHF values obtained from the nanofluid and deposition surface experiments. The CHF enhancement was evident for the 0.0001% and 0.01% nanofluid conditions, and the 0.0001% and 0.01% deposited conditions.

The wettability characteristics of nanoparticles play a crucial role in influencing the behavior of vapor bubbles during boiling[145, 146]. When nanoparticles adsorb onto the gas-liquid interface, they hinder liquid discharge, thereby preventing bubble aggregation, which strongly affects the boiling performance. This phenomenon is illustrated in Figure 20, which shows the distribution of the nanoparticles under a vapor bubble. The effectiveness of enhancing boiling heat transfer is higher for nanoparticles with medium hydrophilicity than for those with strong hydrophilicity, because nanoparticles with lower hydrophilicity can enhance surface roughness [147].

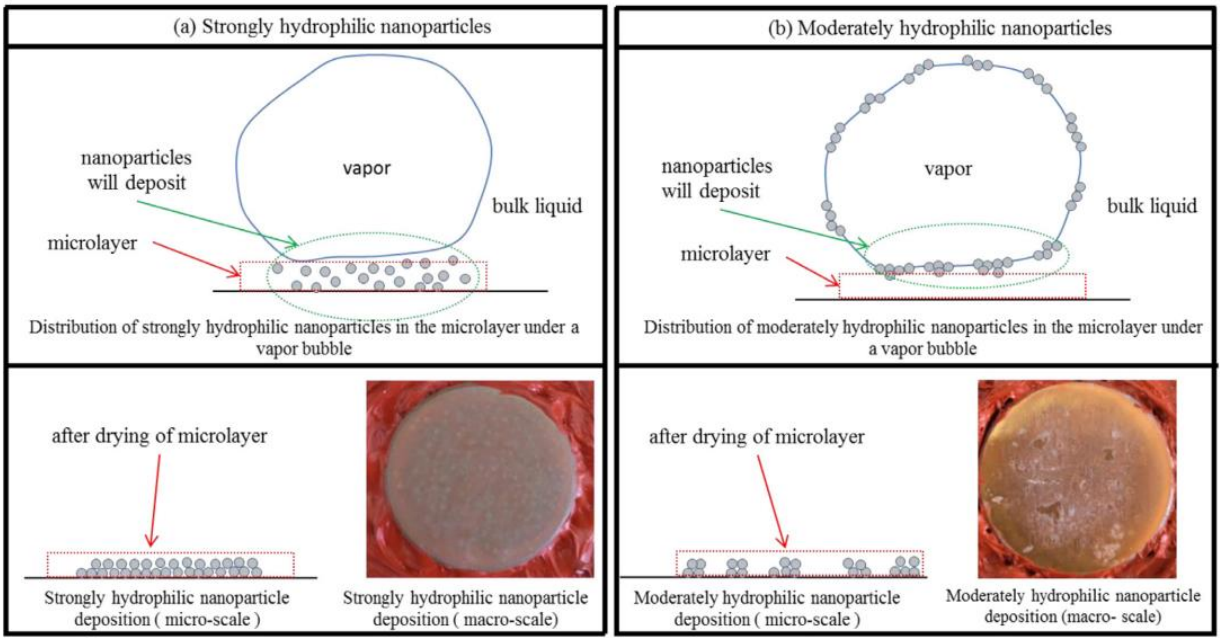


Figure 20. Distribution of strongly/moderately hydrophilic nanoparticles in the microlayer under a vapor bubble in the nucleate pool boiling process. Reproduced with permission from Int. J. Heat Mass Transfer. 108, 32-40 (2017). Copyright 2016 Elsevier Ltd.[147].

Under atmospheric pressure conditions, White et al. [148] conducted a pool boiling experiment using a nanofluid consisting of 2.3 vol% zinc oxide and deionized water, and they observed an improvement in boiling heat transfer. An experiment by Wang and Cheng [149] demonstrated that medium-hydrophilic nanoparticles deposited at the bubble interface may enhance the liquid drainage resistance while also stiffening the bubble interface, thus prolonging the time for bubble agglomeration. Consequently, the level of bubble aggregation in pool boiling is reduced, leading to smaller bubble sizes. Nanoparticles placed on a surface enhance the surface wettability and improve the heat transfer efficiency between the surface and liquid, as revealed in a flow boiling experiment by Yin et al. [150] using a copper/argon nanofluid. Both the duration of bubble nucleation and the deposition of nanoparticles could be leveraged to enhance the impact of pool and flow boiling, as suggested by researchers. However, the enhanced effect of nanoparticles on heat transfer in flow boiling was more

significant due to the additional influence of the rotational motion of suspended nanoparticles, which could enhance both the fluid momentum transfer and heat diffusion.

5.2.3. Surface roughness

The variation in boiling heat transfer is influenced by a combination of factors, including the relative sizes and interactions of the particles suspended in the liquid medium and the shape of the heated surface. The concentration of nanoparticles has a limited impact on the boiling heat transfer when rough surfaces are used. However, when nanoparticles are deposited on initially smooth surfaces, the surface becomes rougher, and the enhancement in boiling heat transfer is directly proportional to the concentration of the nanoparticles [151]. The nucleate boiling of copper oxide and aluminum oxide nanofluids in deionized water was investigated in a study by Niu and Li [152], who used nanoparticles with a diameter of 20 nm at a concentration of 0.015 vol%. Their findings revealed that nanofluids generated larger bubbles than deionized water. Surface porosity significantly influences the size of the bubbles. Notably, the particle size of the nanofluids was found not to directly impact the pool boiling heat transfer in their research [152]. In another investigation conducted by Vafaei [153] involving pool boiling, α-aluminum oxide/water nanofluids with particle sizes ranging from 20 to 150 nm were studied at increasing concentrations of 0.001, 0.01, and 0.1 vol%. The results indicated that the roughness of the nanoparticle-formed layer on the surface increased as the particle concentration in the nanofluid increased, leading to a subsequent increase in cavity size[153].

In a pool boiling experiment, Narayan et al. [154] employed an aluminum oxide/water nanofluid (with a pH of 5.5) containing nanoparticles ranging in size from 47 to 150 nm and concentrations of 0.5, 1, and 2% by weight. That study revealed that even at a very low concentration of 0.5% by weight, the rate of heat transfer increased by 70% for a heater with an average roughness of 524 nm and nanoparticles of 47 nm size. Utilizing titanium dioxide/water

nanofluid and conducting nucleate pool boiling, Suriyawong and Wongwises [121] investigated the effects of the surface roughness and particle concentration. Their results indicated that regardless of how the surface roughness was controlled, the HTC of nanofluids with concentrations greater than 0.0001 vol% was consistently lower than that of the base fluid. In a pool boiling experiment conducted by Ganapathy and Sajith [155], an aluminum oxide/water nanofluid with a particle diameter of 50 nm and concentrations of 0.5, 1, and 2 vol% was used. Their findings suggested that in the presence of a smooth surface, the heat transfer efficiency of the base fluid was reduced owing to the fewer nucleation sites available. This led to a decrease of up to 30% in heat transfer from boiling nanofluids to smooth surfaces. Convective boiling was explored on the same nanofluids (with a particle diameter of 20–30 nm) at a concentration of 0.25 vol% by Setoodeh et al. [156] who observed a direct relationship between the heat flux, fluid velocity, and surface roughness. Furthermore, they found that adding nanoparticles improved the flow boiling heat transfer of pure water by 79%, 59%, and 56% at surface roughness values of 0.65, 4.4, and 15.1 μm, respectively.

5.2.4. Deposition

A lower boiling HTC results from the deposition of nanoparticles from a thin layer on the surface during pool boiling, as per Ciloglu [157]. When nanoparticles are deposited, they may lower the contact angle between the surface and the particles; as the nanoparticle concentration increases, the contact angle will further decrease, improving the surface wettability and increasing the CHF. In an experimental study conducted by Sarafraz et al. [158] on pool boiling using zirconium dioxide/water-ethylene glycol at varying concentrations of 0.025, 0.05, 0.075, and 0.1% by weight, it was observed that the capillary wicking action was enhanced because of the porous layer formed on the surface with the deposition of zirconia nanoparticles, which in turn led to an improvement in the CHF value. They also found that when the heat flux was large, the bubble

coalescence phenomenon intensified, increasing the probability of a CHF crisis. Phan et al. [159] reported that titanium dioxide deposition considerably decreased the pool-boiling HTC of water.

In their research using aluminum oxide/water nanofluid at a concentration of 0.01 vol%, Park et al. [160] observed a consistent decrease in the CHF. This decrease was attributed to the reduced porosity of the deposited layer with longer pre-coating times and increased surface wettability. When the nanofluid concentration was raised above 0.05 vol% by volume, the CHF tended to decrease because of the impact of the porous layer on the increased wettability. Another study conducted by Ham et al. [161] involving an aluminum oxide/water nanofluid at concentrations ranging from 0.001 to 0.1 vol% also showed that the CHF is influenced by both the decrease in contact angle and the increase in the wettability caused by the porous layer formed by nanoparticles.

Diao et al. [162] observed that the deposition layers of nanoparticles on surfaces caused enlargement of the evaporation area and an improved boiling heat transfer process. This improvement is due to the increased density of the nucleation sites. Interestingly, Liu and Liao [163] found that even after cleaning the sorption layer on a heating surface with a water jet, a residual thin layer persisted, causing a reduction in the surface roughness and contact angle.

In the case of nucleate boiling, the deposition of nanoparticles to form a porous layer has been shown to decrease the static contact angle of the surface, leading to improved surface wetting and enhanced CHF [164]. In addition, when nanoparticles are applied as nanocoatings on heater surfaces, they alter the surface wettability, ultimately leading to an increase in the CHF during nanofluid boiling. According to Kwark et al. [165], an optimal thickness and structure exists for nanocoatings that maximize the CHF without compromising the overall heat transfer efficiency. A study by other researchers such as Truong et al. [166] found that the boiling deposition of nanoparticles on sandblasted plate heaters led to significant changes in the wettability of the metal oxide-coated heater surfaces, consequently enhancing the CHF.

Kim et al. [167] performed a flow boiling experiment using varying concentrations of aluminum oxide/water, zinc oxide/water, and diamond/water (0.001, 0.01, and 0.1 vol%) and found that nanoparticle deposition occurs during boiling of the nanofluid, increasing surface wettability and reducing microcavities on the surface. It was shown in another study by Kim et al. [168] using 0.0001 and 0.001 vol% concentrations of aluminum oxide/deionized water, that the nanoparticles formed on the inner surface of the test section tube were responsible for the CHF increase of the nanofluid.

5.3. Experimental conditions

5.3.1. Surfactants

Although the addition of surfactants can accelerate boiling heat transfer and improve the performance of nucleation boiling heat transfer, owing to the reduction in bubble size at the beginning and departure of nucleation, boiling heat transfer is weakened when the concentration of the added surfactant reaches a certain limiting value [169]. In a pool boiling experiment with silicon dioxide/deionized water with a concentration of 1 vol% and cetyltrimethylammonium bromide, polysorbate 20, and sodium laureth sulfate as a surfactant, Etedali et al. [177] noticed that in nanofluids containing sodium laureth sulfate and cetyltrimethylammonium bromide, the HTC decreased with increasing concentration of the nanofluid. In the case of nanofluids containing polysorbate 20, the HTC increased as the concentration increases from 0.01 to 0.1 vol%, as the concentration was further increased to 1 vol%, the heat transfer decreased significantly. A similar pool boiling experiment was conducted by Jung et al. [170] with titanium dioxide/water with concentrations of 0.00001–1 vol% and found that the coating structure of the nanoparticles produced in the suspension containing 0.001 M nitric acid and without any additives was different, and that the presence of nitric acid may restrict the ability of nanofluids to improve the CHF.

Peng et al. [171] conducted experiments in pool boiling with a copper/R113 system at concentrations 0.1, 0.5, and 1.0% by weight with surfactants selected as cetyltrimethylammonium bromide, sodium dodecyl sulfate, and sorbitan monooleate (Span-80). They found that adding a surfactant could promote the CHF increase rate of boiling heat transfer, but when the surfactant concentration was increased further, the CHF increase rate decreased. This result suggests that the addition of a surfactant might limit the ability to increase the CHF of the nanofluid boiling heat exchange. The optimum concentrations of sodium dodecyl sulfate, cetyltrimethylammonium bromide, and sorbitan monooleate were 2000, 500, and 1000 ppm, respectively. Another study by Kathiravan et al. [172] used copper/deionized water with concentrations of 0.25, 0.5, 1.0% by weight and 9.0% by weight sodium lauryl sulfate anionic surfactant to conduct a pool boiling experiment. They found, because of active bubble dynamics and a decrease in surface tension, that the CHF decreased by 75%, 68%, and 62%, respectively, for nanoparticle concentrations of 0.25%, 0.5%, and 1.0% in pure water. A study on nucleate pool boiling by Tang et al. [173] with aluminum oxide/R141b at concentrations of 0.001, 0.01, and 0.1 vol% and sodium dodecyl benzene sulfonate as a surfactant, found that the addition of sodium dodecyl benzene sulfonate weakens the enhancement of the HTC in liquids with a particle concentration of 0.001 vol% but strengthens the enhancement of the HTC in liquids with particle concentrations of 0.01 vol% and 0.1 vol%.

5.3.2. Effect of pressure

The boiling HTC and CHF have been shown to increase as the pressure is significantly reduced, with a corresponding reduction in the saturation temperature [174]. Naphon and Thongjing [175] conducted a pool boiling experiment with titanium dioxide/R141b and titanium dioxide/ethyl alcohol at concentrations of 0.01, 0.025, 0.05, and 0.075 vol% at pressures of 50 and 100 kPa, and

discovered that the boiling heat transfer rate and boiling HTC increased with increasing boiling pressure. In another study, Sakashita [176] conducted a pool boiling experiment using a titanium dioxide/water nanofluid with a concentration of 0.002% by weight at pressures ranging from 0.1 to 1 kPa, and found that the CHF of both nanofluids and pure water is sharply increased with increasing the pressure. However, the enhancement effect of the CHF for nanofluids was found to decrease proportionally with an increase in pressure, eventually approaching zero at a pressure of 0.8 MPa. Lee et al. [177] investigated the impact of pressure on boiling behavior using an aluminum oxide/water nanofluid (20–30 nm) with pH values of 6.6–6.7 and Fe_3O_4/water (4.1–4.5). They observed that the bubble formation frequency of nanofluids was approximately twice as high as that of pure water within a pressure range of 100–1199 kPa. Notably, an increase in the pressure led to a decrease in the weight of the deposited nanoparticles during pool boiling.

5.4. External field and microphysical influence mechanisms

5.4.1. Magnetic field

To explore the effects of a magnetic field, Rostami et al. [43] conducted a pool boiling experiment using nickel oxide/deionised water nanofluids with varying concentrations (0.005, 0.01, 0.05, 0.1, and 0.2 vol%) and the addition of a surfactant. They concluded that a magnetic field could enhance the HTC of diluted nanofluids. They also discovered that a high-intensity magnetic field can decrease the HTC of nickel oxide nanofluids in concentrated solutions. Furthermore, the application of magnetic fields increased sedimentation in concentrated solutions while reducing sedimentation in dilute solutions of nickel oxide. In a different study, Aminfar et al. [123] performed a pool boiling experiment using ferric oxide and water nanofluids at concentrations of 0.01 and 0.1 vol% to investigate the influence of a magnetic field. Their research demonstrated that the enhancement of CHF in ferrofluids is influenced by surface nanoparticle deposition, changes in surface wettability, and alterations in the contact angle. They also noted that a CHF

reduction occurred under zero-flow conditions, and that the attraction of nanoparticles to the heated surface led to the formation of fewer nanoparticles on the surface.

5.4.2. Motion of nanoparticles due to field gradients

Li et al. [178] emphasized the significance of the Brownian motion of nanoparticles in dissipating the surface heat. They pointed out that the heat transfer attributed to the Brownian motion of nanoparticles is influenced by the particle volume concentration, which is inversely proportional to particle size. Michaelides [47] showed that thermophoresis is a consequence of Brownian motion in temperature gradients, and derived the thermophoretic velocity using random molecular impulses that create Brownian motion. The external heat flux also influences the Brownian motion of the nanoparticles. Notably, the thermophoresis phenomenon influenced the heat transfer, with smaller nanoparticles tending to accelerate heat transfer more than larger nanoparticles [179]. In a simulation involving pool boiling with aluminum oxide/water nanofluids at a concentration of 0.02 vol%, Gobinath et al. [180] observed that the viscosity and thermophoresis combine to reduce particle mobility near the heater surface, a phenomenon that has been known for fluid-solid interfaces and called “hindered diffusion” [181]. Their study introduced a modified Peclet number tailored for pool boiling by considering the thermophoretic velocity. Furthermore, Karthikeyan et al. [182] highlighted the influence of pressure, buoyancy, viscosity, and temperature gradient on thermophoretic velocity. A zero thermophoretic velocity near the heater indicates the absence of temperature gradients in the system.

5.4.3. Aggregation and contact angle

Wang et al. [183] observed that nanoparticles aggregating near the triple-phase line can decrease the contact angle. This issue, in turn, could cause an increase in the wettability of the heated surface, as the deposited nanoparticles create a porous sublayer. Conversely, more uniformly

distributed nanoparticles were observed to deposit on the heating surface when agglomeration was not prevalent, thereby increasing the CHF enhancement [184]. Notably, the surface roughness and suspended nanoparticles in the nanofluid were observed to have a relatively minor impact on the peak heat flux compared with the significant influence of changes in the static surface contact angle resulting from particle deposition on the heated surface during boiling [185].

5.4.4. Nanoparticle migration

Nanoparticle migration (dispersion) occurs opposite to particle concentration and is inversely proportional to particle size. The migration of nanoparticles from the liquid phase to the vapor phase in nanofluid pool boiling, based on the refrigerant, can be categorized into four methods: removal of bubbles from the heated surface, movement of bubbles and nanoparticles in the liquid phase, capture of nanoparticles by bubbles, and release of nanoparticles at the liquid-vapor interface [12]. A theoretical study by Zendehboudi et al. [186] investigated pool boiling using copper, aluminum, aluminum oxide, and copper oxide nano-refrigerants. They examined the migration ratios of these nanoparticles during the pool boiling of nano-refrigerants using artificial intelligence. Another investigation by Ding et al. [187] focused on the migratory properties of nanoparticles during pool boiling using copper oxide/R113 nano-refrigerants and nanorefrigerant-oil combinations. They noted that as the initial mass of the nanoparticles and the refrigerant mass increased, the migrating mass of the particles also increased. Figure 21 illustrates the process of nanoparticle migration via bubble adhesion. The effects of different factors on the nano-enhanced boiling process are illustrated in Figure 22.

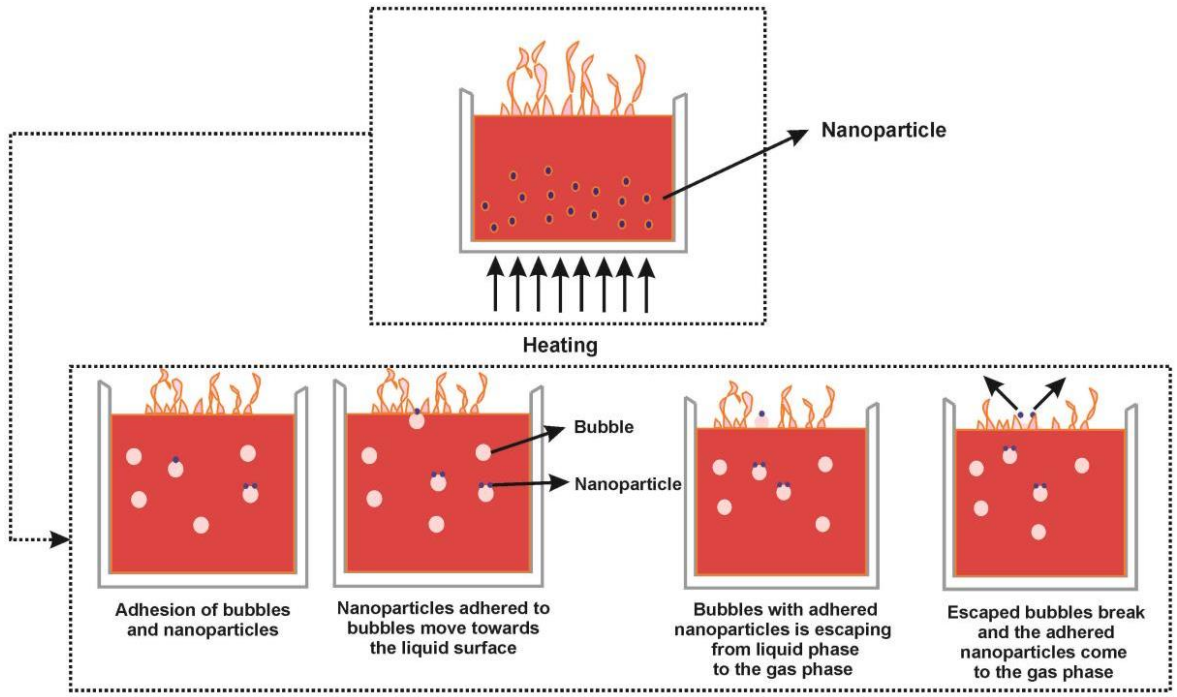


Figure 21. Representation of nanoparticle migration by bubble adhesion. Adapted from Ref. [187].

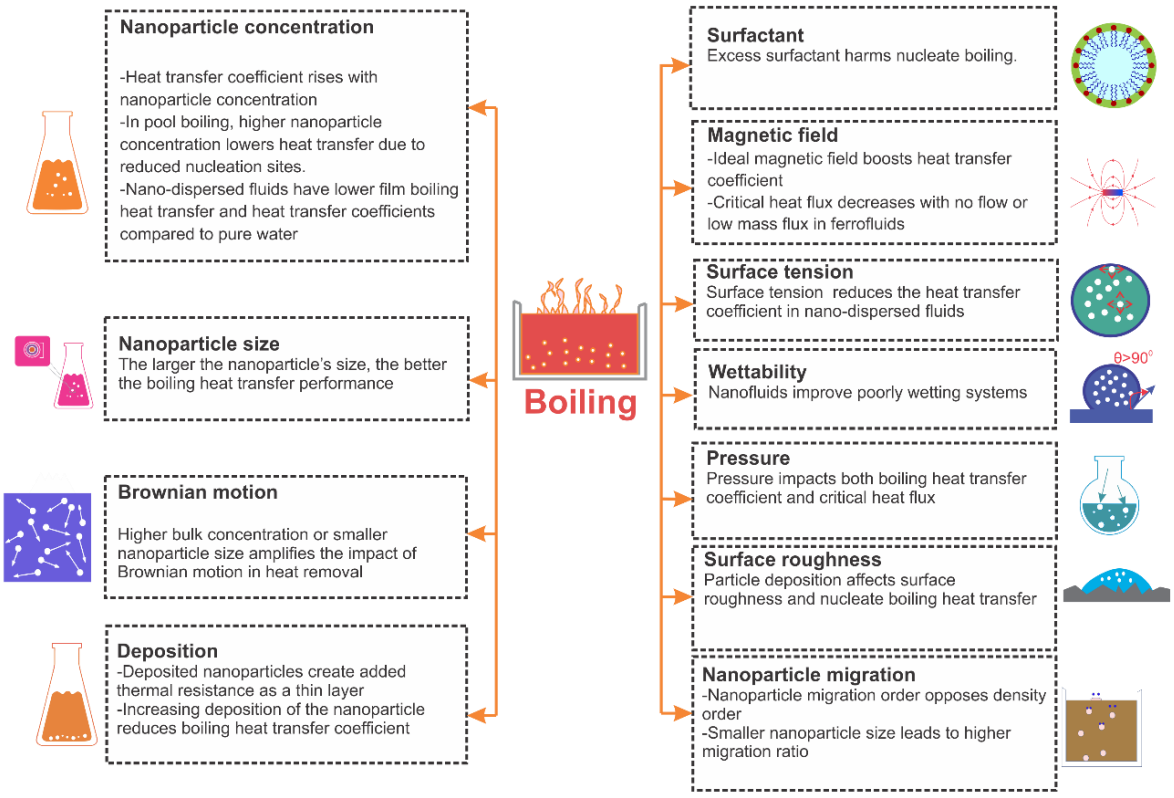


Figure 22. Effects of different factors on the nano-enhanced boiling process [187].

6. Evaporation

Evaporation can occur at any temperature and typically occurs at the surface of a liquid without the formation and movement of bubbles, in contrast to the boiling process described earlier [28]. Evaporation occurs when the saturation pressure of the liquid at the prevailing temperature is higher than the partial pressure of vapor in the surrounding environment. The liquid evaporation phenomenon plays a significant role in various applications such as refrigeration, phase change cooling, and aviation, which utilize the heat absorption and cooling effects of evaporation. Droplet evaporation is a common phenomenon in daily life and has various applications. For instance, in the medical field, the evaporation characteristics of healthy and patient blood droplets on a substrate, and the drying patterns after evaporation, can be used for initial disease diagnosis. When nanoparticles are introduced into the droplets, evaporation is enhanced, leading to higher heat-transfer rates. However, the presence of nanoparticles, along with factors such as nanoparticle type, concentration, droplet surface tension, wettability, and Marangoni effect, can give rise to unique phenomena during evaporation, such as the formation of "coffee rings." These phenomena can significantly affect the evaporation rate [188-191]. Figure 23 shows the experimental setup and working principle of the evaporation process for the nanofluids. The effects of different factors on the evaporation rate of the nano-dispersed fluids are discussed in the following sections.

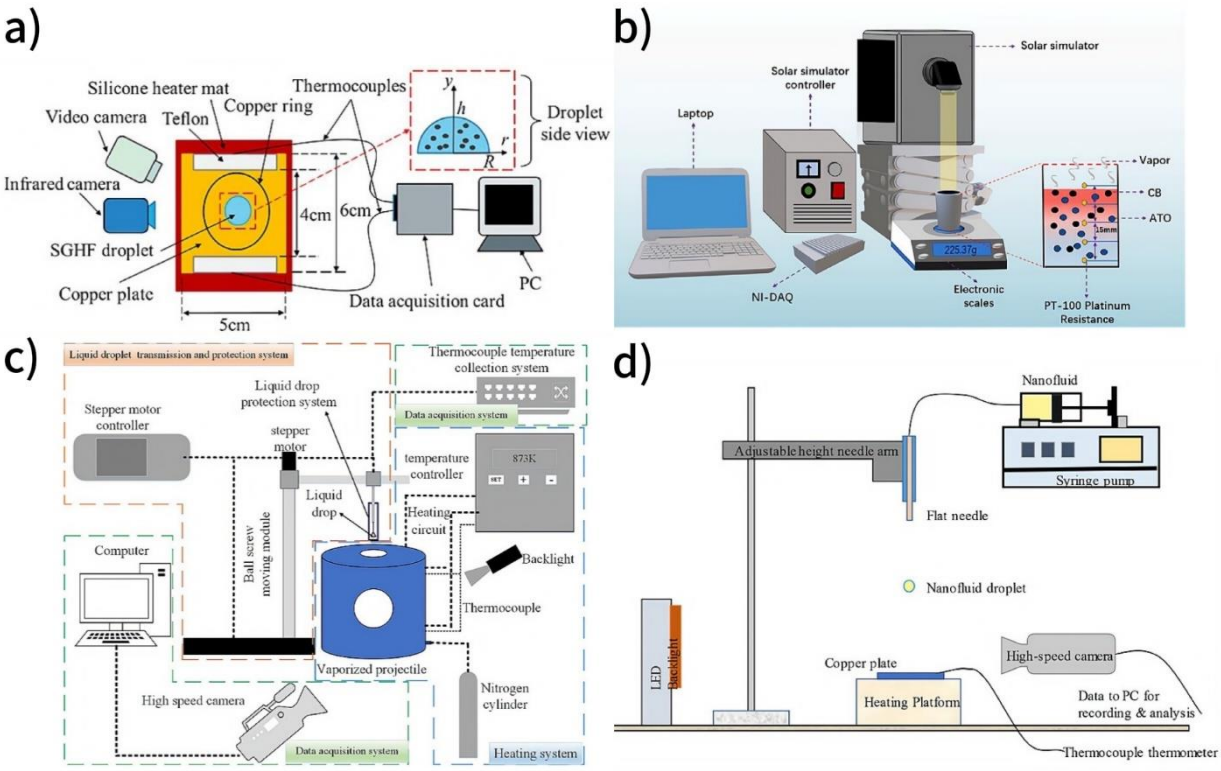


Figure 23. Schematic diagram of the experimental setup and the working principle of the evaporation process for nanofluids: a) SGHF droplet evaporation and boiling. Reproduced with permission from Int. J. Heat Mass Transfer. 180, 121786 (2021). Copyright 2021 Elsevier Ltd.[192] b) evaporation generation. Reproduced with permission from Renewable Energy. 199, 509-516 (2022). Copyright 2022 Elsevier Ltd.[193] c) droplet evaporation process. Reproduced with permission from Fuel. 254, 115633 (2019). Copyright 2019 Elsevier Ltd.[194] d) droplet morphology analysis. Reproduced with permission from Int. J. Heat Mass Transfer. 183, 122172 (2022). Copyright 2021 Elsevier Ltd.[195].

6.1. Effects of nanoparticle concentration and morphology

6.1.1. Nanoparticle type

When analyzing different types of nanoparticles such as titanium oxide, zirconium oxide, iron oxide, and nickel/iron-water, researchers have observed that the addition of iron oxide, nickel/iron-water, and zirconium oxides to deionized water led to a gradual decrease in the evaporation rate

[11]. The nanoparticle concentration was identified as the primary factor influencing the reduction in the evaporation efficiency. This result showed that achieving a high evaporation reduction efficiency required maintaining a low concentration of nickel and iron in the water.

Gan and Qiao [196] conducted experiments using multiwalled carbon nanotubes (MWCNTs) in ethanol, aluminum in ethanol, and carbon nanoparticles (CNPs) at a fixed concentration of 0.1% by weight. They reported that adding MWCNTs or CNPs to ethanol-based nanofluids resulted in a higher droplet evaporation rate than that of pure ethanol. Among these, the MWCNTs in the ethanol-based nanofluid led to the highest droplet evaporation rate. In a study involving quantum dot water (Silwet L-77) at concentrations of 0.5 and 0.007% by weight, it was found that incorporating nanoparticles into surfactant aqueous solutions caused a deterioration of dispersion (or diffusion) rates and the formation of double coffee rings [197]. Furthermore, studies have shown that the dispersion of graphene nanoparticles can be enhanced using GO and polyethylene glycol (PEG), thereby increasing the evaporation rate [198]. Chen et al. [198] observed that reduced GO- and PEG-based nanofluids, unlike pure water, demonstrated higher evaporation rates at ambient temperature.

6.1.2. Nanoparticle concentration

Numerous studies have shown that the addition of nanoparticles can improve the droplet evaporation rate. In other words, fluid droplets with higher nanoparticle concentrations tend to exhibit faster transient evaporation rates [199]. However, when the nanoparticle concentration was low, the evaporation rate of the nanofluid droplets did not show significant differences from that of the pure water droplets. Research also indicates that nanofluids have substantial potential for solar vapor generation because of their excellent absorptivity, especially in scenarios involving free-convection turbulent evaporation [200]. Therefore, a proportional relationship exists between the nanoparticle concentration and residual deposits [201].

In droplet evaporation driven by radiative heat transfer, nanoparticles in the fluid alter their overall light absorption properties, leading to differences in radiation and evaporation characteristics compared with ordinary fluids. Increasing the nanoparticle concentration decreased the transmittance and absorptivity of certain nanofluid solutions, allowing them to absorb more energy. This change results in higher interfacial temperatures and evaporation rates [202]. Furthermore, the nanoparticle concentration also influences the evaporation temperature. For example, higher nanoparticle concentrations can facilitate higher evaporation temperatures under forced convective laminar flow [203].

The concentration of nanoparticles in a nanofluid affects both the viscosity of the fluid and surface tension of the droplets formed during evaporation. Higher nanoparticle concentrations typically result in an increased nanofluid viscosity and surface tension. This phenomenon is often disadvantageous for droplet evaporation because it creates a greater resistance that needs to be overcome during the evaporation process. Consequently, more heat absorption is required to achieve effective evaporation [204]. Lin et al. [205] conducted experiments to analyze the contact angle of nanofluid droplets using silicon dioxide-water nanofluids at various concentrations (0.01, 0.5, 1.0, and 5.0% by weight). Their findings demonstrated that the setback of the contact angle of the surface was consistently higher than that of nanofluid droplets. A higher initial nanoparticle concentration was also necessary to generate larger residual deposits.

6.1.3. Nanoparticle size

The size of the nanoparticles plays a crucial role in influencing the evaporation behavior of nanofluid droplets, with smaller nanoparticle sizes leading to decreased enthalpy of evaporation [199]. Nanofluid evaporation can be categorized into three distinct stages. In the initial stage, the evaporation process is primarily dominated by the liquid phase. During this

stage, the behavior of the nanofluid evaporation closely resembles that of pure water. The liquid volume decreases during the intermediate stage. Here, the physical and thermal conductivities of the nanoparticles become more significant. The excellent thermal conductivity of the nanoparticles resulted in intermittent temperature and heat flux fluctuations. Finally, in the final stage, as the evaporation approaches completion, the liquid diminishes, and the solution approaches a nearly dried state. During this phase, the size of the nanoparticles is a critical factor that significantly influences the remaining evaporation process [206].

In a study by Ganesan et al. [207], it was observed that the size of particle clusters increased with higher nanofluid concentrations. This growth of clusters was attributed to the increasing volume of the nanofluid, which caused the suspended particles to aggregate as fractal structures. Another study, focusing on nanoparticle size as the primary influencer, highlighted the fact that nanofluid droplets containing 60 wt% by weight nanoparticles maintained a substantial contact angle [208]. In contrast, reducing the nanoparticle concentration to 5% by weight decreased the droplet diameter, contact angle, and droplet height. Wasik et al. [209] investigated the evaporation of a nanofluid containing zinc oxide nanoparticles. Upon completion of the liquid evaporation, residual hierarchical surface structures associated with the nanoparticles were observed. The formation of these structures is linked to the morphology, size, and crystallinity of the zinc oxide particles. These characteristics affect the rapid dissolution of isobutylamine-coated zinc oxide nanocrystals, which is influenced by the initial moisture content.

6.2. Surface factors

6.2.1. Surface tension

A comprehensive study was conducted to analyze the impact of nanoparticles on the evaporation process under natural convection conditions, with a specific focus on surface tension and intermolecular van der Waals forces [210]. During the initial evaporation stage,

when the nanoparticles were still in a relatively low concentration within the solution, their dispersed state did not influence the surface tension. However, as evaporation progressed to later stages, most of the liquid evaporated, causing nanoparticles to accumulate near the substrate. In this phase, the few remaining nanoparticles within the liquid were significantly affected by the surface tension owing to the thin liquid layer and limited space for nanoparticle movement.

Investigating aluminum nanoparticle-ethanol nanofluids with a concentration of 3% by weight, Gerken et al. [211] found no discernible correlation between surface tension and the concentration of aluminum nanoparticles. Instead, they observed a gradual reduction in the D-square evaporation rate with increasing concentration of aluminum nanoparticles. Moreover, when comparing the effect of nanoparticle agglomerate packing near the droplet surface, it became evident that there was a second-order effect on the evaporation of aluminum nanoparticle-ethanol pendant droplets during the initial stages.

6.2.2. Wettability

The evaporation of nanofluid droplets was also significantly influenced by wettability. The evaporation rate of the nanofluid droplets on the surface of the residue left after evaporation showed a distinct correlation with the size of the residue. When droplets diffuse across a wetted residue, they come into increased contact with air, resulting in an expanded contact area and an accelerated evaporation rate. Computational investigations revealed that silver-graphene nanofluids exhibit significantly higher evaporation rates, up to 370% higher than silver nanofluid droplets. This enhanced performance can be attributed to the increased wettability of the residue surface [188].

In a study involving gold-argon nanodroplets, numerical simulations focused on wettability as the key parameter [39]. Experimental observations demonstrated that an increased nanoparticle volume within the droplet hindered its overall evaporation, revealing a

direct relationship between the nanoparticle volume percentage and evaporation rate. For wetted surfaces, the localized evaporation of the droplet was most prominent around the three-phase line and gradually diminished along the vertical axis. Conversely, for the non-wetted surfaces, the areas of maximum evaporation were situated in the middle and upper regions of the droplet.

6.3. Microphysical influence mechanisms

6.3.1. Motion of nanoparticles due to field gradient

In a computational study conducted by Wang et al. [212] focusing on copper-water nanofluids undergoing free convection and influenced by Brownian motion, the distribution of nanoparticles was found to significantly impact both the evaporation rate and surface tension. The introduction of lyophilic nanoparticles led to an exponent 'h' in the D^h law of less than 2, signifying a distinct divergence from the norm. Adding lyophobic nanoparticles resulted in an exponent 'h' higher than 2. Notably, their investigation revealed a trend where lyophilic nanoparticles with a higher volume fraction exhibited a substantially higher 'h' value, while lyophobic nanoparticles with a lower volume fraction demonstrated a smaller 'h' value.

6.3.2. Microconvection

Albernaz et al. [213] employed hexane as a nanofluid to investigate its forced-convection behavior and conducted a numerical study. Their research examined the Marangoni effect, where the temperature difference at the droplet surface was directly linked to the velocity of the center of the droplet. Given that the evaporation process of a droplet involves heat absorption, this gives rise to a lower temperature region at the droplet's boundary, resulting in a higher evaporation rate. Moreover, the internal flow within the droplet during evaporation is vigorous. Experimental observations revealed that the maximum concentration of

nanoparticles occurred both at the droplet's surface and at the center, whereas the smallest particle concentration was located at a distance of $1/\sqrt{2}$ times the radius from the center [214, 215]. It must be noted that microconvection is also associated with the enhancement of the local heat transfer that leads to bubble nucleation and evaporation rates [216].

6.3.3. Nanoparticle migration

The evaporation of the droplets creates a complex flow pattern within the droplets, where the flow direction varies with time. The liquid flow during evaporation was designed to balance the spatial distribution of evaporation and the effect of the capillary pressure on the droplet interface shape. Porous media undergoing evaporation have significantly different deposition mechanisms compared to porous media undergoing drainage [217]. An experimental study using nanoparticles at a concentration of 0–0.004% during sessile droplet evaporation revealed that deposition patterns showed scattered dots and radial spokes. In addition, multiple rings were observed to occur repeatedly owing to the constant contact radius and contact angle [218].

6.3.4. Radiation

The application of laser irradiance, which is preferentially absorbed by the nanoparticles, leads to an enhanced evaporation rate, influenced by factors such as the power of the laser beam and nanoparticle concentration [219]. A combined numerical and experimental analysis involving graphite-ethanol nanofluids at concentrations of 1%, 3%, and 5%, exposed to a 2-mW infrared radiation field, revealed that the absorption of radiation by the particles caused a temperature rise, resulting in increased evaporation. Interestingly, the accumulation of particles on the droplet surface reduced the effective area ratio and suppressed evaporation [220, 221]. Figure 24 illustrates the various parameters of a single particle trapped at the liquid-particle-gas interface.

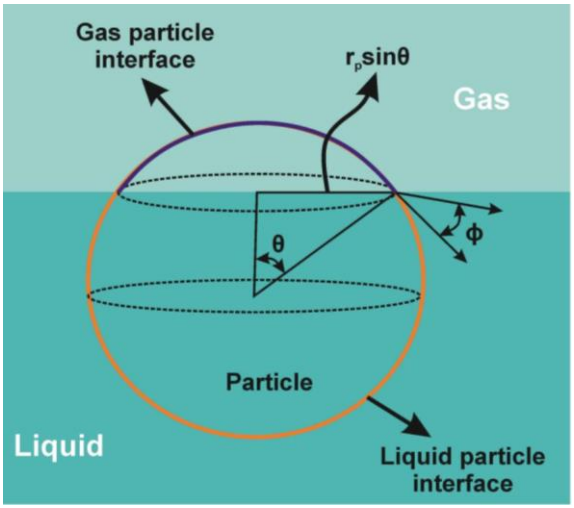


Figure 24. Illustration of parameters associated with the single particle trapped at liquid–particle–gas interface. Adapted from Ref. [192].

Radiation has been established as an influential factor for enhancing the evaporation rate of nanofluids, particularly in ethanol-based systems that evaporate at lower temperatures. Adding MWCNTs and CNPs to ethanol-based nanofluids has been shown to achieve an increased evaporation rate. Subsequent experimental investigations demonstrated that the evaporation rate of MWCNT-doped ethanol surpasses that of CNP or aluminum-doped ethanol, indicating varying enhancement effects [196]. In a different context, an experimental analysis involving polystyrene-water nanofluids with a concentration of 0.3% by weight, exposed to a high-power laser with a wavelength of 2.9 μm, revealed that the laser-induced flow induces selective aggregation of particles of distinct sizes and pattern manners due to localized heating effects [222].

6.3.5. Sonication

Ultrasound has been shown to significantly influence the performance and stability of nanofluids. Research has demonstrated that under the impact of ultrasound, the evaporation rate increases, with a higher ultrasound power yielding greater effects. Interestingly, distilled

water subjected to ultrasound evaporated faster at equivalent evaporation temperatures than distilled water without ultrasound treatment. This phenomenon also extends to nanofluids, where ultrasonic waves lead to analogous effects on the evaporation rate of the liquid droplets. Applying ultrasound at 120-minute intervals to nanofluid droplets enhanced their light absorption capacity and evaporation rate [223]. Furthermore, an increase in the nanofluid concentration contributes to a small increase in the sensibility efficiency. A comprehensive visualization of the impact of various parameters on the nano-enhanced evaporation process is shown in Figure 25.

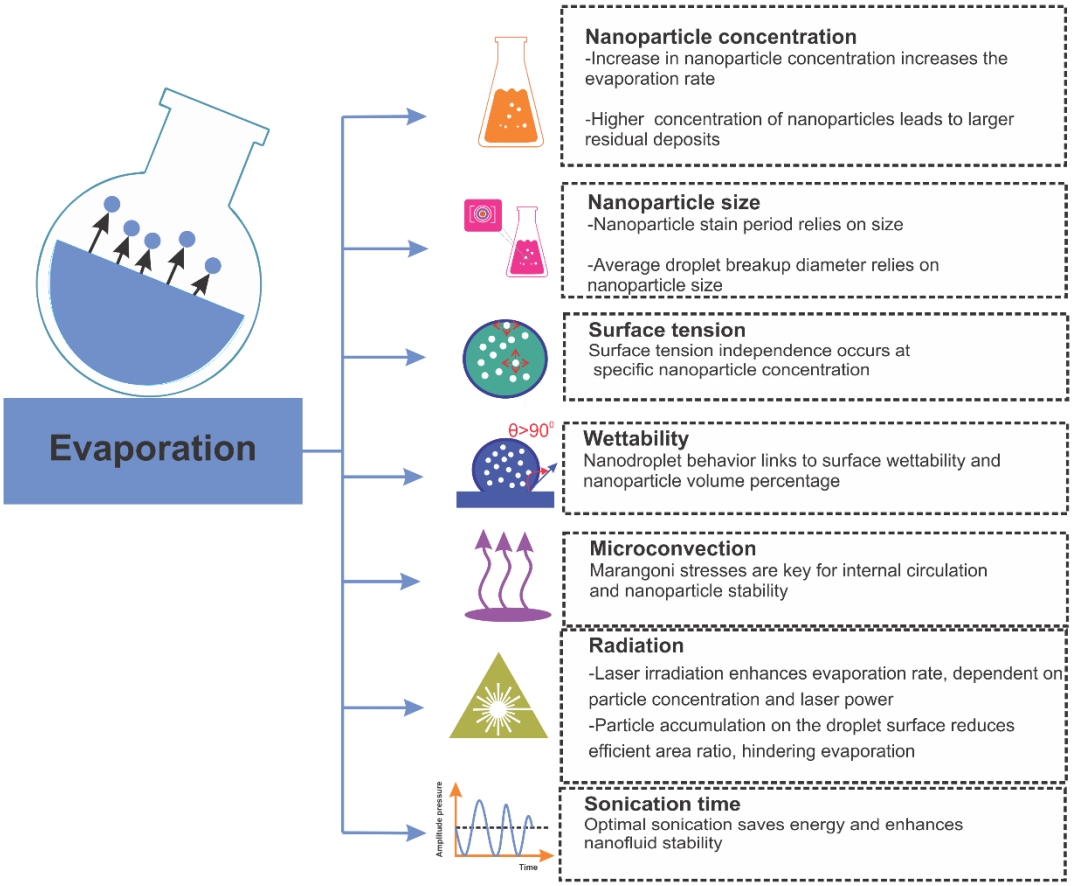


Figure 25. Influences of different parameters on the nano-enhanced evaporation process [223].

7. Condensation

From the perspective of heat and mass transfer, condensation involves the migration of vapor molecules, accompanied by a phase transition at the vapor-liquid boundary that releases latent heat. This heat was then conveyed to the cooling equipment through the condensation layer. This process releases a substantial amount of latent heat, even with minute temperature differences. As a result, it substantially enhances the heat transfer capacity of heat exchange surfaces, significantly improves the total energy transfer and conversion efficiency, and has broad applications in the petrochemical industry, electronics manufacturing, building energy conservation, and waste heat recovery [224]. In general, condensation can be categorized into film and dropwise condensation.

In the case of film condensation, the condensate initially wets the cooling surface to form a liquid film, which then descends under the influence of gravity. As vapor condenses onto the film, the thickness of the liquid layer increases. Bead condensation involves the formation of condensed vapor droplets, which dot the cooling surface with numerous droplets of varying sizes [28]. A schematic illustration of the film and dropwise condensation is shown in Figure 26. Typically, the HTC associated with dropwise condensation is considerably higher than that associated with thin-film condensation. Nevertheless, thin-film condensation is dominant in most applications [225]. Recently, significant attention has been directed toward nanostructured superhydrophilic/hydrophobic surfaces that exhibit the potential to enhance condensation heat transfer. The various experimental setups for investigating these surfaces are shown in Figure 27. The subsequent sections examine the effect of introducing nanomaterials on the condensation phase transition phenomenon.

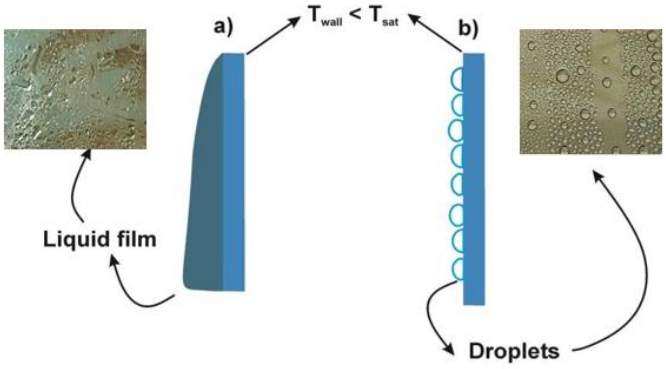


Figure 26. Representation of condensation process: a) film condensation, and b) dropwise condensation (photographs are reproduced with permission from J Clean Prod. 265, 121758 (2020). Copyright 2020 Elsevier Ltd. [226]).

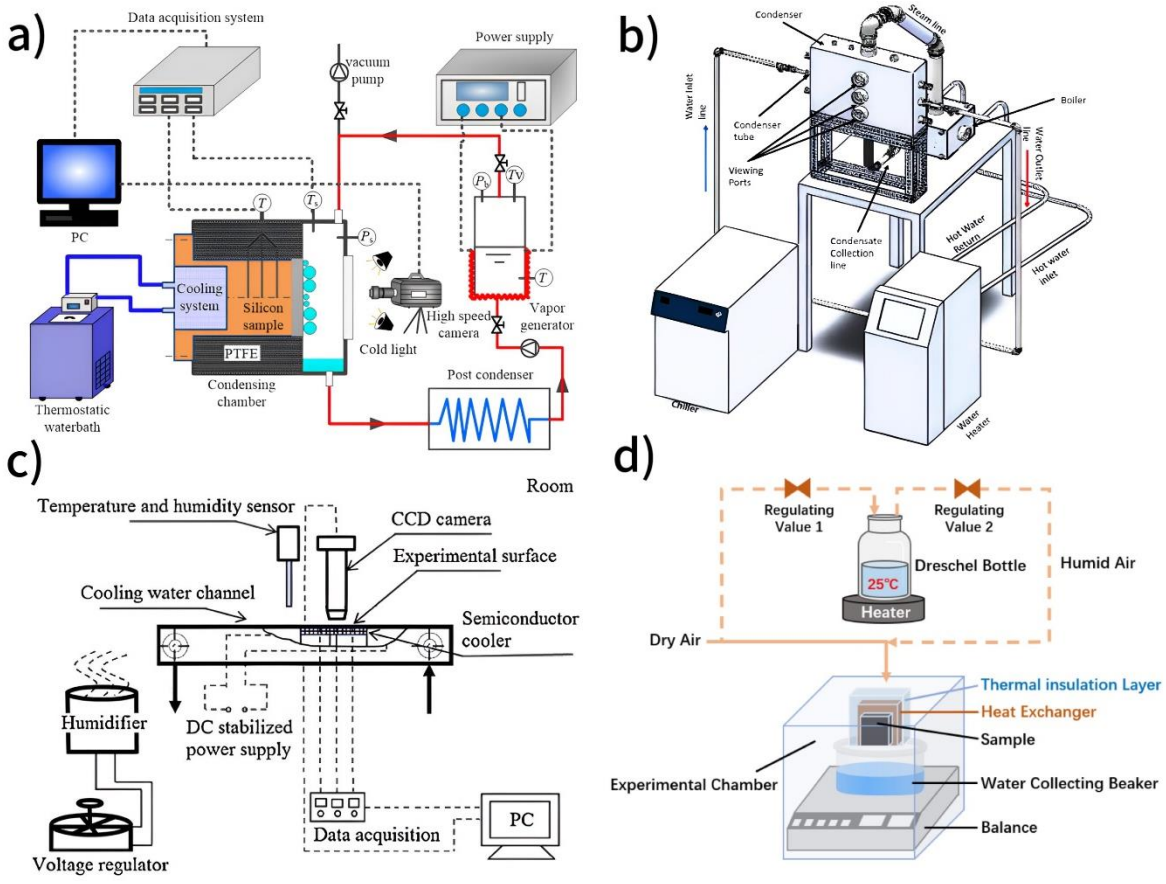


Figure 27. Schematics of the experimental setup on nanostructured superhydrophilic/hydrophobic surfaces for enhanced condensation heat transfer: a) experimental setup of pure steam condensation. Reproduced with permission from Int. J. Heat Mass Transfer. 177, 121526 (2021). Copyright 2021

Elsevier Ltd. [227, 228] b) external condensation apparatus for heat transfer measurement in drop condensation. Reproduced with permission from Int. J. Heat Mass Transfer. 65, 619-626 (2013). Copyright 2013 Elsevier Ltd.[229] c) condensation characteristics of fabricated metallic superhydrophobic surfaces setup. Reproduced with permission from Appl. Surf. Sci. 371, 322-328 (2016). Copyright 2016 Elsevier B.V.[230] d) composite adsorbent-coated superhydrophilic-nanostructured heterogeneous surface setup. Adapted from Ref. [231].

7.1. Effects of nanoparticle concentration and morphology

7.1.1. Nanoparticle type principles of effects

In a typical condensation process, heat transfer primarily occurs within the condensing film and is primarily influenced by the thickness of the film and the rate of condensation. These parameters are intricately related to the thermophysical properties of the fluid and can be controlled by adding nanoparticles. Nanoparticles enhance the thermal conductivity of conventional fluids, thereby enhancing the overall efficiency of the heat-exchange process. It is worth noting that the type of nanoparticles introduced had a direct impact on the thermal properties of the fluid. For instance, in a study conducted by Cui et al. [232], copper nanoparticles were incorporated into an argon fluid using molecular dynamics simulations. The results of this investigation substantiate the positive effect of nanoparticles on improving the thermal behavior of the fluid and enhancing its structural thermal conductivity.

7.1.2. Nanoparticle concentration

Several studies have examined the influence of the nanoparticle concentration on condensation heat transfer, revealing noteworthy insights. Ghorbani et al. [233] conducted experiments involving various copper oxide nanoparticle concentrations and observed a significant enhancement in the condensation HTC, registering a 14% increase at a nanoparticle mass fraction

of approximately 1.5% compared with an oil/refrigerant mixture. Another investigation led by Ahmadpour and Akhavan-Behabadi [13] explored the impact of different MWCNTs on condensation flow. The results highlighted the remarkable contribution of nanoparticles, particularly in scenarios involving low and medium steam masses. Specifically, the local heat transfer of R600a/oil/MWCNT showed a substantial improvement of 68% compared to R600a under specific conditions involving a mass velocity of 280 kg/m^2s and nanoparticle mass fraction of 0.3%.

The impact of copper oxide nanoparticle concentration on flow condensation was investigated by Peng et al. [234]. Their research highlighted that the condensation HTC is directly correlated with the nanoparticle concentration and vapor mass flux. Notably, the most significant improvement in heat transfer occurred at a 1% mass fraction of nanoparticles, leading to a remarkable 40% increase in the HTC. However, it is important to note that increasing the nanoparticle concentration may also increase the pressure drop. Moreover, high concentrations can lead to the aggregation and settling of many nanoparticles, potentially obstructing the pipeline. Strict control over the nanoparticle concentration may be recommended to prevent the adverse effects of severe pressure drops on heat-mass transfer [234].

In addition to experimental investigations, researchers have developed mathematical models to quantify the influence of nanoparticle concentrations on the condensation transition process. Famileh et al. [235] constructed a mathematical model to examine how the concentration of nanoparticles such as silicon dioxide, sodium chloride, and copper affects condensation. Their model demonstrated that higher-density nanoparticles exhibited lower deposition efficiency and particle turbulence, thus enhancing heat-mass transfer. Under various conditions, the utilization of nanoparticles consistently led to improvements in the mass

transfer coefficient, resulting in accelerated condensation rates. Famileh et al. [235] emphasized that the extent of this impact depends on the inlet velocity.

7.1.3. Nanoparticle size

The effect of nanoparticle size on heat-mass transfer during condensation is as significant as that of nanoparticle concentration. Recent research by Ghahremanian et al. [236] examined the influence of argon-copper nanoparticle size on nanofluid condensation. They observed that an increase in nanoparticles within the condensate flow not only enhanced the heat flux correlation, but also hastened the attainment of equilibrium, effectively reducing the time required to reach it. Interestingly, their study demonstrated that using larger-diameter nanoparticles at a specific volume fraction yielded superior thermal conductivity and condensation performance compared with utilizing larger mass nanoparticles.

Another numerical investigation by Heysiattalab et al. [237] sought to determine the heat-transfer rate of Fe_3O_4 nanoparticles of varying sizes. Their findings revealed that larger-diameter nanoparticles facilitated greater migration within the membrane, thereby enhancing the nanoparticle volume fraction at the cold wall. However, an increased nanoparticle concentration resulted in a higher velocity profile within the membrane, which was not conducive to improving HTC. Consequently, the research indicated that smaller diameter nanoparticles at lower concentrations had a more pronounced effect on improving HTC.

7.2. Surface and environmental factors

7.2.1. Wettability

Exploring hybrid wettability surface patterns is important for advancing condensation heat transfer. Hybrid wetting surfaces can regulate the generation of condensate droplets within a superhydrophobic region. In addition, these surfaces facilitated the creation and detachment of

liquid bridges, effectively preventing the accumulation of droplets along the hydrophobic region. This mechanism accelerates the renewal process of the surface in the hydrophobic region, leading to an amplified heat-exchange capacity on the superhydrophobic surface. Consequently, these advancements collectively contribute to the enhancement of the condensation heat transfer. Among various patterns, implementing a stripe pattern with a specific inclination angle on mixed-wettability surfaces has been notably effective in bolstering condensation heat transfer on superhydrophobic surfaces [238].

7.2.2. Temperature and pressure

Peng et al. [234] examined the impact of copper oxide nanoparticles on condensation. They observed a reduction in the thickness of the liquid film, which was attributed to the interactions between the vapor and liquid velocities. Moreover, the HTC increased owing to the nanoparticle concentration and the superheat temperature. Interestingly, the enhancement in heat transfer was more pronounced at lower mass flux levels.

7.3. Microphysical influence mechanisms

7.3.1. Motion of nanoparticles due to field gradient

Sheikholeslami et al. [239] conducted a study on the influence of Brownian motion and frictional pressure drop on the condensation heat transfer enhancement with nanoparticles. For copper oxide nanoparticles, their findings revealed that adding nanoparticles increased the frictional pressure drop of the channel. This result can be attributed to the combined effects of Brownian motion and the accumulation of nanoparticles within the tube, leading to enhanced fluid conduction and micro-convection. On a related note, Avramenko et al. [240] reported that the diffusion driven by thermophoresis positively impacted the heat transfer in channels.

However, the role of Brownian diffusion was observed to have an opposite effect on the heat transfer enhancement during condensation.

7.3.2. Agglomeration

Li et al. [241] made an interesting observation regarding the solidification process of Fe-Ni-Cr clusters in their investigation of inert-gas condensation involving ternary nanoparticles. They noted that the solidification of these clusters proceeded gradually from the inner region and was facilitated by the development of multifold twins. Their findings also revealed a linear correlation between the solidification temperature and particle size, suggesting a linear size inhibition effect on the solidification behavior of the nanoparticles.

7.3.3. Nanoparticles migration

Nanoparticles in a base liquid undergo random migration owing to thermal and Brownian motions. The distribution of the nanoparticle volume fraction was influenced by Brownian motion, leading to an uneven concentration. On the other hand, the thermophoretic force drives nanoparticles to migrate against the temperature gradient from warmer regions to cooler ones, further affecting the distribution. Manipulating the nanoparticle diameter can affect intramembrane migration, increase the nanoparticle concentration at the cold wall, and enhance the velocity distribution within the membrane. This change emphasizes the advantages of utilizing smaller nanoparticles to improve the cooling performance [237].

The optimal cooling performance is achieved when the magnetic field aligns with the temperature gradient. The effects of different factors on the enhancement of nano-enhanced phase-change processes, including freezing, melting, boiling, evaporation, and condensation, are illustrated in Figure 28. To summarize recent research findings, Table 1 provides a concise overview of the effects of several parameters on phase change phenomena.

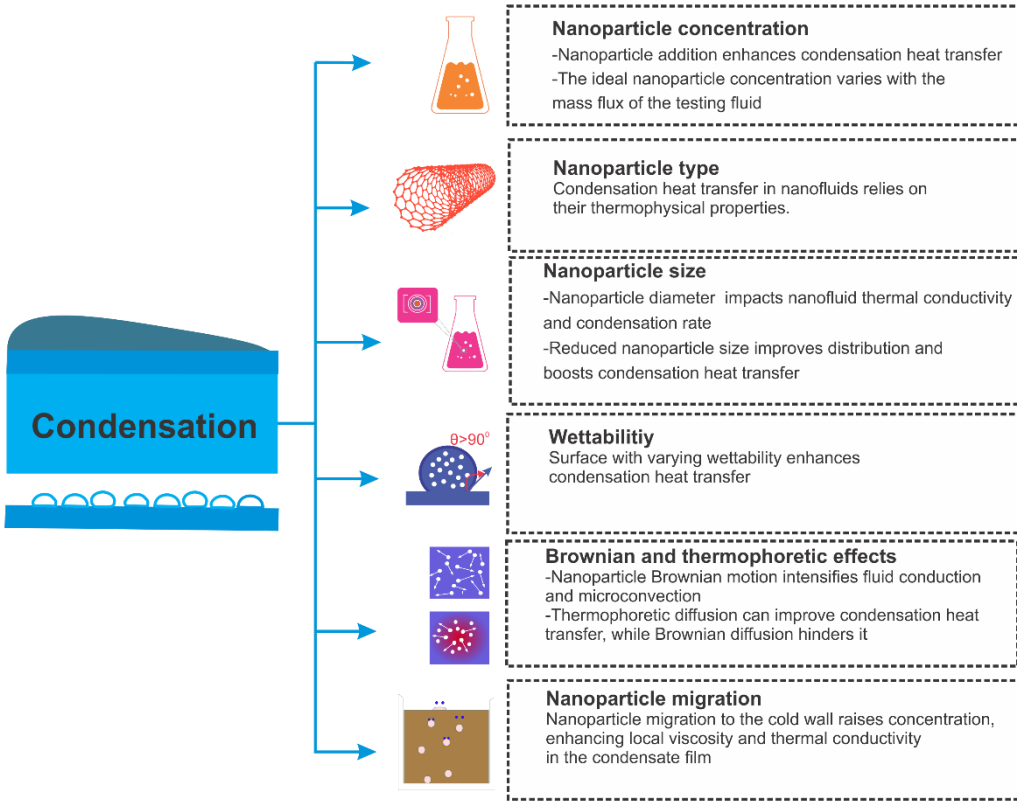
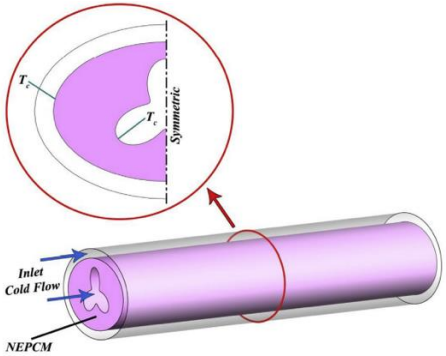
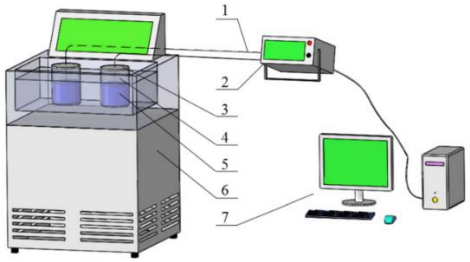
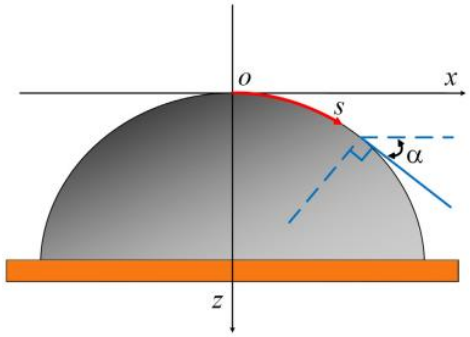
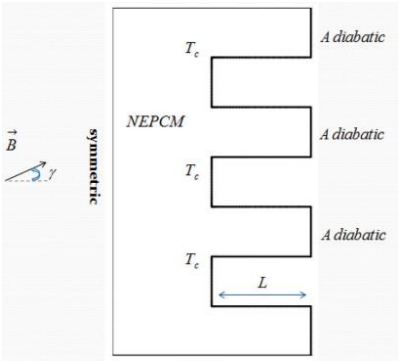
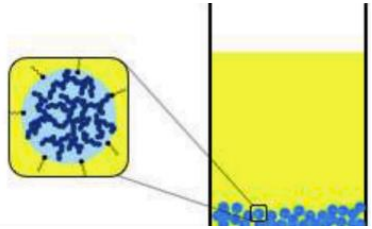
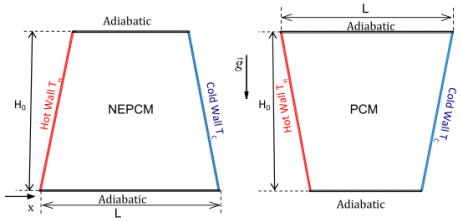
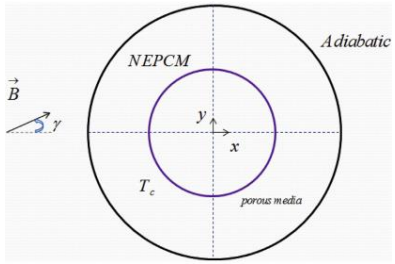
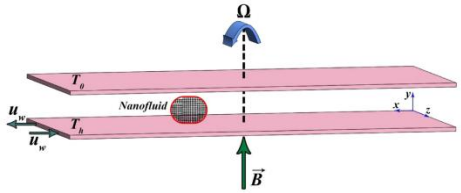
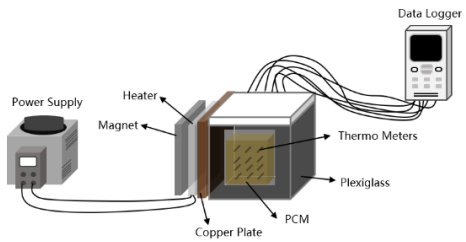


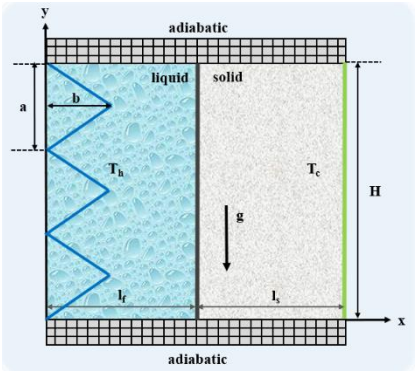
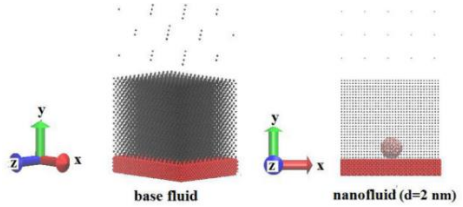
Figure 28. Effects of different factors on nano-enhanced condensation process [237].

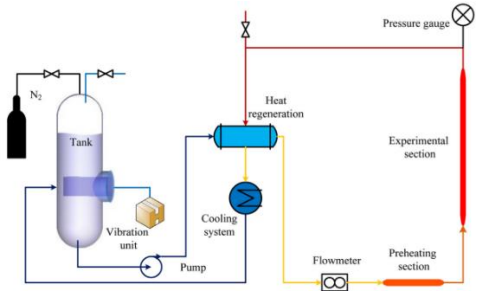
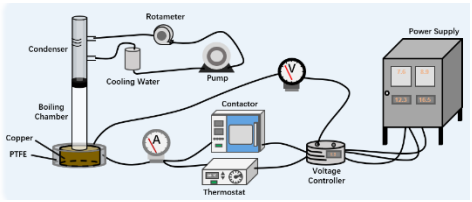
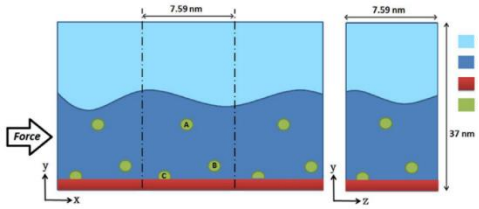
Table 1. Influences of different factors on nano-enhanced phase change phenomena.

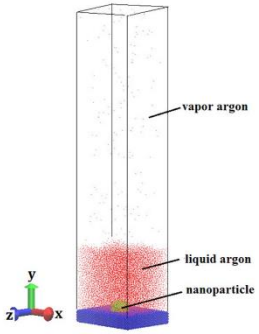
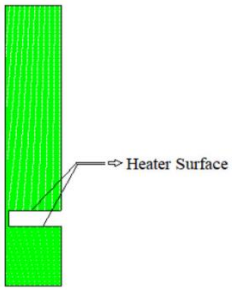
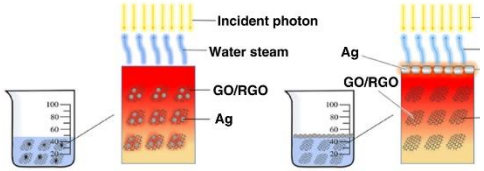
Phase change phenomenon	Method	Nanoparticle/ Nanofluid	Influences	Schematic/geometry	Remarks	Ref
Freezing	Numerical	Copper oxide/water	Concentration	 Thermal storage with two cold flows from the side	Enhancing the shape factor and adding nanomaterial to pure water could result in a shortened solidification timeframe.	[62] Reproduced with permission from J. Mol. Liq. 296, 111731 (2019). Copyright 2019 Elsevier B.V.
	Experimental	Expanded graphite / Octanoic acid and Myristic acid	Surfactant	 Constant low-temperature tank device for measuring thermal performance	When immersed in expanded graphite with up to 93% n-octanoic acid-myristic acid, the thermal conductivity is significantly enhanced by >230%.	[72] Reproduced with permission from J. Mol. Liq. 288, 111092 (2019). Copyright 2019 Elsevier B.V.

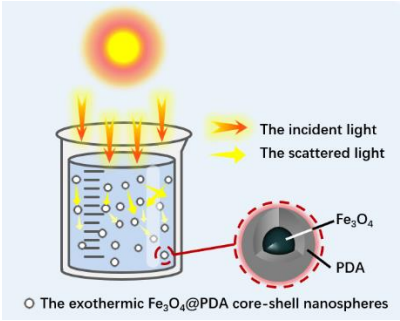
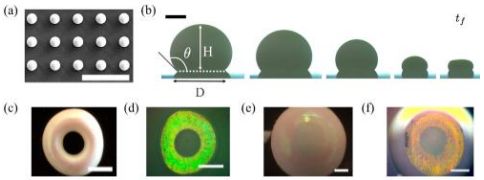
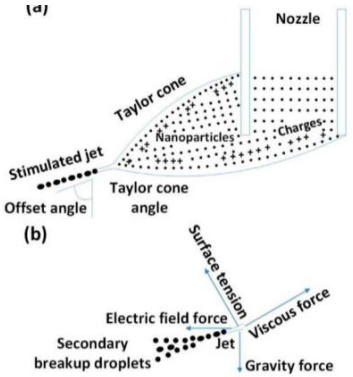
Experimental	Copper /ferrofluid	Magnetic field	 Coordinate system of ferromagnetic droplet analysis attached to the substrate surface.	Through magnetic or compressive conditions, extension or reduction of droplet freezing duration was observed.	[76] Reproduced with permission from Appl. Therm. Eng. 176, 115444 (2020). Copyright 2020 Elsevier Ltd.
Numerical	CuO/water	Magnetic field	 Latent heat storage configuration	The entropy output was increased with greater buoyancy forces, while it was decreased with higher magnetic field strength.	[63] Reproduced with permission from Int. Commun. Heat Mass Transfer. 117, 104715 (2020). Copyright 2020 Elsevier Ltd.
Experimental	Silica nanoparticle aqueous suspensions	Agglomeration	 Flocculated silica microparticle sedimentation after freezing	Nanoparticles were transformed into flocculated masses, and the fraction of emulsion volume and droplet size determined the resulting microstructure.	[82] Reproduced with permission from Int. Microporous Mesoporous Mater. 305, 110362 (2020). Copyright 2020 Elsevier Inc.

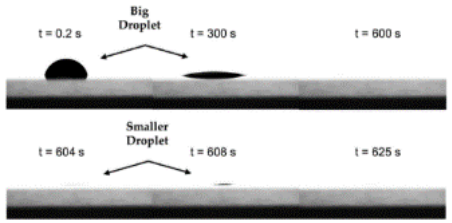
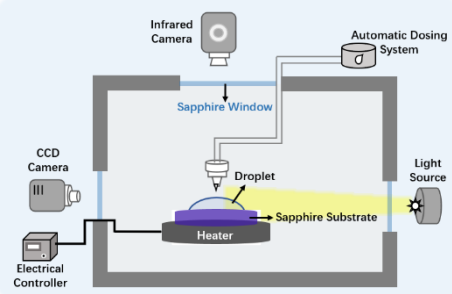
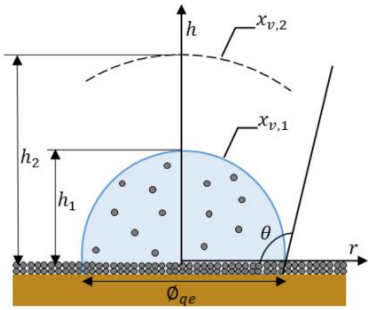
	Numerical	Graphene-PCM	Concentration	 (a) Case I (b) Case II Schematic diagram of boundary dimensions and heat transfer parameters of the model.	The melting rate of NePCM did not monotonically change with the concentration of nanoparticles.	[90] Reproduced with permission from J. Mol. Liq. 292, 110592 (2019). Copyright 2019 Elsevier B.V.
	Numerical	CuO-water	Concentration, magnetic field, Rayleigh number	 Influence of external magnetic field on heat storage	Using a magnetic field and adding nanoparticles could facilitate the solidification of the PCM. The time required to freeze PCM was increased with increasing Rayleigh number.	[110] Reproduced with permission from J. Cleaner Prod. 215, 963-977 (2019). Copyright 2019 Elsevier Ltd.
Melting	Numerical	CuO-water	Rotation viscosity, magnetic melting, concentration	 Physical model	With the increase of nanofluid concentration, the temperature was increased, and the melting parameters were decreased.	[92] Reproduced with permission from Physica A. 541, 123036 (2020). Copyright 2019 Elsevier B.V.
	Experimental	Fe_3O_4	Concentration, magnetic field		Fe_3O_4 magnetic nanoparticles could diminish the horizontal temperature gradient, reducing melting time. Applying a magnetic field could further decrease melting time and augment heat transfer in paraffin.	Adapted from Ref. [112].

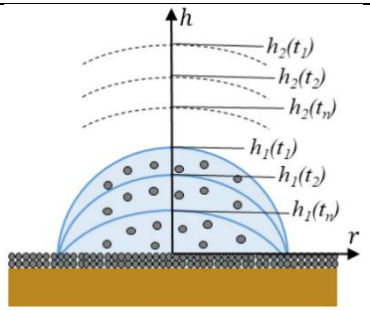
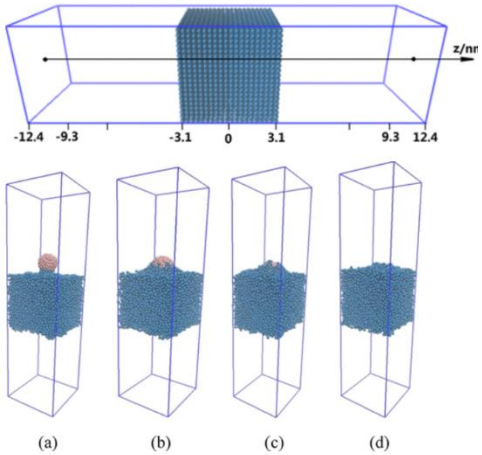
			Schematic of the experimental setup		
Numerical	CNT-water	Concentration, Hartmann number, magnetic inclination angle, corrugation number and height	 Physical model and boundary conditions	An increase in the quantity and height of corrugation waves led to a decrease in heat transfer and alterations in the characteristics of the melt front curve. Compared to pure water, heat transfer was enhanced with the presence of nanofluid regardless of applying a magnetic field.	Adapted from Ref. [113].
Experimental	NiO/Deionized water	Magnetic field	 The picture of the boiling copper surface	A high-intensity magnetic field could reduce the HTC of NiO nanofluid at high concentrations. The magnetic field could minimize sedimentation at diluted NiO concentrations and benefit sedimentation at high concentrations.	[43] Reproduced with permission from Powder Technol. 376, 398-409 (2020). Copyright 2020 Elsevier B.V.
Simulation	Cu/water	Deposition, wettability of the surface, nanoparticle size	 Initiation boiling model	Compared to the base fluid, the deposition of nanoparticles improved the surface wettability and the boiling conditions of the fluid. The heat transfer capacity of nanofluids was increased by decreasing particle size.	[143] Reproduced with permission from Int. J. Multiphase Flow. 115, 9-18 (2019). Copyright 2019 Elsevier Ltd.

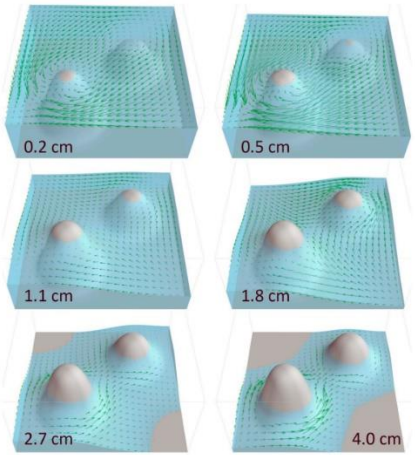
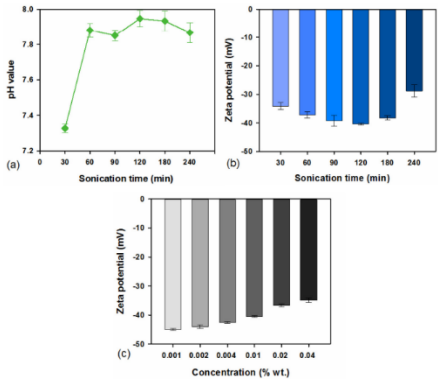
Boiling	Experimental	SiC/water, Graphite/water	Aggregation, Deposition, Contact angle	 Experimental device diagram of nanofluid flow boiling.	Nanoparticle aggregation near the triple-phase axis led to a reduction in the contact angle. The deposition of nanoparticles on the heated surface resulted in an increased porous sub-layer and improved wettability. Experimental facility of nanofluid flow boiling.	[183] Reproduced with permission from Int. J. Heat Mass Transfer. 158, 119985 (2020). Copyright 2020 Elsevier Ltd.
	Experimental	SiO_2/ Deionized water	Surfactant	 A view of boiling heat transfer apparatus.	The boiling HTC of SiO_2 nanofluid containing sodium laureth sulfate and cetyltrimethylammonium bromide surfactants tended to decrease with increasing concentration, while with the polysorbate 20 surfactant, the HTC was increased.	Adapted from Ref. [242].
	Simulation	Cu/Ar	Deposition, wettability of the surface	 Model established for nanofluids flow boiling investigation	The heat transfer efficiency caused by the nanoparticle deposition could be attributed to: In both pool boiling and flow boiling, the frequency of bubble nucleation was increased, and surface wettability was enhanced.	[150] Reproduced with permission from Int. J. Heat Mass Transfer. 162, 120338 (2020). Copyright 2020 Elsevier Ltd.

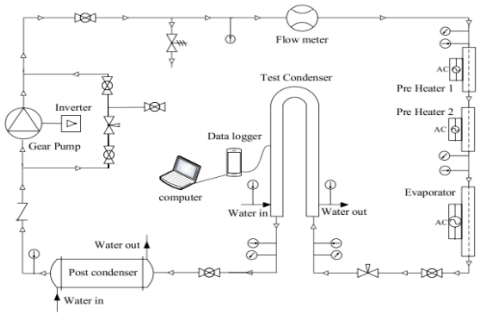
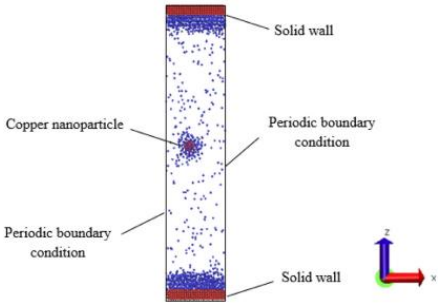
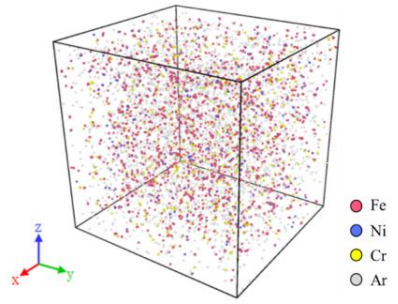
Simulation	Cu/water	Wettability of nanoparticles	 Simulation system after nanoparticle deposition.	Nanoparticles with diverse wettability characteristics were shown to enhance heat transfer during explosive boiling. The wettability alteration due to nanoparticle deposition pronouncedly impacted the interactions at the solid/liquid interface and thermal resistance.	[243] Reproduced with permission from Int. J. Therm. Sci. 145, 105977 (2019). Copyright 2019 Elsevier Masson SAS.
Numerical	Al_2O_3/water	Thermophoresis	 Meshed model of the geometry (2-D).	Gradient temperature, heat, viscosity, and buoyancy significantly influenced the thermophoresis velocity relationship.	[182] Reproduced with permission from J. Mol. Liq. 301, 112459 (2020). Copyright 2020 Elsevier B.V.
Experimental	GO-water, Reduced GO +Ag-Water, GO+Ag-Water	Concentration, Type	 RGO/GO+Ag nanofluid	The RGO nanofluid had a stronger solar vapor generation capacity due to its greater absorption capacity. The efficiency of RGO-Ag was greater than that of GO-Ag, GO-Ag, and RGO-Ag.	[200] Reproduced with permission from Energy Convers. Manage. 199, 112019 (2019). Copyright 2019 Elsevier Ltd.

	Experimental	Fe_3O_4 @Polydopamine	Concentration, surfactant	 Graphical abstract	Due to its high light-absorbing ability, Fe_3O_4@polydopamine nanofluid provided a high evaporation efficiency of 70% at low irradiation.	Adapted from Ref. [244].
	Numerical	SiO_2-Water	Size	 Side-view snapshots of an evaporating droplet containing 5% by weight silica nanoparticles on a superhydrophobic substrate	The droplets of nanofluid containing 60% by weight nanoparticles exhibited a sustained wide contact angle during the initial drying phase. In contrast, droplets loaded with 5% by weight nanoparticles showed a decrease in contact angle, droplet diameter, and droplet height.	[208] Reproduced with permission from Langmuir. 36(17), 4835-4841 (2020). Copyright 2020 American Chemical Society.
Evaporation	Numerical	Al/n-decane	Size	 Electrostatic breakup mechanism of nanofluid fuel and the force analysis of the stimulated jet	Smaller-sized Al nanoparticles exhibited a more significant tendency towards agglomeration and precipitation behaviors. The relationship between the diameter of the average breakup droplet and nanoparticle size followed a nonlinear trend.	[245] Reproduced with permission from Energy Fuels. 34(1), 1082-1092 (2020). Copyright 2020 American Chemical Society.

Experiential	Quantum dots-water, Silwet L-77—water	Type	 Diffusion and evaporation of Silwet L-77 critical aggregation concentration aqueous solution containing quantum dots	When nanoparticles were introduced into an aqueous surfactant solution, their spreading velocity tended to degrade, forming a double coffee ring pattern.	[197] Reproduced with permission from Langmuir. 36(14), 3798-3813 (2020). Copyright 2020 American Chemical Society.
Experimental	PEGylated GO and RGO	Type	 Schematic of the experimental setup	PEGylated GO functionalization could accelerate the dispersion of graphene nanoparticles and the evaporation rate. RGOylated PEG nanofluid droplets experienced a greater evaporation rate at ambient temperature than water.	Adapted from Ref. [198].
Experimental and numerical	0.1 Ag-0.9 GNP (graphene nanoplates), 0.9 Ag-0.1 GNP	Type and Wettability		The presence of wetting residues on the nanofluid droplets of GNP and MR-1 increased the contact area between droplets and air and improved the droplet evaporation rate. With the high wettability of the residue surface at V_{fd}/V_{sd}=20, the maximum evaporation rate of MR-1 mixed nanofluid droplets was 370% higher than that of Ag.	[188] Reproduced with permission from Int. J. Heat Mass Transfer. 153, 119618 (2020). Copyright 2020 Elsevier Ltd.

			 Droplet and pinned droplet evaporation		
Numerical	Cu-Water	Brownian motion	 Simulation box and indrawn nanoparticle.	The arrangement of nanoparticles played a pivotal role in dictating the rate of evaporation and surface tension. Including hydrophilic nanoparticles resulted in an index less than 2, and the higher the volume fraction, the larger the h value, whereas hydrophobic nanoparticles have the opposite effect.	[212] Reproduced with permission from Langmuir. 36(4), 919-930 (2020). Copyright 2020 American Chemical Society.

Numerical	-	Nanoparticles migration	 Six simulation results at different capillary pressures	Evaporation caused by pore water flow could lead to the deposition of suspended nanoparticles even without good adhesion.	[217] Reproduced with permission from J. Contam. Hydrol. 226, 103524 (2019). Copyright 2019 Elsevier B.V.
Experimental	MWCNT/ GNP	Sonication	 Zeta potential at different pH values, sonication times, and concentrations	Incorporating nanofluid concentration could facilitate energy localization by transferring photothermal heat to the nanofluid, consequently elevating the surface temperature of the nanofluid. This temperature rise resulted in a slight enhancement of the responsive efficiency by increasing the nanofluid concentration.	[223] Reproduced with permission from Ultrason. Sonochem. 61, 104817 (2020). Copyright 2019 Elsevier B.V.

Condensation	Experimental	MWCNT	Nanoparticle concentration	 Schematic diagram of the test condenser system	Incorporating MWCNT nanoparticles demonstrated a more pronounced improvement in heat transfer. The highest local heat transfer enhancement in the R600a/oil/MWCNT system was achieved at a nanoparticle concentration of 0.3%.	[13] Reproduced with permission from Int. J. Therm. Sci. 146, 106110 (2019). Copyright 2019 Elsevier Masson SAS.
	Numerical	Argon-Copper	Nanoparticle size	 Two solid walls and one copper nanoparticle position atoms in the computational domain	At a constant nanoparticle volume fraction, increasing particle diameter could improve the thermal conductivity of nanofluid condensation better than increasing particle number.	[236] Reproduced with permission from J. Mol. Liq. 311, 113310 (2020). Copyright 2020 Elsevier B.V.
	Numerical	Fe-Ni-Cr	Agglomeration	 Typical equilibrated mixture atomic configuration	Cluster solidification was initiated in the inner region, marked by structural relaxation by creating layered face-centered cubic and hexagonal close-packed structure layers or multiple twins. This process gradually extended toward the surface as solidification progressed.	[241] Reproduced with permission from Comput. Mater. Sci. 177, 109579 (2020). Copyright 2020 Elsevier B.V.

8. Outlook, challenges, and future scope

This article emphasizes the substantial enhancement in thermal performance resulting from the incorporation of nanomaterials into phase-change processes. Further research is essential for our comprehensive understanding of the underlying mechanisms, determining the effects of key parameters, and establishing optimal operating conditions for the impact of nanomaterials on phase change. These findings demonstrate that increasing the concentration of the nanoparticles can accelerate the melting rate. It is noteworthy, however, that higher concentrations also extended the melting time, indicating the existence of an optimal concentration. Conversely, during the curing process, the influence of nanomaterials on the curing rate remains less pronounced at lower concentrations, but it significantly increases upon reaching the optimal concentration.

Studies have shown that nanoparticles exhibit more pronounced effectiveness in enhancing solidification than in melting. Therefore, optimizing the phase-change heat-transfer mechanisms necessitates a holistic consideration of key parameters, including the temperature, molecular structure of the base fluid, nanoparticle morphology, type, concentration, and nanoparticle interactions. For boiling phenomena, it is evident that surface nanoparticles can adversely affect the boiling characteristics. An elevated concentration of nanofluids can lead to an increase in viscosity, subsequently impeding the efficiency of boiling heat transfer. However, enhancing the surface wetting with nanoparticles presents a promising avenue for significantly augmenting the heat transfer. A more intriguing inquiry pertains to maintaining an optimal boiling heat transfer rate.

For condensation, it becomes evident that the thermal resistance within the liquid film is the main hindrance to the heat transfer. This phenomenon, known as membrane condensation heat transfer, revolves around the dynamics of the liquid film. The film thickness and prevailing flow conditions significantly influenced the overall condensation heat-transfer process. Elevating the efficiency of condensation heat transfer necessitates a vital step: mitigating the impact of noncondensable gases, which form a protective gaseous layer around the cooling

surfaces. In this endeavor, the use of nanoparticles has emerged as a valuable strategy. These nanoparticles not only enhance local adhesion but also facilitate the efficient conduction of heat within the film by inducing controlled migration of the cold wall. Looking into the future, further inquiries should investigate innovative methods for enhancing film condensation performance through the well-planned integration of nanoparticles.

Nanoparticles manufactured with robust interfacial effects and substantial specific surface areas undoubtedly hold an upper hand in enhancing the heat conduction of PCMs. The preparation of composite PCMs by incorporating nanoparticles with high thermal conductivity has emerged as a burgeoning area of research. Phase-change energy storage is a potent means to greatly enhance thermal management, finding versatile applications in battery thermal management, industrial heat recovery, solar thermal utilization, and building thermal regulation. Notwithstanding the capacity of PCMs to absorb or release significant latent heat with higher energy storage density and temperature stability, their limited thermal conductivity constrains their operational efficiency and performance. Thus, the integration of nanomaterials has emerged as a pivotal strategy for augmenting the thermal conductivity of PCMs.

The practical application of nanomaterials presents several challenges; the selection of suitable nanomaterials and determination of their optimal concentration remain key considerations. The diverse thermal conductivity and compatibility properties of different nanomaterials necessitate thorough evaluation. In addition, the influence of nanomaterial quantity and dispersion on PCM thermal conductivity requires in-depth scrutiny to ensure even dispersion and maximize the thermal conductivity effect within the PCM.

In the future, the trajectory of research encompasses the development of novel nanomaterials, fine-tuning of addition methods, enhancement of PCM thermal conductivity, exploration of synergistic applications of PCMs with other thermal storage technologies, and evaluation of economic feasibility. These multifaceted endeavors collectively pave the way for

the advancement and broader application of PCM technology to meet the demands of future sustainable energy development.

While simpler models for phase change processes have emerged in recent years, their applicability to real-world scenarios remains limited. In numerical simulations of nano-phase transitions, the ability to forecast the behavior of multiphase flow systems is indispensable. In addition, it is crucial to integrate phase transition models to obtain the heat and mass transfer source terms, which can then be incorporated into the energy or mass equations. This comprehensive approach facilitates an accurate portrayal of the nano-phase transition heat transfer processes, broadening the horizons of their application.

In summary, utilizing nanotechnology to optimize thermal systems and adopt advanced waste-to-energy recovery systems can effectively address energy and environmental problems and achieve sustainable development [246]. Approximately 40 TWh of energy is projected to be conserved annually in the UK by employing waste heat recovery techniques [247]. Therefore, there is a pressing need to prioritize the development of advanced waste-to-energy recovery systems utilizing various techniques such as nanoparticles, which can effectively decrease both energy consumption and CO_2 emissions.

9. Conclusion

A thorough and critical analysis of recent studies on the introduction of nanoparticles into phase transition phenomena has been performed, including freezing (solidification), melting, boiling, evaporation, and condensation. In this study, several key observations were made.

Freezing (solidification):

- The solidification rate of the liquid phase is affected by both the morphology and concentration of nanoparticles. Within certain limits of the particle size and concentration, nanoparticles with small size and high concentration can lead to higher solidification rates.

- The surfactant concentration influences the subcooling and freezing times of the nanofluid. Moreover, the initial temperature influences the latent heat release and accelerates solidification.
- Nanomaterials aggregate, with the microstructure of particle agglomerates being influenced by factors such as the emulsion volume fraction and droplet size.
- External electric or magnetic fields influence the particle motion and enhance the velocity at the solid-liquid interface during solidification. Notably, ferrohydrodynamic and magnetohydrodynamic effects hold substantial sway over conductive ferromagnetic fluids, resulting in shortened solidification times.
- The phenomenon of "repulsion" at the solid-liquid interface influences the solidification process in the PCMs. In nanoparticle interactions, a high particle volume fraction leads to decelerated formation of the solid-liquid interface, whereas the impact of particle size on the rate of interface formation becomes more pronounced.
- Surfactants on the surface of nanoparticles are effective in preventing particles from colliding and aggregating with each other, which in turn improves nucleation efficiency.
- Micro- and nano-bubbles can significantly increase the rate at which the solutions freeze. When combined, micro- and nano-bubbles increase nucleation and crystal growth rates.

Melting:

- As the melting process progresses, the influence of some metal and metal oxide nanoparticles becomes progressively pronounced, resulting in higher melting rates at higher volume fractions.
- Research has indicated that incorporating nanoparticles reduces the temperature gradients and causes a subsequent decrease in the melting time. This result is due to the increased heat conduction enabled by the nanoparticles, which can be further enhanced by a magnetic field.
- An increase in the magnetic number leads to a decrease in the melting rate. Moreover, the melting rate decreased at a certain magnetic number as the Hartmann number increased.

Furthermore, the temperature gradients inside the bulk material were enhanced at higher melting parameters and Rayleigh numbers.

- Longer fin lengths contribute to improved heat absorption and heat transfer effectiveness, whereas thinner fins allow for greater energy absorption. The addition of fins to tubing leads to higher transfer rates and reduced charging times.

Boiling:

- Boiling HTC is usually inversely proportional to the particle volume concentration. In addition, the influence of pressure on the boiling HTC decreases with an increase in particle concentration. As the nanoparticles were adsorbed onto the surface, the rate of boiling is dramatically decreased with an increase in concentration, minimizing the surface roughness.
- The boiling heat transfer of nanofluids is affected by the Brownian motion of nanoparticles. Brownian motion is improved when the volume concentration of the nanoparticles increases or the particle size decreases.
- Thermal swimming phenomena lead to the accumulation of nanoparticles at gas-liquid interfaces, resulting in maximum concentration, whereas the heating wall exhibits the lowest concentrations, leading to an uneven overall particle distribution. Moreover, smaller nanoparticles enhance the heat transfer rates, whereas larger nanoparticles can impede the heat transfer.
- Nanoparticle deposition enhances surface wettability, thereby increasing the critical heat flux (CHF) of nanofluids during boiling. The wettability of the deposited nanoparticles significantly influences the solid-liquid interactions and thermal resistance at the interface. The improved wettability contributes to more effective heat transfer.
- During pool boiling, the deposition of nanoparticles in a thin surface layer reduces bubble generation, leading to a lower boiling point and an enhanced HTC. The deposited nanoparticles

can decrease the contact angle, with the degree of reduction proportional to the nanoparticle concentration. This change contributed to the improved surface wetting and increased CHF.

Evaporation:

- The viscosity of nanofluids and surface tension both increase with the concentration of particles, a phenomenon that is detrimental to evaporation because of the need to overcome a greater transport resistance, which also means that more heat must be absorbed.
- The impact of nanodroplets on the surface wetting and evaporative activity is closely related to the surface wettability. A higher nanoparticle volume fraction resulted in a larger contact angle, which reduced the evaporation rate on hydrophilic surfaces. The influence of nanoparticle concentration on evaporation was more pronounced for neutral and hydrophobic surfaces, and diminished with increasing concentration.
- Ultrasound significantly affects the stability and properties of the nanofluids. For a given evaporation temperature, the evaporation rate of distilled water with ultrasound applied was higher than that of distilled water without the ultrasound effect, and the evaporation rate was positively correlated with the applied ultrasonic power. For nanofluids, ultrasonic waves have the same effect on the evaporation rate of the liquid droplets.

Condensation:

- Nanoparticles enhance the condensation HTC, and optimal nanoparticle concentrations maximize the HTC of various types of fluids.
- The condensation HTC increases with an increase in nanoparticle concentration and steam mass flux, and at a low mass flux, nanoparticles can enhance heat transfer more significantly.
- Using denser nanoparticles results in lower deposition efficiencies and lower levels of particle turbulence, leading to enhanced heat and mass transfer rates.
- Surface-modified nanoparticles introduce higher wettability and better condensation and heat transfer performance.

- Employing smaller nanoparticles can yield an improved cooling performance owing to nanoparticle migration driven by thermophoresis (a consequence of Brownian motion). The optimal cooling was achieved when the magnetic field was aligned with the temperature gradient.

Acknowledgements

The work in this article has been financially supported by the National Natural Science Foundation of China (Grant number 52176061 and 52476186) and the Scientific and Technological Innovation Project of Carbon Emission Peak and Carbon Neutrality of Jiangsu Province (Grant number BE2022028-4). This work was also supported by the UK Engineering and Physical Sciences Research Council (EPSRC) (Grant numbers EP/T03338X/1 and EP/S032622/1). Data supporting this publication can be obtained on request from the first author. For the purpose of Open Access, the authors have applied a CC BY public copyright licence to any Author Accepted Manuscript version arising from this submission.

Conflict of interest

The authors have no conflicts to declare.

Credit Author Statement

Liu Yang: Conceptualization (lead); Writing – original draft (equal); Writing – review and editing (equal); Investigation (equal); Project administration (lead); Validation (lead); Funding Acquisition(lead). **Jialu Tian:** Writing – original draft (supporting); Writing – review and editing (equal); Investigation (equal). **Yulong Ding:** Writing – review and editing (equal). **Avinash Alagumalai:** Conceptualization (supporting); Writing – original draft (equal); Writing – review and editing (equal). **Fatih Selimefendigil**: Writing – review and editing (equal).

Mortaza Aghbashlo: Writing – review and editing (equal). **Meisam Tabatabaei:** Writing – review and editing (equal). **L. Godson Asirvatham:** Writing – review and editing (equal). **Somchai Wongwises:** Supervision (supporting); Writing – review and editing (equal). **S.A. Sherif**: Review and editing (equal), Investigation (equal). **Efstathios E. Michaelides**: Writing – review, and editing(equal). **Christos N. Markides**: Writing – review and editing (equal), Investigation (equal). **Omid Mahian:** Supervision (lead); Project administration (supporting); Writing – review and editing (equal).

Data availability

The data that support the findings of this study are available from the corresponding author upon reasonable request.

Nomenclature

A	$Surface\ area, \quad m^2$
C_p	$Isobaric\ specific\ heat, \quad J/kg \cdot K$
D_T	$Translational\ diffusion\ coefficient, \quad m^2/s$
g_0	$Force\ conversion\ factor(dimentionless)$
K_B	$Boltzmann\ constant, \quad 1.38 \times 10^{-23}\ J/K$
R_a	$Rayleigh\ number$
R_e	$Reynolds\ number$
T_∞	$Surrounding\ temperature, \quad K$
T_b	$Base\ temperature, \quad K$
T_c	$Critical\ temperature, \quad K$
T_s	$Surface\ temperature, \quad K$
Bo	$Bond\ number$
D	$Diffusion\ coefficient, \quad m^2/s$
F	$Faraday\ constant, \quad C/mol$
g	$Acceleration\ due\ to\ gravity, \quad m/s^2$
h	$Heat\ transfer\ coefficient, \quad W/m^2 \cdot K$
Ha	$Hartmann\ number$
J	$Current\ density, \quad A/m^2$
k	$Thermal\ conductivity, \quad W/m \cdot K$
Nu	$Nusselt\ number$
P_r	$Prandtl\ number$
q	$Charge\ density, \quad C/m^3$
Sh	$Sherwood\ number$

St	$Stefan\ number$
T	$Temperature,\quad K$
v	$Velocity,\quad m/s$
We	$Weber\ number$
ΔT_e	$Excess\ temperature,\quad K$

Greek symbols

μ_0	$Vacuum\ permeability,\quad N/A^2$
$\Delta\gamma$	$Magnetic\ susceptibility,\quad m^3/kg$
μ	$Dynamic\ viscosity,\quad Pa \cdot s$
ρ	$Density,\quad kg/m^3$
σ	$Surface\ tension,\quad N/m$
Φ	$Electric\ potential,\quad V$

Subscripts

f	$Saturated\ liquid$
$f\ g$	$Difference\ between\ the\ saturated\ vapor\ and\ saturated\ liquid\ values\ of\ the\ same\ property$
l	$Liquid\ phase$
v	$Vapor\ phase$

References

1. K. Binder, "Introductory Statistical Mechanics," *Eur. J. Phys.* 21(2), 197 (2000). https://doi.org/10.1088/0143-0807/21/2/701
2. A. Faghri and Y. Zhang, "1 - INTRODUCTION TO TRANSPORT PHENOMENA," *Academic Press*. 1-106 (2006). https://doi.org/10.1016/B978-0-12-370610-2.50006-4
3. T. Yamaguchi, G. Nagayama, T. Tsuruta, Y. Jiang, S. Maruyama, K. Okuyama, Y. Saito, K. Suzuki, M. Tange and I. Ueno, "Chapter 6 - Topics on Boiling: From Fundamentals to Applications," *Elsevier*. 443-777 (2017). https://doi.org/10.1016/B978-0-08-101010-5.00006-3
4. M. J. Pitkethly, "Nanomaterials – the driving force," *Mater. Today*. 7(12, Supplement), 20-29 (2004). https://doi.org/10.1016/S1369-7021(04)00627-3
5. T. Mahbub and M. E. Hoque, "Chapter 1 - Introduction to nanomaterials and nanomanufacturing for nanosensors," *Elsevier*. 1-20 (2020). https://doi.org/10.1016/B978-0-12-820702-4.00001-5
6. C. Dhand, N. Dwivedi, X. J. Loh, A. N. J. Ying, N. K. Verma, R. W. Beuerman, R. Lakshminarayanan and S. Ramakrishna, "Methods and strategies for the synthesis of diverse nanoparticles and their applications: a comprehensive overview," *Rsc Advances*. 5(127), 105003-105037 (2015). https://doi.org/10.1039/c5ra19388e
7. S. Link and M. A. El-Sayed, "Shape and size dependence of radiative, non-radiative and photothermal properties of gold nanocrystals," *Int. Rev. Phys. Chem.* 19(3), 409-453 (2000). https://doi.org/10.1080/01442350050034180
8. K. L. Kelly, E. Coronado, L. L. Zhao and G. C. Schatz, "The Optical Properties of Metal Nanoparticles: The Influence of Size, Shape, and Dielectric Environment," *The Journal of Physical Chemistry B*. 107(3), 668-677 (2003). https://doi.org/10.1021/jp026731y
9. V. A. A. Raj and R. Velraj, "Review on free cooling of buildings using phase change materials," *Renewable Sustainable Energy Rev.* 14(9), 2819-2829 (2010). https://doi.org/10.1016/j.rser.2010.07.004
10. N. Hajighafoori Boukani, A. Dadvand and A. J. Chamkha, "Melting of a Nano-enhanced Phase Change Material (NePCM) in partially-filled horizontal elliptical capsules with different aspect ratios," *Int. J. Mech. Sci.* 149, 164-177 (2018). https://doi.org/10.1016/j.ijmecsci.2018.09.056
11. M. Moghiman and B. Aslani, "Influence of nanoparticles on reducing and enhancing evaporation mass transfer and its efficiency," *Int. J. Heat Mass Transfer*. 61, 114-118 (2013). https://doi.org/10.1016/j.ijheatmasstransfer.2013.01.057
12. H. Peng, G. Ding, W. Jiang, H. Hu and Y. Gao, "Heat transfer characteristics of refrigerant-based nanofluid flow boiling inside a horizontal smooth tube," *Int. J. Refrig.* 32(6), 1259-1270 (2009). https://doi.org/10.1016/j.ijrefrig.2009.01.025
13. M. M. Ahmadpour and M. A. Akhavan-Behabadi, "Experimental investigation of heat transfer during flow condensation of HC-R600a based nano-refrigerant inside a horizontal U-shaped tube," *Int. J. Therm. Sci.* 146, 106110 (2019). https://doi.org/10.1016/j.ijthermalsci.2019.106110
14. I. M. Shahrul, I. M. Mahbubul, S. S. Khaleduzzaman, R. Saidur and M. F. M. Sabri, "A comparative review on the specific heat of nanofluids for energy perspective," *Renewable Sustainable Energy Rev.* 38, 88-98 (2014). https://doi.org/10.1016/j.rser.2014.05.081
15. M. Gupta, V. Singh, R. Kumar and Z. Said, "A review on thermophysical properties of nanofluids and heat transfer applications," *Renewable Sustainable Energy Rev.* 74, 638-670 (2017). https://doi.org/10.1016/j.rser.2017.02.073
16. J. Chai, J. Wang and Q. Ni, "Experiment on heat transfer performance of phase change materials strengthened by nanoparticles and fins," *Energy Storage Science and Technology*. 11(10), 3161-3170 (2022). https://doi.org/10.19799/j.cnki.2095-4239.2022.0021
17. X. Wu, Q. Wang, K. Wang, L. Gao, H. Liu, C. Wang and Y. Wang, "Review on thermophysical property and application of organic composite phase change material

enhanced by nano-particle," *New Chemical Materials*. 49(04), 40-45 (2021). https://doi.org/10.19817/j.cnki.issn1006-3536.2021.04.009
18. L. Landau, "The Theory of Phase Transitions," *Nat.* 138(3498), 840-841 (1936). https://doi.org/10.1038/138840a0
19. G. Bulai and O. F. Caltun, "1 - Fundamentals of magnetism," *Woodhead Publishing*. 3-15 (2023). https://doi.org/10.1016/B978-0-12-823717-5.00028-0
20. C. N. Nanev, "7 - Theory of Nucleation," *Elsevier*. 315-358 (2015). https://doi.org/10.1016/B978-0-444-56369-9.00007-1
21. J. W. Gibbs, "On the equilibrium of heterogeneous substances," *Am. J. Sci.* s3-16(96), 441 (1878). https://doi.org/10.2475/ajs.s3-16.96.441
22. A. J. M. Garrett, "Entropy," *Contemp. Phys.* 33(4), 271-274 (1992). https://doi.org/10.1080/00107519208223976
23. L. M. Siqveland and S. M. Skjæveland, "Derivations of the Young-Laplace equation," *Capillarity*. 4(2), 23-30 (2021). https://doi.org/10.46690/capi.2021.02.01
24. H. Ibach, "Physics of surfaces and interfaces,"*Springer Berlin, Heidelberg*. 12((2006). https://doi.org/10.1007/3-540-34710-0
25. N. Das, Y. Takata, M. Kohno and S. Harish, "Effect of carbon nano inclusion dimensionality on the melting of phase change nanocomposites in vertical shell-tube thermal energy storage unit," *Int. J. Heat Mass Transfer*. 113, 423-431 (2017). https://doi.org/10.1016/j.ijheatmasstransfer.2017.05.101
26. Z.-R. Li, N. Hu, J. Liu, R.-H. Zhang and L.-W. Fan, "Revisiting melting heat transfer of nano-enhanced phase change materials (NePCM) in differentially-heated rectangular cavities using thermochromic liquid crystal (TLC) thermography," *Int. J. Heat Mass Transfer*. 159, 120119 (2020). https://doi.org/10.1016/j.ijheatmasstransfer.2020.120119
27. P. Estellé, D. Cabaleiro, G. Żyła, L. Lugo and S. M. S. Murshed, "Current trends in surface tension and wetting behavior of nanofluids," *Renewable Sustainable Energy Rev.* 94, 931-944 (2018). https://doi.org/10.1016/j.rser.2018.07.006
28. Y. A. Cengel, "Heat Transfer: A Pratical Approach,"*McGraw-Hill* (1997).
29. M. M. Rahman, J. Pollack and M. McCarthy, "Increasing Boiling Heat Transfer using Low Conductivity Materials," *Sci. Rep.* 5(1), 13145 (2015). https://doi.org/10.1038/srep13145
30. J. Chinnam, D. K. Das, R. S. Vajjha and J. R. Satti, "Measurements of the surface tension of nanofluids and development of a new correlation," *Int. J. Therm. Sci.* 98, 68-80 (2015). https://doi.org/10.1016/j.ijthermalsci.2015.07.008
31. J. H. Lienhard and R. Eichhorn, "Peak boiling heat flux on cylinders in a cross flow," *Int. J. Heat Mass Transfer*. 19(10), 1135-1142 (1976). https://doi.org/10.1016/0017-9310(76)90146-0
32. R. Wen, X. Ma, Y.-C. Lee and R. Yang, "Liquid-Vapor Phase-Change Heat Transfer on Functionalized Nanowired Surfaces and Beyond," *Joule*. 2(11), 2307-2347 (2018). https://doi.org/10.1016/j.joule.2018.08.014
33. H. J. Cho, D. J. Preston, Y. Zhu and E. N. Wang, "Nanoengineered materials for liquid–vapour phase-change heat transfer," *Nat. Rev. Mater.* 2(2), 16092 (2016). https://doi.org/10.1038/natrevmats.2016.92
34. S. Vafaei and D. Wen, "Flow boiling heat transfer of alumina nanofluids in single microchannels and the roles of nanoparticles," *J. Nanopart. Res.* 13(3), 1063-1073 (2011). https://doi.org/10.1007/s11051-010-0095-z
35. J. S. Coursey and J. Kim, "Nanofluid boiling: The effect of surface wettability," *Int. J. Heat Fluid Flow*. 29(6), 1577-1585 (2008). https://doi.org/10.1016/j.ijheatfluidflow.2008.07.004
36. A. R. Harikrishnan, P. Dhar, P. K. Agnihotri, S. Gedupudi and S. K. Das, "Wettability of Complex Fluids and Surfactant Capped Nanoparticle-Induced Quasi-Universal Wetting Behavior," *The Journal of Physical Chemistry B*. 121(24), 6081-6095 (2017). https://doi.org/10.1021/acs.jpcb.7b02723

37. A. Karthikeyan, S. Coulombe and A. M. Kietzig, "Wetting behavior of multi-walled carbon nanotube nanofluids," *Nanotechnol.* 28(10), 105706 (2017). https://doi.org/10.1088/1361-6528/aa5a5f
38. Y.-A. Lee, L.-S. Kuo, T.-W. Su, C.-C. Hsu and P.-H. Chen, "Orientation effects of nanoparticle-modified surfaces with interlaced wettability on condensation heat transfer," *Appl. Therm. Eng.* 98, 1054-1060 (2016). https://doi.org/10.1016/j.applthermaleng.2016.01.003
39. W. Qiang, B. Wang, Q. Li and W. Wang, "Molecular dynamics simulation of wetting and evaporation characteristics for sessile nanofluid nanodroplets," *Chem. Phys. Lett.* 695, 112-118 (2018). https://doi.org/10.1016/j.cplett.2018.02.001
40. G. Wang, Z. Zhang, R. Wang and Z. Zhu, "A Review on Heat Transfer of Nanofluids by Applied Electric Field or Magnetic Field," *Nanomater.* 10(12), 2386 (2020). https://doi.org/10.3390/nano10122386
41. S. Mittal, B. Nigam, A. Prakash, S. Satsangi, P. K. Mahto and B. P. Swain, "Review of Magnetohydrodynamics flow in Nanofluids," *IOP Conf. Ser.: Mater. Sci. Eng.* 377(1), 012176 (2018). https://doi.org/10.1088/1757-899X/377/1/012176
42. M. Rostami Dibavar, M. Mohammadpourfard, F. Mohseni and S. Zeinali Heris, "Numerical study on the effect of non-uniform magnetic fields on melting and solidification characteristics of NEPCMs in an annulus enclosure," *Energy Convers. Manage.* 171, 879-889 (2018). https://doi.org/10.1016/j.enconman.2018.06.040
43. S. Rostami, E. Raki, A. Abdollahi and A. S. Goldanlou, "Effects of different magnetic fields on the boiling heat transfer coefficient of the NiO/deionized water nanofluid, an experimental investigation," *Powder Technol.* 376, 398-409 (2020). https://doi.org/10.1016/j.powtec.2020.08.045
44. J. Ranville and M. D. Montano, "Chapter 3 - Size Distributions," *Elsevier*. 8, 91-121 (2015). https://doi.org/10.1016/B978-0-08-099948-7.00003-8
45. T. Hao, "Chapter 6-Physics of electrorheological fluids," *Electrorheological Fluids*. 235-340 (2005). https://doi.org/10.1016/S1383-7303(05)80021-3
46. D.-L. Liu, "Chapter 1 - Particle Deposition onto Enclosure Surfaces," *William Andrew Publishing*. 1-56 (2010). https://doi.org/10.1016/B978-1-4377-7830-4.10001-5
47. E. E. Michaelides, "Brownian movement and thermophoresis of nanoparticles in liquids," *Int. J. Heat Mass Transfer*. 81, 179-187 (2015). https://doi.org/10.1016/j.ijheatmasstransfer.2014.10.019
48. B. R. Sehgal, "Chapter 5 - Fission Product Release and Transport," *Academic Press*. 425-517 (2012). https://doi.org/10.1016/B978-0-12-388446-6.00005-8
49. M. Sheikholeslami and H. B. Rokni, "Effect of melting heat transfer on nanofluid flow in existence of magnetic field considering Buongiorno Model," *Chin. J. Phys.* 55(4), 1115-1126 (2017). https://doi.org/10.1016/j.cjph.2017.04.019
50. E. E. Michaelides, "Nanoparticle diffusivity in narrow cylindrical pores," *Int. J. Heat Mass Transfer*. 114, 607-612 (2017). https://doi.org/10.1016/j.ijheatmasstransfer.2017.06.098
51. F. A. Soomro, M. Usman, R. Ul Haq and W. Wang, "Melting heat transfer analysis of Sisko fluid over a moving surface with nonlinear thermal radiation via Collocation method," *Int. J. Heat Mass Transfer*. 126, 1034-1042 (2018). https://doi.org/10.1016/j.ijheatmasstransfer.2018.05.099
52. T. Hayat, G. Bashir, M. Waqas and A. Alsaedi, "MHD 2D flow of Williamson nanofluid over a nonlinear variable thicked surface with melting heat transfer," *J. Mol. Liq.* 223, 836-844 (2016). https://doi.org/10.1016/j.molliq.2016.08.104
53. M. Lacroix and M. Benmadda, "NUMERICAL SIMULATION OF NATURAL CONVECTION-DOMINATED MELTING AND SOLIDIFICATION FROM A FINNED VERTICAL WALL," *Numer. Heat Transfer, Part A.* 31(1), 71-86 (1997). https://doi.org/10.1080/10407789708914026
54. A. M. Abdulateef, J. Abdulateef, K. Sopian, S. Mat and A. Ibrahim, "Optimal fin parameters used for enhancing the melting and solidification of phase-change material in a heat

exchanger unite," *Case Stud. Therm. Eng.* 14, 100487 (2019). https://doi.org/10.1016/j.csite.2019.100487
55. K. Hosseinzadeh, M. Alizadeh and D. D. Ganji, "Solidification process of hybrid nano-enhanced phase change material in a LHTESS with tree-like branching fin in the presence of thermal radiation," *J. Mol. Liq.* 275, 909-925 (2019). https://doi.org/10.1016/j.molliq.2018.11.109
56. G. H. Yeoh and J. Tu, "Chapter 8 - Freezing/Solidification," *Butterworth-Heinemann*. 501-539 (2010). https://doi.org/10.1016/B978-0-08-046733-7.00008-4
57. J. Dirker, D. Juggurnath, A. Kaya, E. A. Osowade, M. Simpson, S. Lecompte, S. M. A. N. R. Abadi, V. Voulgaropoulos, A. O. Adelaja, M. Z. Dauhoo, A. Khoodaruth, S. O. Obayopo, O. T. Olakoyejo, M. K. Elahee, M. De Paepe, J. P. Meyer and C. N. Markides, "Thermal Energy Processes in Direct Steam Generation Solar Systems: Boiling, Condensation and Energy Storage," *Front. Energy Res.* 6, (2019). https://doi.org/10.3389/fenrg.2018.00147
58. R. Elarem, T. Alqahtani, S. Mellouli, F. Askri, A. Edacherian, T. Vineet, I. A. Badruddin and J. Abdelmajid, "A comprehensive review of heat transfer intensification methods for latent heat storage units," *Energy Storage*. 3(1), (2020). https://doi.org/10.1002/est2.127
59. M. Sheikholeslami, "Numerical modeling of nano enhanced PCM solidification in an enclosure with metallic fin," *J. Mol. Liq.* 259, 424-438 (2018). https://doi.org/10.1016/j.molliq.2018.03.006
60. Y. M. F. El Hasadi and J. M. Khodadadi, "One-dimensional Stefan problem formulation for solidification of nanostructure-enhanced phase change materials (NePCM)," *Int. J. Heat Mass Transfer*. 67, 202-213 (2013). https://doi.org/10.1016/j.ijheatmasstransfer.2013.07.095
61. H. Yang, Y. A. Rothan, S. Althobaiti and M. M. Selim, "Simulation for influence of Y-shape fin on phase change of paraffin inside triplex pipe with using Al_2O_3 nanoparticles," *J. Energy Storage*. 46, 103878 (2022). https://doi.org/10.1016/j.est.2021.103878
62. R. Wang, M. Sheikholeslami, B. S. Mahmood, A. Shafee and T. Nguyen-Thoi, "Simulation of triplex-tube heat storage including nanoparticles, solidification process," *J. Mol. Liq.* 296, 111731 (2019). https://doi.org/10.1016/j.molliq.2019.111731
63. Z. Shah, M. R. Hajizadeh, Ikramullah, N. A. Alreshidi, W. Deebani and M. Shutaywi, "Entropy optimization and heat transfer modeling for Lorentz forces effect on solidification of NEPCM," *Int. Commun. Heat Mass Transfer*. 117, 104715 (2020). https://doi.org/10.1016/j.icheatmasstransfer.2020.104715
64. L. Fan and J. M. Khodadadi, "An experimental investigation of enhanced thermal conductivity and expedited unidirectional freezing of cyclohexane-based nanoparticle suspensions utilized as nano-enhanced phase change materials (NePCM)," *Int. J. Therm. Sci.* 62, 120-126 (2012). https://doi.org/10.1016/j.ijthermalsci.2011.11.005
65. R. Elbahjaoui and H. El Qarnia, "Thermal analysis of nanoparticle-enhanced phase change material solidification in a rectangular latent heat storage unit including natural convection," *Energy Build.* 153, 1-17 (2017). https://doi.org/10.1016/j.enbuild.2017.08.003
66. Y. M. F. El Hasadi and J. M. Khodadadi, "Numerical Simulation of the Effect of the Size of Suspensions on the Solidification Process of Nanoparticle-Enhanced Phase Change Materials," *J. Heat Transfer*. 135(5), (2013). https://doi.org/10.1115/1.4023542
67. T. S. Zhu and M. Li, "Size-dependent freezing temperature of metallic and semi-metallic nanoparticles," *Mater. Res. Bull.* 63, 253-255 (2015). https://doi.org/10.1016/j.materresbull.2014.12.010
68. L.-W. Fan, Z.-Q. Zhu and M.-J. Liu, "A similarity solution to unidirectional solidification of nano-enhanced phase change materials (NePCM) considering the mushy region effect," *Int. J. Heat Mass Transfer*. 86, 478-481 (2015). https://doi.org/10.1016/j.ijheatmasstransfer.2015.03.018
69. J. M. Khodadadi and S. F. Hosseinizadeh, "Nanoparticle-enhanced phase change materials (NEPCM) with great potential for improved thermal energy storage," *Int. Commun. Heat Mass Transfer*. 34(5), 534-543 (2007). https://doi.org/10.1016/j.icheatmasstransfer.2007.02.005

70. A. K. Mishra, B. B. Lahiri and J. Philip, "Thermal conductivity enhancement in organic phase change material (phenol-water system) upon addition of Al_2O_3, SiO_2 and TiO_2 nano-inclusions," *J. Mol. Liq.* 269, 47-63 (2018). https://doi.org/10.1016/j.molliq.2018.08.001
71. S. P. Mo, Y. Chen, J. Y. Yang and X. L. Luo, "Experimental Study on Solidification Behavior of Carbon Nanotube Nanofluid," *Adv. Mater. Res.* 171-172, 333-336 (2011). https://doi.org/10.4028/www.scientific.net/amr.171-172.333
72. Y. Wang, X. Zhang, J. Ji, Y. Li, J. M. Munyalo, B. Liu, X. Xu and S. Liu, "Thermal conductivity modification of n-octanoic acid-myristic acid composite phase change material," *J. Mol. Liq.* 288, 111092 (2019). https://doi.org/10.1016/j.molliq.2019.111092
73. J. You, L. Wang, Z. Wang, J. Li, J. Wang, X. Lin and W. Huang, "Interfacial undercooling in solidification of colloidal suspensions: analyses with quantitative measurements," *Sci. Rep.* 6(1), (2016). https://doi.org/10.1038/srep28434
74. R. K. Sharma, H. S. C. Metselaar and P. Ganesan, "Numerical study of freezing of Cu-water nanofluid in a trapezoidal cavity," *Institution of Engineering and Technology*. (2014). https://doi.org/10.1049/cp.2014.1513
75. L. Jia, Y. Chen, S. Lei, S. Mo, X. Luo and X. Shao, "External electromagnetic field-aided freezing of CMC-modified graphene/water nanofluid," *Appl. Energy*. 162, 1670-1677 (2016). https://doi.org/10.1016/j.apenergy.2015.08.067
76. H. Zhang, Y. Zhao, W. Fang, C. Zhang, F. Zhu, L. Jin and C. Yang, "Active control of the freezing process of a ferrofluid droplet with magnetic fields," *Appl. Therm. Eng.* 176, 115444 (2020). https://doi.org/10.1016/j.applthermaleng.2020.115444
77. M. Sheikholeslami, Z. Li and A. Shafee, "Lorentz forces effect on NEPCM heat transfer during solidification in a porous energy storage system," *Int. J. Heat Mass Transfer*. 127, 665-674 (2018). https://doi.org/10.1016/j.ijheatmasstransfer.2018.06.087
78. E. Shi, S. Ahangar Zonouzi, H. Aminfar and M. Mohammadpourfard, "Enhancement of the performance of a NEPCM filled shell-and-multi tube thermal energy storage system using magnetic field: A numerical study," *Appl. Therm. Eng.* 178, 115604 (2020). https://doi.org/10.1016/j.applthermaleng.2020.115604
79. J. Abdollahzadeh and J. Park, "Effects of Brownian motion on freezing of PCM containing nanoparticles," *Therm. Sci.* 20(5), 1533-1541 (2016). https://doi.org/10.2298/tsci140413094a
80. B. Saint-Michel, M. Georgelin, S. Deville and A. Pocheau, "Interaction of Multiple Particles with a Solidification Front: From Compacted Particle Layer to Particle Trapping," *Langmuir*. 33(23), 5617-5627 (2017). https://doi.org/10.1021/acs.langmuir.7b00472
81. L. Jia, L. Peng, Y. Chen, S. Mo and X. Li, "Improving the supercooling degree of titanium dioxide nanofluids with sodium dodecylsulfate," *Appl. Energy*. 124, 248-255 (2014). https://doi.org/10.1016/j.apenergy.2014.03.019
82. M. Nespoulous, M. Antoni, C. Chassigneux and R. Denoyel, "Porous silica beads produced by nanofluid emulsion freezing," *Microporous Mesoporous Mater.* 305, 110362 (2020). https://doi.org/10.1016/j.micromeso.2020.110362
83. E. E. Michaelides, "Wall Effects on the Brownian Movement, Thermophoresis, and Deposition of Nanoparticles in Liquids," *ASME J. Fluids Eng.* 138(5), (2016). https://doi.org/10.1115/1.4032030
84. R. P. Singh, S. C. Kaushik and D. Rakshit, "Solidification behavior of binary eutectic phase change material in a vertical finned thermal storage system dispersed with graphene nano-plates," *Energy Convers. Manage.* 171, 825-838 (2018). https://doi.org/10.1016/j.enconman.2018.06.037
85. Z. Zhu, D.-W. Sun, Z. Zhang, Y. Li and L. Cheng, "Effects of micro-nano bubbles on the nucleation and crystal growth of sucrose and maltodextrin solutions during ultrasound-assisted freezing process," *LWT*. 92, 404-411 (2018). https://doi.org/10.1016/j.lwt.2018.02.053
86. E. E. Michaelides, "Thermodynamics, Energy Dissipation, and Figures of Merit of Energy Storage Systems-A Critical Review," *Energies*. 14(19), (2021). https://doi.org/10.3390/en14196121

87. M. Bashar and K. Siddiqui, "Experimental investigation of transient melting and heat transfer behavior of nanoparticle-enriched PCM in a rectangular enclosure," *J. Energy Storage*. 18, 485-497 (2018). https://doi.org/10.1016/j.est.2018.06.006
88. Y. Feng, H. Li, L. Li, L. Bu and T. Wang, "Numerical investigation on the melting of nanoparticle-enhanced phase change materials (NEPCM) in a bottom-heated rectangular cavity using lattice Boltzmann method," *Int. J. Heat Mass Transfer*. 81, 415-425 (2015). https://doi.org/10.1016/j.ijheatmasstransfer.2014.10.048
89. N. Kousha, M. J. Hosseini, M. R. Aligoodarz, R. Pakrouh and R. Bahrampoury, "Effect of inclination angle on the performance of a shell and tube heat storage unit – An experimental study," *Appl. Therm. Eng.* 112, 1497-1509 (2017). https://doi.org/10.1016/j.applthermaleng.2016.10.203
90. F. Iachachene, Z. Haddad, H. F. Oztop and E. Abu-Nada, "Melting of phase change materials in a trapezoidal cavity: Orientation and nanoparticles effects," *J. Mol. Liq.* 292, 110592 (2019). https://doi.org/10.1016/j.molliq.2019.03.051
91. K. Muhammad, T. Hayat and A. Alsaedi, "Numerical study for melting heat in dissipative flow of hybrid nanofluid over a variable thicked surface," *Int. Commun. Heat Mass Transfer*. 121, 104805 (2021). https://doi.org/10.1016/j.icheatmasstransfer.2020.104805
92. M. Tran Dinh, I. Tlili, R. N. Dara, A. Shafee, Y. Y. Y. Al-Jahmany and T. Nguyen-Thoi, "Nanomaterial treatment due to imposing MHD flow considering melting surface heat transfer," *Physica A*. 541, 123036 (2020). https://doi.org/10.1016/j.physa.2019.123036
93. R. Elbahjaoui and H. El Qarnia, "Transient behavior analysis of the melting of nanoparticle-enhanced phase change material inside a rectangular latent heat storage unit," *Appl. Therm. Eng.* 112, 720-738 (2017). https://doi.org/10.1016/j.applthermaleng.2016.10.115
94. Z. Cui, B. Ji, Q. Fu, H. Duan, Y. Xue and Z. Li, "Research on size dependent integral melting thermodynamic properties of Cu nanoparticles," *The Journal of Chemical Thermodynamics*. 149, 106148 (2020). https://doi.org/10.1016/j.jct.2020.106148
95. M. H. Shojaeefard, M. Jourabian, A. A. Rabienataj Darzi and A. Bayat, "Inward Melting inside a Horizontal Multilobed Capsule with Conductive Wall Affected by Ag-MgO/Water Hybrid and MgO/Water Nanofluids," *J. Heat Mass Transfer Res.* 8(2), 205-223 (2021). https://doi.org/10.22075/jhmtr.2021.22194.1326
96. C. J. Ho and J. Y. Gao, "An experimental study on melting heat transfer of paraffin dispersed with Al_2O_3 nanoparticles in a vertical enclosure," *Int. J. Heat Mass Transfer*. 62, 2-8 (2013). https://doi.org/10.1016/j.ijheatmasstransfer.2013.02.065
97. M. H. Shojaeefard, M. Jourabian and A. A. R. Darzi, "Rectangular heat sink filled with PCM/ hybrid nanoparticles composites and cooled by intruded T-shaped cavity: Numerical investigation of thermal performance," *Int. Commun. Heat Mass Transfer*. 127, 105527 (2021). https://doi.org/10.1016/j.icheatmasstransfer.2021.105527
98. M. H. Shojaeefard, M. Jourabian and A. A. R. Darzi, "Interactions between hybrid nanosized particles and convection melting inside an enclosure with partially active walls: 2D lattice Boltzmann-based numerical investigation," *Heat Transf.* 50(5), 4908-4936 (2021). https://doi.org/10.1002/htj.22109
99. M. Arıcı, E. Tütüncü, Ç. Yıldız and D. Li, "Enhancement of PCM melting rate via internal fin and nanoparticles," *Int. J. Heat Mass Transfer*. 156, 119845 (2020). https://doi.org/10.1016/j.ijheatmasstransfer.2020.119845
100. Y. Pahamli, M. J. Hosseini, A. A. Ranjbar and R. Bahrampoury, "Effect of nanoparticle dispersion and inclination angle on melting of PCM in a shell and tube heat exchanger," *J. Taiwan Inst. Chem. Eng.* 81, 316-334 (2017). https://doi.org/10.1016/j.jtice.2017.09.044
101. A. Ebrahimi and A. Dadvand, "Simulation of melting of a nano-enhanced phase change material (NePCM) in a square cavity with two heat source–sink pairs," *Alexandria Eng. J.* 54(4), 1003-1017 (2015). https://doi.org/10.1016/j.aej.2015.09.007
102. A. A. Rabienataj Darzi, M. Jourabian and M. Farhadi, "Melting and solidification of PCM enhanced by radial conductive fins and nanoparticles in cylindrical annulus," *Energy Convers. Manage.* 118, 253-263 (2016). https://doi.org/10.1016/j.enconman.2016.04.016

103. M. Al-Jethelah, S. H. Tasnim, S. Mahmud and A. Dutta, "Melting of nano-PCM in an enclosed space: Scale analysis and heatline tracking," *Int. J. Heat Mass Transfer*. 119, 841-859 (2018). https://doi.org/10.1016/j.ijheatmasstransfer.2017.11.106
104. H. Faraji, M. El Alami and A. Arshad, "Investigating the effect of single and hybrid nanoparticles on melting of phase change material in a rectangular enclosure with finite heat source," *Int. J. Energy Res.* 45(3), 4314-4330 (2020). https://doi.org/10.1002/er.6095
105. J. M. Mahdi and E. C. Nsofor, "Melting enhancement in triplex-tube latent heat energy storage system using nanoparticles-metal foam combination," *Appl. Energy*. 191, 22-34 (2017). https://doi.org/10.1016/j.apenergy.2016.11.036
106. M. Parsazadeh and X. Duan, "Numerical and statistical study on melting of nanoparticle enhanced phase change material in a shell-and-tube thermal energy storage system," *Appl. Therm. Eng.* 111, 950-960 (2017). https://doi.org/10.1016/j.applthermaleng.2016.09.133
107. S. S. Sebti, M. Mastiani, H. Mirzaei, A. Dadvand, S. Kashani and S. A. Hosseini, "Numerical study of the melting of nano-enhanced phase change material in a square cavity," *Journal of Zhejiang University: SCIENCE A.* 14(5), 307-316 (2013). https://doi.org/10.1631/jzus.a1200208
108. S. H. Tasnim, R. Hossain, S. Mahmud and A. Dutta, "Convection effect on the melting process of nano-PCM inside porous enclosure," *Int. J. Heat Mass Transfer*. 85, 206-220 (2015). https://doi.org/10.1016/j.ijheatmasstransfer.2015.01.073
109. M. Ghalambaz, A. Doostani, A. J. Chamkha and M. A. Ismael, "Melting of nanoparticles-enhanced phase-change materials in an enclosure: Effect of hybrid nanoparticles," *Int. J. Mech. Sci.* 134, 85-97 (2017). https://doi.org/10.1016/j.ijmecsci.2017.09.045
110. M. Sheikholeslami and O. Mahian, "Enhancement of PCM solidification using inorganic nanoparticles and an external magnetic field with application in energy storage systems," *J. Cleaner Prod.* 215, 963-977 (2019). https://doi.org/10.1016/j.jclepro.2019.01.122
111. T. Hayat, M. Imtiaz and A. Alsaedi, "Melting heat transfer in the MHD flow of Cu–water nanofluid with viscous dissipation and Joule heating," *Adv. Powder Technol.* 27(4), 1301-1308 (2016). https://doi.org/10.1016/j.apt.2016.04.024
112. S. S. Sadegh, A. Aghababaei, O. Mohammadi, H. J. Mosleh, M. B. Shafii and M. H. Ahmadi, "An experimental investigation into the melting of phase change material using Fe_3O_4 magnetic nanoparticles under magnetic field," *J. Therm. Anal. Calorim.* 146(1), 381-392 (2020). https://doi.org/10.1007/s10973-020-09958-4
113. F. Selimefendigil and H. F. Öztop, "Natural convection and melting of NEPCM in a corrugated cavity under the effect of magnetic field," *J. Therm. Anal. Calorim.* 140(3), 1427-1442 (2019). https://doi.org/10.1007/s10973-019-08667-x
114. B. J. Gireesha, B. Mahanthesh, I. S. Shivakumara and K. M. Eshwarappa, "Melting heat transfer in boundary layer stagnation-point flow of nanofluid toward a stretching sheet with induced magnetic field," *Eng. Sci. Technol. Int. J.* 19(1), 313-321 (2016). https://doi.org/10.1016/j.jestch.2015.07.012
115. F. Mabood, T. A. Yusuf and W. A. Khan, "Cu–Al2O3–H2O hybrid nanofluid flow with melting heat transfer, irreversibility analysis and nonlinear thermal radiation," *J. Therm. Anal. Calorim.* 143(2), 973-984 (2020). https://doi.org/10.1007/s10973-020-09720-w
116. F. Mabood and A. Mastroberardino, "Melting heat transfer on MHD convective flow of a nanofluid over a stretching sheet with viscous dissipation and second order slip," *J. Taiwan Inst. Chem. Eng.* 57, 62-68 (2015). https://doi.org/10.1016/j.jtice.2015.05.020
117. N. S. Dhaidan, J. M. Khodadadi, T. A. Al-Hattab and S. M. Al-Mashat, "Experimental and numerical investigation of melting of NePCM inside an annular container under a constant heat flux including the effect of eccentricity," *Int. J. Heat Mass Transfer*. 67, 455-468 (2013). https://doi.org/10.1016/j.ijheatmasstransfer.2013.08.002
118. M. Tausif Sk, K. Das and P. K. Kundu, "Presence of different shapes of ZrO_2 nanoparticles in the melting heat transfer of a Casson flow," *Eur. Phys. J. Plus*. 132(10), 425 (2017). https://doi.org/10.1140/epjp/i2017-11680-8
119. B. W. Martin, "Heat Transfer: J.P. Holman," *Int. J. Heat Fluid Flow*. 3(1), 51-52 (1982). https://doi.org/10.1016/0142-727X(82)90045-5

120. H. R. Moran, D. Zogg, V. Voulgaropoulos, W. J. Van den Bergh, J. Dirker, J. P. Meyer, O. K. Matar and C. N. Markides, "An experimental study of the thermohydraulic characteristics of flow boiling in horizontal pipes: Linking spatiotemporally resolved and integral measurements," *Appl. Therm. Eng.* 194, (2021). https://doi.org/10.1016/j.applthermaleng.2021.117085
121. A. Suriyawong and S. Wongwises, "Nucleate pool boiling heat transfer characteristics of TiO_2–water nanofluids at very low concentrations," *Exp. Therm Fluid Sci.* 34(8), 992-999 (2010). https://doi.org/10.1016/j.expthermflusci.2010.03.002
122. T. Sayahi and M. Bahrami, "Investigation on the Effect of Type and Size of Nanoparticles and Surfactant on Pool Boiling Heat Transfer of Nanofluids," *J. Heat Transfer*. 138(3), (2015). https://doi.org/10.1115/1.4031883
123. H. Aminfar, M. Mohammadpourfard and R. Maroofiazar, "Experimental study on the effect of magnetic field on critical heat flux of ferrofluid flow boiling in a vertical annulus," *Exp. Therm Fluid Sci.* 58, 156-169 (2014). https://doi.org/10.1016/j.expthermflusci.2014.06.023
124. H. S. Ahn, H. Kim, H. Jo, S. Kang, W. Chang and M. H. Kim, "Experimental study of critical heat flux enhancement during forced convective flow boiling of nanofluid on a short heated surface," *Int. J. Multiphase Flow*. 36(5), 375-384 (2010). https://doi.org/10.1016/j.ijmultiphaseflow.2010.01.004
125. Z.-h. Liu, J.-g. Xiong and R. Bao, "Boiling heat transfer characteristics of nanofluids in a flat heat pipe evaporator with micro-grooved heating surface," *Int. J. Multiphase Flow*. 33(12), 1284-1295 (2007). https://doi.org/10.1016/j.ijmultiphaseflow.2007.06.009
126. V. Trisaksri and S. Wongwises, "Nucleate pool boiling heat transfer of TiO_2–R141b nanofluids," *Int. J. Heat Mass Transfer*. 52(5-6), 1582-1588 (2009). https://doi.org/10.1016/j.ijheatmasstransfer.2008.07.041
127. S. K. Das, N. Putra and W. Roetzel, "Pool boiling characteristics of nano-fluids," *Int. J. Heat Mass Transfer*. 46(5), 851-862 (2003). https://doi.org/10.1016/s0017-9310(02)00348-4
128. M. M. Sarafraz and F. Hormozi, "Nucleate pool boiling heat transfer characteristics of dilute Al_2O_3–ethyleneglycol nanofluids," *Int. Commun. Heat Mass Transfer*. 58, 96-104 (2014). https://doi.org/10.1016/j.icheatmasstransfer.2014.08.028
129. I. C. Bang and S. Heung Chang, "Boiling heat transfer performance and phenomena of Al_2O_3–water nano-fluids from a plain surface in a pool," *Int. J. Heat Mass Transfer*. 48(12), 2407-2419 (2005). https://doi.org/10.1016/j.ijheatmasstransfer.2004.12.047
130. H. S. Park, D. Shiferaw, B. R. Sehgal, D. K. Kim and M. Muhammed, "Film Boiling Heat Transfer on a High Temperature Sphere in Nanofluid," In *ASME 2004 Heat Transfer/Fluids Engineering Summer Conference*, 4, 469-476(2004). http://doi.org/10.1115/ht-fed2004-56471
131. B. Sun and D. Yang, "Flow boiling heat transfer characteristics of nano-refrigerants in a horizontal tube," *Int. J. Refrig.* 38, 206-214 (2014). https://doi.org/10.1016/j.ijrefrig.2013.08.020
132. J. T. Cieśliński and T. Z. Kaczmarczyk, "Pool Boiling of Water–Al_2O_3 and Water–Cu Nanofluids Outside Porous Coated Tubes," *Heat Transfer Eng.* 36(6), 553-563 (2015). https://doi.org/10.1080/01457632.2014.939046
133. B. Sun and D. Yang, "Flow boiling heat transfer characteristics of nano-refrigerants in a horizontal tube," *Int. J. Refrig*. 38, 206-214 (2014). https://doi.org/10.1016/j.ijrefrig.2013.08.020
134. S. Soltani, S. G. Etemad and J. Thibault, "Pool boiling heat transfer of non-Newtonian nanofluids," *Int. Commun. Heat Mass Transfer*. 37(1), 29-33 (2010). https://doi.org/10.1016/j.icheatmasstransfer.2009.08.005
135. D. Wen and Y. Ding, "Experimental investigation into the pool boiling heat transfer of aqueous based γ-alumina nanofluids," *J. Nanopart. Res.* 7(2-3), 265-274 (2005). https://doi.org/10.1007/s11051-005-3478-9
136. S. W. Lee, K. M. Kim and I. C. Bang, "Study on flow boiling critical heat flux enhancement of graphene oxide/water nanofluid," *Int. J. Heat Mass Transfer*. 65, 348-356 (2013). https://doi.org/10.1016/j.ijheatmasstransfer.2013.06.013

137. D. Milanova and R. Kumar, "Heat Transfer Behavior of Silica Nanoparticles in Pool Boiling Experiment," *J. Heat Transfer*. 130(4), (2008). https://doi.org/10.1115/1.2787020
138. P. Vassallo, R. Kumar and S. D'Amico, "Pool boiling heat transfer experiments in silica–water nano-fluids," *Int. J. Heat Mass Transfer*. 47(2), 407-411 (2004). https://doi.org/10.1016/s0017-9310(03)00361-2
139. A. Amiri, M. Shanbedi, H. Amiri, S. Z. Heris, S. N. Kazi, B. T. Chew and H. Eshghi, "Pool boiling heat transfer of CNT/water nanofluids," *Appl. Therm. Eng.* 71(1), 450-459 (2014). https://doi.org/10.1016/j.applthermaleng.2014.06.064
140. M. M. Sarafraz and F. Hormozi, "Comparatively experimental study on the boiling thermal performance of metal oxide and multi-walled carbon nanotube nanofluids," *Powder Technol.* 287, 412-430 (2016). https://doi.org/10.1016/j.powtec.2015.10.022
141. S. Yao, X. Huang, Y. Song, Y. Shen and S. Zhang, "Effects of nanoparticle types and size on boiling feat transfer performance under different pressures," *AIP Adv.* 8(2), 025005 (2018). https://doi.org/10.1063/1.5010809
142. R. Kumar and D. Milanova, "Effect of surface tension on nanotube nanofluids," *Appl. Phys. Lett.* 94(7), 073107 (2009). https://doi.org/10.1063/1.3085766
143. X. Yin, C. Hu, M. Bai and J. Lv, "Molecular dynamic simulation of rapid boiling of nanofluids on different wetting surfaces with depositional nanoparticles," *Int. J. Multiphase Flow*. 115, 9-18 (2019). https://doi.org/10.1016/j.ijmultiphaseflow.2019.03.022
144. S. L. Song, J. H. Lee and S. H. Chang, "CHF enhancement of SiC nanofluid in pool boiling experiment," *Exp. Therm Fluid Sci.* 52, 12-18 (2014). https://doi.org/10.1016/j.expthermflusci.2013.08.008
145. B. D. Bock, M. Bucci, C. N. Markides, J. R. Thome and J. P. Meyer, "Falling film boiling of refrigerants over nanostructured and roughened tubes: Heat transfer, dryout and critical heat flux," *Int. J. Heat Mass Transfer*. 163, (2020). https://doi.org/10.1016/j.ijheatmasstransfer.2020.120452
146. B. D. Bock, M. Bucci, C. N. Markides, J. R. Thome and J. P. Meyer, "Pool boiling of refrigerants over nanostructured and roughened tubes," *Int. J. Heat Mass Transfer*. 162, (2020). https://doi.org/10.1016/j.ijheatmasstransfer.2020.120387
147. X. Quan, D. Wang and P. Cheng, "An experimental investigation on wettability effects of nanoparticles in pool boiling of a nanofluid," *Int. J. Heat Mass Transfer*. 108, 32-40 (2017). https://doi.org/10.1016/j.ijheatmasstransfer.2016.11.098
148. S. B. White, A. J. Shih and K. P. Pipe, "Effects of nanoparticle layering on nanofluid and base fluid pool boiling heat transfer from a horizontal surface under atmospheric pressure," *J. Appl. Phys.* 107(11), 114302 (2010). https://doi.org/10.1063/1.3342584
149. D. Wang and P. Cheng, "Effects of nanoparticles' wettability on vapor bubble coalescence in saturated pool boiling of nanofluids: A lattice Boltzmann simulation," *Int. J. Heat Mass Transfer*. 154, 119669 (2020). https://doi.org/10.1016/j.ijheatmasstransfer.2020.119669
150. X. Yin, C. Hu, M. Bai and J. Lv, "An investigation on the heat transfer characteristics of nanofluids in flow boiling by molecular dynamics simulations," *Int. J. Heat Mass Transfer*. 162, 120338 (2020). https://doi.org/10.1016/j.ijheatmasstransfer.2020.120338
151. D. Wen, M. Corr, X. Hu and G. Lin, "Boiling heat transfer of nanofluids: The effect of heating surface modification," *Int. J. Therm. Sci.* 50(4), 480-485 (2011). https://doi.org/10.1016/j.ijthermalsci.2010.10.017
152. G. Niu and J. Li, "Comparative studies of pool boiling heat transfer with nano-fluids on porous surface," *Heat Mass Transfer*. 51(12), 1769-1777 (2015). https://doi.org/10.1007/s00231-015-1542-2
153. S. Vafaei, "Nanofluid pool boiling heat transfer phenomenon," *Powder Technol.* 277, 181-192 (2015). https://doi.org/10.1016/j.powtec.2015.02.040
154. G. P. Narayan, K. B. Anoop and S. K. Das, "Mechanism of enhancement/deterioration of boiling heat transfer using stable nanoparticle suspensions over vertical tubes," *J. Appl. Phys.* 102(7), 074317 (2007). https://doi.org/10.1063/1.2794731

155. H. Ganapathy and V. Sajith, "Semi-analytical model for pool boiling of nanofluids," *Int. J. Heat Mass Transfer*. 57(1), 32-47 (2013). https://doi.org/10.1016/j.ijheatmasstransfer.2012.09.056
156. H. Setoodeh, A. Keshavarz, A. Ghasemian and A. Nasouhi, "Subcooled flow boiling of alumina/water nanofluid in a channel with a hot spot: An experimental study," *Appl. Therm. Eng.* 90, 384-394 (2015). https://doi.org/10.1016/j.applthermaleng.2015.07.016
157. D. Ciloglu, "An Experimental Investigation of Nucleate Pool Boiling Heat Transfer of Nanofluids From a Hemispherical Surface," *Heat Transfer Eng.* 38(10), 919-930 (2016). https://doi.org/10.1080/01457632.2016.1212571
158. M. M. Sarafraz, T. Kiani and F. Hormozi, "Critical heat flux and pool boiling heat transfer analysis of synthesized zirconia aqueous nano-fluids," *Int. Commun. Heat Mass Transfer*. 70, 75-83 (2016). https://doi.org/10.1016/j.icheatmasstransfer.2015.12.008
159. H. T. Phan, N. Caney, P. Marty, S. Colasson and J. Gavillet, "Surface wettability control by nanocoating: The effects on pool boiling heat transfer and nucleation mechanism," *Int. J. Heat Mass Transfer*. 52(23-24), 5459-5471 (2009). https://doi.org/10.1016/j.ijheatmasstransfer.2009.06.032
160. S. D. Park, S. B. Moon and I. C. Bang, "Effects of thickness of boiling-induced nanoparticle deposition on the saturation of critical heat flux enhancement," *Int. J. Heat Mass Transfer*. 78, 506-514 (2014). https://doi.org/10.1016/j.ijheatmasstransfer.2014.06.090
161. J. Ham, H. Kim, Y. Shin and H. Cho, "Experimental investigation of pool boiling characteristics in Al_2O_3 nanofluid according to surface roughness and concentration," *Int. J. Therm. Sci.* 114, 86-97 (2017). https://doi.org/10.1016/j.ijthermalsci.2016.12.009
162. Y. Diao, Y. Liu, R. Wang, Y. Zhao and L. Guo, "Experimental investigation of the Cu/R141b nanofluids on the evaporation/boiling heat transfer characteristics for surface with capillary micro-channels," *Heat Mass Transfer*. 50(9), 1261-1274 (2014). https://doi.org/10.1007/s00231-014-1325-1
163. Z.-h. Liu and L. Liao, "Sorption and agglutination phenomenon of nanofluids on a plain heating surface during pool boiling," *Int. J. Heat Mass Transfer*. 51(9-10), 2593-2602 (2008). https://doi.org/10.1016/j.ijheatmasstransfer.2006.11.050
164. S. J. Kim, I. C. Bang, J. Buongiorno and L. W. Hu, "Surface wettability change during pool boiling of nanofluids and its effect on critical heat flux," *Int. J. Heat Mass Transfer*. 50(19-20), 4105-4116 (2007). https://doi.org/10.1016/j.ijheatmasstransfer.2007.02.002
165. S. M. Kwark, R. Kumar, G. Moreno, J. Yoo and S. M. You, "Pool boiling characteristics of low concentration nanofluids," *Int. J. Heat Mass Transfer*. 53(5-6), 972-981 (2010). https://doi.org/10.1016/j.ijheatmasstransfer.2009.11.018
166. B. Truong, L.-w. Hu, J. Buongiorno and T. McKrell, "Modification of sandblasted plate heaters using nanofluids to enhance pool boiling critical heat flux," *Int. J. Heat Mass Transfer*. 53(1-3), 85-94 (2010). https://doi.org/10.1016/j.ijheatmasstransfer.2009.10.002
167. S. J. Kim, T. McKrell, J. Buongiorno and L.-w. Hu, "Subcooled flow boiling heat transfer of dilute alumina, zinc oxide, and diamond nanofluids at atmospheric pressure," *Nucl. Eng. Des.* 240(5), 1186-1194 (2010). https://doi.org/10.1016/j.nucengdes.2010.01.020
168. T. I. Kim, W. J. Chang and S. H. Chang, "Flow boiling CHF enhancement using Al_2O_3 nanofluid and an Al_2O_3 nanoparticle deposited tube," *Int. J. Heat Mass Transfer*. 54(9-10), 2021-2025 (2011). https://doi.org/10.1016/j.ijheatmasstransfer.2010.12.029
169. M. Chopkar, A. K. Das, I. Manna and P. K. Das, "Pool boiling heat transfer characteristics of ZrO_2–water nanofluids from a flat surface in a pool," *Heat Mass Transfer*. 44(8), 999-1004 (2007). https://doi.org/10.1007/s00231-007-0345-5
170. J.-Y. Jung, H. Kim and M. H. Kim, "Effect of ionic additive on pool boiling critical heat flux of titania/water nanofluids," *Heat Mass Transfer*. 49(1), 1-10 (2012). https://doi.org/10.1007/s00231-012-1055-1
171. H. Peng, G. Ding and H. Hu, "Effect of surfactant additives on nucleate pool boiling heat transfer of refrigerant-based nanofluid," *Exp. Therm Fluid Sci.* 35(6), 960-970 (2011). https://doi.org/10.1016/j.expthermflusci.2011.01.016

172. R. Kathiravan, R. Kumar, A. Gupta and R. Chandra, "Preparation and pool boiling characteristics of copper nanofluids over a flat plate heater," *Int. J. Heat Mass Transfer*. 53(9-10), 1673-1681 (2010). https://doi.org/10.1016/j.ijheatmasstransfer.2010.01.022
173. X. Tang, Y.-H. Zhao and Y.-h. Diao, "Experimental investigation of the nucleate pool boiling heat transfer characteristics of δ-Al_2O_3-R141b nanofluids on a horizontal plate," *Exp. Therm Fluid Sci.* 52, 88-96 (2014). https://doi.org/10.1016/j.expthermflusci.2013.08.025
174. Z.-H. Liu, X.-F. Yang and J.-G. Xiong, "Boiling characteristics of carbon nanotube suspensions under sub-atmospheric pressures," *Int. J. Therm. Sci.* 49(7), 1156-1164 (2010). https://doi.org/10.1016/j.ijthermalsci.2010.01.023
175. P. Naphon and C. Thongjing, "Pool boiling heat transfer characteristics of refrigerant-nanoparticle mixtures," *Int. Commun. Heat Mass Transfer*. 52, 84-89 (2014). https://doi.org/10.1016/j.icheatmasstransfer.2014.01.014
176. H. Sakashita, "Pressure effect on CHF enhancement in pool boiling of nanofluids," *J. Nucl. Sci. Technol.* 53(6), 797-802 (2015). https://doi.org/10.1080/00223131.2015.1072482
177. J. H. Lee, T. Lee and Y. H. Jeong, "The effect of pressure on the critical heat flux in water-based nanofluids containing Al_2O_3 and Fe_3O_4 nanoparticles," *Int. J. Heat Mass Transfer*. 61, 432-438 (2013). https://doi.org/10.1016/j.ijheatmasstransfer.2013.02.018
178. X. Li, Y. Yuan and J. Tu, "A theoretical model for nucleate boiling of nanofluids considering the nanoparticle Brownian motion in liquid microlayer," *Int. J. Heat Mass Transfer*. 91, 467-476 (2015). https://doi.org/10.1016/j.ijheatmasstransfer.2015.07.116
179. A. Malvandi, S. Heysiattalab and D. D. Ganji, "Thermophoresis and Brownian motion effects on heat transfer enhancement at film boiling of nanofluids over a vertical cylinder," *J. Mol. Liq.* 216, 503-509 (2016). https://doi.org/10.1016/j.molliq.2016.01.030
180. N. Gobinath, T. Venugopal, K. Palani and A. A. Samuel, "Numerical modelling of thermophoresis in water-alumina nanofluid under pool boiling conditions," *Int. J. Therm. Sci.* 129, 1-13 (2018). https://doi.org/10.1016/j.ijthermalsci.2018.02.025
181. R. B. Bird, "Five decades of transport phenomena," *AlChE J.* 50(2), 273-287 (2004). https://doi.org/10.1002/aic.10026
182. C. P. Karthikeyan, G. Kalpana, V. Krishnamoorthy and A. A. Samuel, "Transient numerical analysis of thermophoresis and particle dynamics in a nanofluid – pool boiling conditions," *J. Mol. Liq.* 301, 112459 (2020). https://doi.org/10.1016/j.molliq.2020.112459
183. Y. Wang, K. Deng, J. Wu, G. Su and S. Qiu, "A mechanism of heat transfer enhancement or deterioration of nanofluid flow boiling," *Int. J. Heat Mass Transfer*. 158, 119985 (2020). https://doi.org/10.1016/j.ijheatmasstransfer.2020.119985
184. N. Kumar, N. Urkude, S. S. Sonawane and S. H. Sonawane, "Experimental study on pool boiling and Critical Heat Flux enhancement of metal oxides based nanofluid," *Int. Commun. Heat Mass Transfer*. 96, 37-42 (2018). https://doi.org/10.1016/j.icheatmasstransfer.2018.05.018
185. M. N. Golubovic, H. D. Madhawa Hettiarachchi, W. M. Worek and W. J. Minkowycz, "Nanofluids and critical heat flux, experimental and analytical study," *Appl. Therm. Eng.* 29(7), 1281-1288 (2009). https://doi.org/10.1016/j.applthermaleng.2008.05.005
186. A. Zendehboudi, B. Wang and X. Li, "Robust model to predict the migration ratios of nanoparticles during the pool-boiling process of nanorefrigerants," *Int. Commun. Heat Mass Transfer*. 84, 75-85 (2017). https://doi.org/10.1016/j.icheatmasstransfer.2017.03.012
187. G. Ding, H. Peng, W. Jiang and Y. Gao, "The migration characteristics of nanoparticles in the pool boiling process of nanorefrigerant and nanorefrigerant–oil mixture," *Int. J. Refrig.* 32(1), 114-123 (2009). https://doi.org/10.1016/j.ijrefrig.2008.08.007
188. F. R. Siddiqui, C. Y. Tso, S. C. Fu, H. H. Qiu and C. Y. H. Chao, "Evaporation and wetting behavior of silver-graphene hybrid nanofluid droplet on its porous residue surface for various mixing ratios," *Int. J. Heat Mass Transfer*. 153, 119618 (2020). https://doi.org/10.1016/j.ijheatmasstransfer.2020.119618
189. F.-C. Wang and H.-A. Wu, "Pinning and depinning mechanism of the contact line during evaporation of nano-droplets sessile on textured surfaces," *Soft Matter*. 9(24), 5703-5709 (2013). https://doi.org/10.1039/c3sm50530h

190. D. Wang and P. Cheng, "Nanoparticles deposition patterns in evaporating nanofluid droplets on smooth heated hydrophilic substrates: A 2D immersed boundary-lattice Boltzmann simulation," *Int. J. Heat Mass Transfer*. 168, 120868 (2021). https://doi.org/10.1016/j.ijheatmasstransfer.2020.120868
191. F. R. Siddiqui, E. C. Y. Tso, S. C. Fu, C. Y. H. Chao and H. Qiu, "Experimental Investigation on Silver-Graphene Hybrid Nanofluid Droplet Evaporation and Wetting Characteristics of its Nanostructured Droplet Residue," In *ASME-JSME-KSME 2019 8th Joint Fluids Engineering Conference*, AJKFluids,4, (2019). http://doi.org/10.1115/ajkfluids2019-5049
192. F. R. Siddiqui, C. Y. Tso, S. C. Fu, H. H. Qiu and C. Y. H. Chao, "Droplet evaporation and boiling for different mixing ratios of the silver-graphene hybrid nanofluid over heated surfaces," *Int. J. Heat Mass Transfer*. 180, 121786 (2021). https://doi.org/10.1016/j.ijheatmasstransfer.2021.121786
193. D. Qu, L. Cheng, Y. Bao, Y. Gao, X. Zheng and G. Qin, "Enhanced optical absorption and solar steam generation of CB-ATO hybrid nanofluids," *Renewable Energy*. 199, 509-516 (2022). https://doi.org/10.1016/j.renene.2022.08.150
194. M. Dai, J. Wang, N. Wei, X. Wang and C. Xu, "Experimental study on evaporation characteristics of diesel/cerium oxide nanofluid fuel droplets," *Fuel*. 254, 115633 (2019). https://doi.org/10.1016/j.fuel.2019.115633
195. Z. Liu, S. Li, X. Pan and H. Fang, "Mechanism study on spreading dynamics of nanofluids droplet coupled with thermal evaporation," *Int. J. Heat Mass Transfer*. 183, 122172 (2022). https://doi.org/10.1016/j.ijheatmasstransfer.2021.122172
196. Y. Gan and L. Qiao, "Optical Properties and Radiation-Enhanced Evaporation of Nanofluid Fuels Containing Carbon-Based Nanostructures," *Energy Fuels*. 26(7), 4224-4230 (2012). https://doi.org/10.1021/ef300493m
197. N. Kubochkin, J. Venzmer and T. Gambaryan-Roisman, "Superspreading and Drying of Trisiloxane-Laden Quantum Dot Nanofluids on Hydrophobic Surfaces," *Langmuir*. 36(14), 3798-3813 (2020). https://doi.org/10.1021/acs.langmuir.0c00337
198. P. Chen, S. Harmand, S. Szunerits and R. Boukherroub, "Evaporation behavior of PEGylated graphene oxide nanofluid droplets on heated substrate," *Int. J. Therm. Sci.* 135, 445-458 (2019). https://doi.org/10.1016/j.ijthermalsci.2018.06.030
199. C. Y. Tso and C. Y. H. Chao, "Study of enthalpy of evaporation, saturated vapor pressure and evaporation rate of aqueous nanofluids," *Int. J. Heat Mass Transfer*. 84, 931-941 (2015). https://doi.org/10.1016/j.ijheatmasstransfer.2015.01.090
200. Z. Hong, J. Pei, Y. Wang, B. Cao, M. Mao, H. Liu, H. Jiang, Q. An, X. Liu and X. Hu, "Characteristics of the direct absorption solar collectors based on reduced graphene oxide nanofluids in solar steam evaporation," *Energy Convers. Manage.* 199, 112019 (2019). https://doi.org/10.1016/j.enconman.2019.112019
201. I. Kim and K. D. Kihm, "Hidden Cavity Formations by Nanocrystalline Self-Assembly on Various Substrates with Different Hydrophobicities," *Langmuir*. 28(25), 9195-9200 (2012). https://doi.org/10.1021/la301526f
202. A. Zeiny, H. Jin, G. Lin, P. Song and D. Wen, "Solar evaporation via nanofluids: A comparative study," *Renewable Energy*. 122, 443-454 (2018). https://doi.org/10.1016/j.renene.2018.01.043
203. M. Najim, M. B. Feddaoui, A. Nait Alla and A. Charef, "Computational study of evaporating nanofluids film along a vertical channel by the two-phase model," *Int. J. Mech. Sci.* 151, 858-867 (2019). https://doi.org/10.1016/j.ijmecsci.2018.12.042
204. M. Mahrukh, A. Kumar, S. Gu, S. Kamnis and E. Gozali, "Modeling the Effects of Concentration of Solid Nanoparticles in Liquid Feedstock Injection on High-Velocity Suspension Flame Spray Process," *Ind. Eng. Chem. Res.* 55(9), 2556-2573 (2016). https://doi.org/10.1021/acs.iecr.5b03956
205. S.-Y. Lin, K.-C. Yang and L.-J. Chen, "Effect of Surface Hydrophobicity on Critical Pinning Concentration of Nanoparticles To Trigger the Coffee Ring Formation during the Evaporation Process of Sessile Drops of Nanofluids," *The Journal of Physical Chemistry C*. 119(6), 3050-3059 (2015). https://doi.org/10.1021/jp509547n

206. C. H. Chon, S. Paik, J. B. Tipton and K. D. Kihm, "Effect of Nanoparticle Sizes and Number Densities on the Evaporation and Dryout Characteristics for Strongly Pinned Nanofluid Droplets," *Langmuir*. 23(6), 2953-2960 (2006). https://doi.org/10.1021/la061661y
207. V. Ganesan, C. Louis and S. P. Damodaran, "Novel Nanofluids Based on Magnetite Nanoclusters and Investigation on Their Cluster Size-Dependent Thermal Conductivity," *J. Phys. Chem. C*. 122(12), 6918-6929 (2018). https://doi.org/10.1021/acs.jpcc.7b12043
208. M. B. Bigdeli and P. A. Tsai, "Making Photonic Crystals via Evaporation of Nanoparticle-Laden Droplets on Superhydrophobic Microstructures," *Langmuir*. 36(17), 4835-4841 (2020). https://doi.org/10.1021/acs.langmuir.0c00193
209. P. Wąsik, C. Redeker, T. G. Dane, A. M. Seddon, H. Wu and W. H. Briscoe, "Hierarchical Surface Patterns upon Evaporation of a ZnO Nanofluid Droplet: Effect of Particle Morphology," *Langmuir*. 34(4), 1645-1654 (2018). https://doi.org/10.1021/acs.langmuir.7b03854
210. J.-y. Jung, Y. W. Kim, J. Y. Yoo, J. Koo and Y. T. Kang, "Forces Acting on a Single Particle in an Evaporating Sessile Droplet on a Hydrophilic Surface," *Anal. Chem.* 82(3), 784-788 (2010). https://doi.org/10.1021/ac902288z
211. W. J. Gerken, A. V. Thomas, N. Koratkar and M. A. Oehlschlaeger, "Nanofluid pendant droplet evaporation: Experiments and modeling," *Int. J. Heat Mass Transfer*. 74, 263-268 (2014). https://doi.org/10.1016/j.ijheatmasstransfer.2014.03.031
212. R. Wang, G. Pan, S. Qian, L. Li and Z. Zhu, "Influence of Nanoparticles on the Evaporation Behavior of Nanofluid Droplets: A Law and Underlying Mechanism," *Langmuir*. 36(4), 919-930 (2020). https://doi.org/10.1021/acs.langmuir.9b02669
213. D. L. Albernaz, G. Amberg and M. Do-Quang, "Simulation of a suspended droplet under evaporation with Marangoni effects," *Int. J. Heat Mass Transfer*. 97, 853-860 (2016). https://doi.org/10.1016/j.ijheatmasstransfer.2016.02.073
214. I. Zaaroura, M. Toubal, H. Reda, J. Carlier, S. Harmand, R. Boukherroub, A. Fasquelle and B. Nongaillard, "Evaporation of nanofluid sessile drops: Infrared and acoustic methods to track the dynamic deposition of copper oxide nanoparticles," *Int. J. Heat Mass Transfer*. 127, 1168-1177 (2018). https://doi.org/10.1016/j.ijheatmasstransfer.2018.07.102
215. Y. Wei, W. Deng and R.-H. Chen, "Effects of internal circulation and particle mobility during nanofluid droplet evaporation," *Int. J. Heat Mass Transfer*. 103, 1335-1347 (2016). https://doi.org/10.1016/j.ijheatmasstransfer.2016.08.037
216. E. E. S. Michaelides, "Nanofluidics: Thermodynamic and Transport Properties,"9783319343105, *Springer Cham*. 1-335 (2014). https://doi.org/10.1007/978-3-319-05621-0
217. S. Yan and T. C. G. Kibbey, "The effect of evaporation-induced flow at the pore scale on nanoparticle transport and deposition in drying unsaturated porous media," *J. Contam. Hydrol.* . 226, 103524 (2019). https://doi.org/10.1016/j.jconhyd.2019.103524
218. Z. Sun, L. Zhou, C. Xiao, X. Du and Y. Yang, "Nanoparticle motion and deposition near the triple line in evaporating sessile water droplet on a superhydrophilic substrate," *Exp. Therm Fluid Sci.* 76, 67-74 (2016). https://doi.org/10.1016/j.expthermflusci.2016.03.009
219. A. R. Harikrishnan and P. Dhar, "Optical thermogeneration induced enhanced evaporation kinetics in pendant nanofluid droplets," *Int. J. Heat Mass Transfer*. 118, 1169-1179 (2018). https://doi.org/10.1016/j.ijheatmasstransfer.2017.11.092
220. Y. Gan and L. Qiao, "Radiation-enhanced evaporation of ethanol fuel containing suspended metal nanoparticles," *Int. J. Heat Mass Transfer*. 55(21-22), 5777-5782 (2012). https://doi.org/10.1016/j.ijheatmasstransfer.2012.05.074
221. S. Tanvir, S. Biswas and L. Qiao, "Evaporation characteristics of ethanol droplets containing graphite nanoparticles under infrared radiation," *Int. J. Heat Mass Transfer*. 114, 541-549 (2017). https://doi.org/10.1016/j.ijheatmasstransfer.2017.06.059
222. V. D. Ta, R. M. Carter, E. Esenturk, C. Connaughton, T. J. Wasley, J. Li, R. W. Kay, J. Stringer, P. J. Smith and J. D. Shephard, "Dynamically controlled deposition of colloidal nanoparticle suspension in evaporating drops using laser radiation," *Soft Matter*. 12(20), 4530-4536 (2016). https://doi.org/10.1039/c6sm00465b

223. M. M. Ghafurian, Z. Akbari, H. Niazmand, R. Mehrkhah, S. Wongwises and O. Mahian, "Effect of sonication time on the evaporation rate of seawater containing a nanocomposite," *Ultrason. Sonochem.* 61, 104817 (2020). https://doi.org/10.1016/j.ultsonch.2019.104817
224. R. Wen, B. Du, S. Yang, Y. Liu, Q. Li, Y. Cheng, Z. Lan and X. Ma, "Progress in the study of vapor condensation heat transfer enhancement," *Journal of Tsinghua University(Science and Technology)*. 61(12), 1353-1370 (2021). https://doi.org/10.16511/j.cnki.qhdxxb.2022.25.002
225. G.-H. Chong, X.-D. Lu, W.-T. Ji, L. Chen, C.-Y. Zhao and W.-Q. Tao, "Deposition of nano-scale polymer film on micro-fins to enhance the film-wise condensation of very low surface tension substances," *Int. J. Heat Mass Transfer*. 177, 121499 (2021). https://doi.org/10.1016/j.ijheatmasstransfer.2021.121499
226. P. Zanganeh, A. S. Goharrizi, S. Ayatollahi and M. Feilizadeh, "Nano-coated condensation surfaces enhanced the productivity of the single-slope solar still by changing the condensation mechanism," *J. Cleaner Prod.* 265, 121758 (2020). https://doi.org/10.1016/j.jclepro.2020.121758
227. X. Wang, B. Xu, Q. Liu, Y. Yang and Z. Chen, "Enhancement of vapor condensation heat transfer on the micro- and nano-structured superhydrophobic surfaces," *Int. J. Heat Mass Transfer*. 177, 121526 (2021). https://doi.org/10.1016/j.ijheatmasstransfer.2021.121526
228. X. Wang, B. Xu and Z. Chen, "Hierarchical microporous superhydrophobic surfaces with nanostructures enhancing vapor condensation heat transfer," *Appl. Therm. Eng.* 219, 119527 (2023). https://doi.org/10.1016/j.applthermaleng.2022.119527
229. S. Lee, K. Cheng, V. Palmre, M. D. M. H. Bhuiya, K. J. Kim, B. J. Zhang and H. Yoon, "Heat transfer measurement during dropwise condensation using micro/nano-scale porous surface," *Int. J. Heat Mass Transfer*. 65, 619-626 (2013). https://doi.org/10.1016/j.ijheatmasstransfer.2013.06.016
230. F. Chu and X. Wu, "Fabrication and condensation characteristics of metallic superhydrophobic surface with hierarchical micro-nano structures," *Appl. Surf. Sci.* 371, 322-328 (2016). https://doi.org/10.1016/j.apsusc.2016.02.208
231. S. Chen, A. Pan, Y. Zhu, T. C. Ho, H. H. Lee, Y. Zeng, C. Wu, H. Qiu and C. Y. Tso, "A novel composite adsorbent coated superhydrophilic-nanostructured heterogeneous surface for condensation heat transfer enhancement," *Int. J. Therm. Sci.* 184, 107978 (2023). https://doi.org/10.1016/j.ijthermalsci.2022.107978
232. H. Cui, S. Saleem, J. E. Jam, M. H. Beni, M. Hekmatifar, D. Toghraie and R. Sabetvand, "Effects of roughness and radius of nanoparticles on the condensation of nanofluid structures with molecular dynamics simulation: Statistical approach," *J. Taiwan Inst. Chem. Eng.* 128, 346-353 (2021). https://doi.org/10.1016/j.jtice.2021.09.005
233. B. Ghorbani, M. A. Akhavan-Behabadi, S. Ebrahimi and K. Vijayaraghavan, "Experimental investigation of condensation heat transfer of R600a/POE/CuO nano-refrigerant in flattened tubes," *Int. Commun. Heat Mass Transfer*. 88, 236-244 (2017). https://doi.org/10.1016/j.icheatmasstransfer.2017.09.011
234. Q. Peng, L. Jia, C. Dang, X. Zhang and Q. Huang, "Experimental investigation on flow condensation of R141b with CuO nanoparticles in a vertical circular tube," *Appl. Therm. Eng.* 129, 812-821 (2018). https://doi.org/10.1016/j.applthermaleng.2017.10.108
235. I. Z. Famileh, J. A. Esfahani and K. Vafai, "Effect of nanoparticles on condensation of humid air in vertical channels," *Int. J. Therm. Sci.* 112, 470-483 (2017). https://doi.org/10.1016/j.ijthermalsci.2016.05.011
236. S. Ghahremanian, A. Abbassi, Z. Mansoori and D. Toghraie, "Investigation the nanofluid flow through a nanochannel to study the effect of nanoparticles on the condensation phenomena," *J. Mol. Liq.* 311, 113310 (2020). https://doi.org/10.1016/j.molliq.2020.113310
237. S. Heysiattalab, A. Malvandi and D. D. Ganji, "Anisotropic behavior of magnetic nanofluids (MNFs) at filmwise condensation over a vertical plate in presence of a uniform variable-directional magnetic field," *J. Mol. Liq.* 219, 875-882 (2016). https://doi.org/10.1016/j.molliq.2016.04.004

238. D. Zhu, X. Xu, J. Liu and L. Jiong, "Study of condensation heat transfer properties of mixed wettability patterned copper-based surfaces," 72, 2528-2546 (2021). https://kns.cnki.net/kcms/detail/11.1946.TQ.20201119.1003.002.html
239. M. Sheikholeslami, M. Darzi and M. K. Sadoughi, "Heat transfer improvement and pressure drop during condensation of refrigerant-based nanofluid; an experimental procedure," *Int. J. Heat Mass Transfer*. 122, 643-650 (2018). https://doi.org/10.1016/j.ijheatmasstransfer.2018.02.015
240. A. A. Avramenko, I. V. Shevchuk, A. I. Tyrinov and D. G. Blinov, "Heat transfer at film condensation of stationary vapor with nanoparticles near a vertical plate," *Appl. Therm. Eng.* 73(1), 391-398 (2014). https://doi.org/10.1016/j.applthermaleng.2014.07.070
241. B. Li, R. Zheng, X. Zhang, G. Zhao and H. Liu, "Molecular dynamics simulation of inert gas condensation of ternary Fe-Ni-Cr nanoparticles," *Comput. Mater. Sci*. 177, 109579 (2020). https://doi.org/10.1016/j.commatsci.2020.109579
242. S. Etedali, M. Afrand and A. Abdollahi, "Effect of different surfactants on the pool boiling heat transfer of SiO_2/deionized water nanofluid on a copper surface," *Int. J. Therm. Sci.* 145, 105977 (2019). https://doi.org/10.1016/j.ijthermalsci.2019.105977
243. X. Yin, C. Hu, M. Bai and J. Lv, "Effects of depositional nanoparticle wettability on explosive boiling heat transfer: A molecular dynamics study," *Int. Commun. Heat Mass Transfer*. 109, 104390 (2019). https://doi.org/10.1016/j.icheatmasstransfer.2019.104390
244. Q. Wang, Y. Qin, F. Jia, S. Song and Y. Li, "Recyclable Fe_3O_4@Polydopamine (PDA) nanofluids for highly efficient solar evaporation," *Green Energy Environ.* 7(1), 35-42 (2022). https://doi.org/10.1016/j.gee.2020.07.020
245. S. Li, H. Du, Z. Zhuo, Y. Lu and X. Huang, "Dispersion Stability, Physical Properties, and Electrostatic Breakup of Surfactant-Loaded Aluminum/*n*-Decane Nanofluid Fuel: Nanoparticle Size Effect," *Energy Fuels*. 34(1), 1082-1092 (2020). https://doi.org/10.1021/acs.energyfuels.9b03332
246. A. Henry, R. Prasher and A. Majumdar, "Five thermal energy grand challenges for decarbonization," *Nat. Energy*. 5(9), 635-637 (2020). https://doi.org/10.1038/s41560-020-0675-9
247. H. Jouhara, N. Khordehgah, S. Almahmoud, B. Delpech, A. Chauhan and S. A. Tassou, "Waste heat recovery technologies and applications," *Therm. Sci. Eng. Prog.* 6, 268-289 (2018). https://doi.org/10.1016/j.tsep.2018.04.017